doi.org/10.26434/chemrxiv.12780044.v1

Radical Tropolone Biosynthesis

Tyler J. Doyon, Kevin Skinner, Di Yang, Leena Mallik, Troy Wymore, Markos Koutmos, Paul M. Zimmerman, Alison Narayan

Submitted date: 07/08/2020 • Posted date: 10/08/2020

Citation information: Doyon, Tyler J.; Skinner, Kevin; Yang, Di; Mallik, Leena; Wymore, Troy; Koutmos, Markos; et al. (2020): Radical Tropolone Biosynthesis. ChemRxiv. Preprint. https://doi.org/10.26434/chemrxiv.12780044.v1

Non-heme iron (NHI) enzymes perform a variety of oxidative rearrangements to advance simple building blocks toward complex molecular scaffolds within secondary metabolite pathways. Many of these transformations occur with selectivity that is unprecedented in small molecule catalysis, spurring an interest in the enzymatic processes which lead to a particular rearrangement. In-depth investigations of NHI mechanisms examine the source of this selectivity and can offer inspiration for the development of novel synthetic transformations. However, the mechanistic details of many NHI-catalyzed rearrangements remain underexplored, hindering full characterization of the chemistry accessible to this functionally diverse class of enzymes. For NHI-catalyzed rearrangements which have been investigated, mechanistic proposals often describe one-electron processes, followed by single electron oxidation from the substrate to the iron(III)-hydroxyl active site species. Here, we examine the ring expansion mechanism employed in fungal tropolone biosynthesis. TropC, an α-ketoglutarate- dependent NHI dioxygenase, catalyzes a ring expansion in the biosynthesis of tropolone natural product stipitatic acid through an under-studied mechanism. Investigation of both polar and radical mechanistic proposals suggests tropolones are constructed through a radical ring expansion. This biosynthetic route to tropolones is supported by X-ray crystal structure data combined with molecular dynamics simulations, alanine-scanning of active site residues, assessed reactivity of putative biosynthetic intermediates, and quantum mechanical (QM) calculations. These studies support a radical ring expansion in fungal tropolone biosynthesis.

File list (2)

Radical tropolone biosynthesis

*Tyler J. Doyon,[1,2] Kevin C. Skinner,[1,3] Di Yang,[1,3] Leena Mallik,[2,3] Troy Wymore,[3] Markos Koutmos,[2,3] Paul M. Zimmerman,[3] Alison R. H. Narayan[1,2,3]**

[1]Life Sciences Institute, University of Michigan, Ann Arbor, Michigan 48109, USA. [2]Program in Chemical Biology, University of Michigan, Ann Arbor, Michigan 48109, USA. [3]Department of Chemistry, University of Michigan, Ann Arbor, Michigan 48109, USA.

*Corresponding author, email: arhardin@umich.edu

Abstract

Non-heme iron (NHI) enzymes perform a variety of oxidative rearrangements to advance simple building blocks toward complex molecular scaffolds within secondary metabolite pathways. Many of these transformations occur with selectivity that is unprecedented in small molecule catalysis, spurring an interest in the enzymatic processes which lead to a particular rearrangement. In-depth investigations of NHI mechanisms examine the source of this selectivity and can offer inspiration for the development of novel synthetic transformations. However, the mechanistic details of many NHI-catalyzed rearrangements remain underexplored, hindering full characterization of the chemistry accessible to this functionally diverse class of enzymes. For NHI-catalyzed rearrangements which have been investigated, mechanistic proposals often describe one-electron processes, followed by single electron oxidation from the substrate to the iron(III)-hydroxyl active site species. Here, we examine the ring expansion mechanism employed in fungal tropolone biosynthesis. TropC, an α-ketoglutarate-dependent NHI dioxygenase, catalyzes a ring expansion in the biosynthesis of tropolone natural product stipitatic acid through an under-studied mechanism. Investigation of both polar and radical mechanistic proposals suggests tropolones are constructed through a radical ring expansion. This biosynthetic route to tropolones is supported by X-ray crystal structure data combined with molecular dynamics simulations, alanine-scanning of active site residues, assessed reactivity of putative biosynthetic intermediates, and quantum mechanical (QM) calculations. These studies support a radical ring expansion in fungal tropolone biosynthesis.

Introduction

Enzymes catalyze challenging transformations with exquisite control over chemo-, site- and stereoselectivity, directing the synthesis of structurally-complex products from bioavailable starting materials. These transformations often take advantage of the three-dimensional architecture of the enzyme active site to guide reactive intermediates toward formation of the desired product.[1] Biocatalytic control over the fate of reactive intermediates is a common mechanistic architype in a variety of enzymes such as cyclases, which leverage active site geometries to induce selective cyclization reactions, polyketide synthases that deliver specific products from large, structurally-complex intermediates, Diels-Alderases, which choreograph the relative position of two reactive components to form a stereo-enriched product, and non-heme iron (NHI) dioxygenases, an enzyme class known to catalyze numerous skeletal rearrangements through radical or polar mechanisms.[1-4] In many cases, reactions of identical intermediates generated outside of the enzyme active site proceed in an uncontrolled fashion, leading to racemic products or fundamentally divergent reactivity.[1-2]

In contrast to the selectivity demonstrated by enzyme-mediated transformations, small molecule-enabled transformations often require careful substrate design to achieve a desired rearrangement, adding synthetic steps and reducing the efficiency and sustainability of the resulting synthesis.[5-6] Radical-based rearrangements are particularly impacted by selectivity challenges, as competing radical pathways often complicate anticipated reaction outcomes.[5-6] As a result, selectivity can be achieved only through optimization of substrate design and reaction conditions to favor the desired reaction pathway.[5-6] In comparison, biocatalysts operate with precise control over the reaction outcome, enabling highly selective and direct synthesis of natural product scaffolds.[7-9] Therefore, thorough examination of the mechanistic details of enzyme-catalyzed rearrangements is critically important to the development of novel, selective approaches to complex molecule synthesis.

Non-heme iron (NHI) enzymes perform an array of oxidative transformations and rearrangements in secondary metabolism.[4, 10-11] Members of the α-ketoglutarate-dependent family of NHI dioxygenases couple the oxidative decarboxylation of α-ketoglutarate (α-KG) to the activation of molecular oxygen, generating an iron(IV)-oxo species (**17**, Fig. 1D).[12-13] Through this common mechanism of oxygen activation, NHI enzymes catalyze a variety of selective transformations that are often initiated by hydrogen atom abstraction, followed by a variety of processes including hydroxylation, desaturation, halogenation, endoperoxidation, epimerization, ring expansion and ring contraction, among others.[4, 11-13] Understanding how the fate of a radical intermediate is controlled by each catalyst has motivated structural, spectroscopic and computational studies of NHI enzymes. In-depth interrogation of NHI-catalyzed reaction mechanisms has revealed critical enzyme-substrate interactions that dictate the reaction outcome in several cases.[7-9] These studies provide mechanistic detail for several NHI-catalyzed rearrangements, including ring contractions and ring expansions.[14-17]

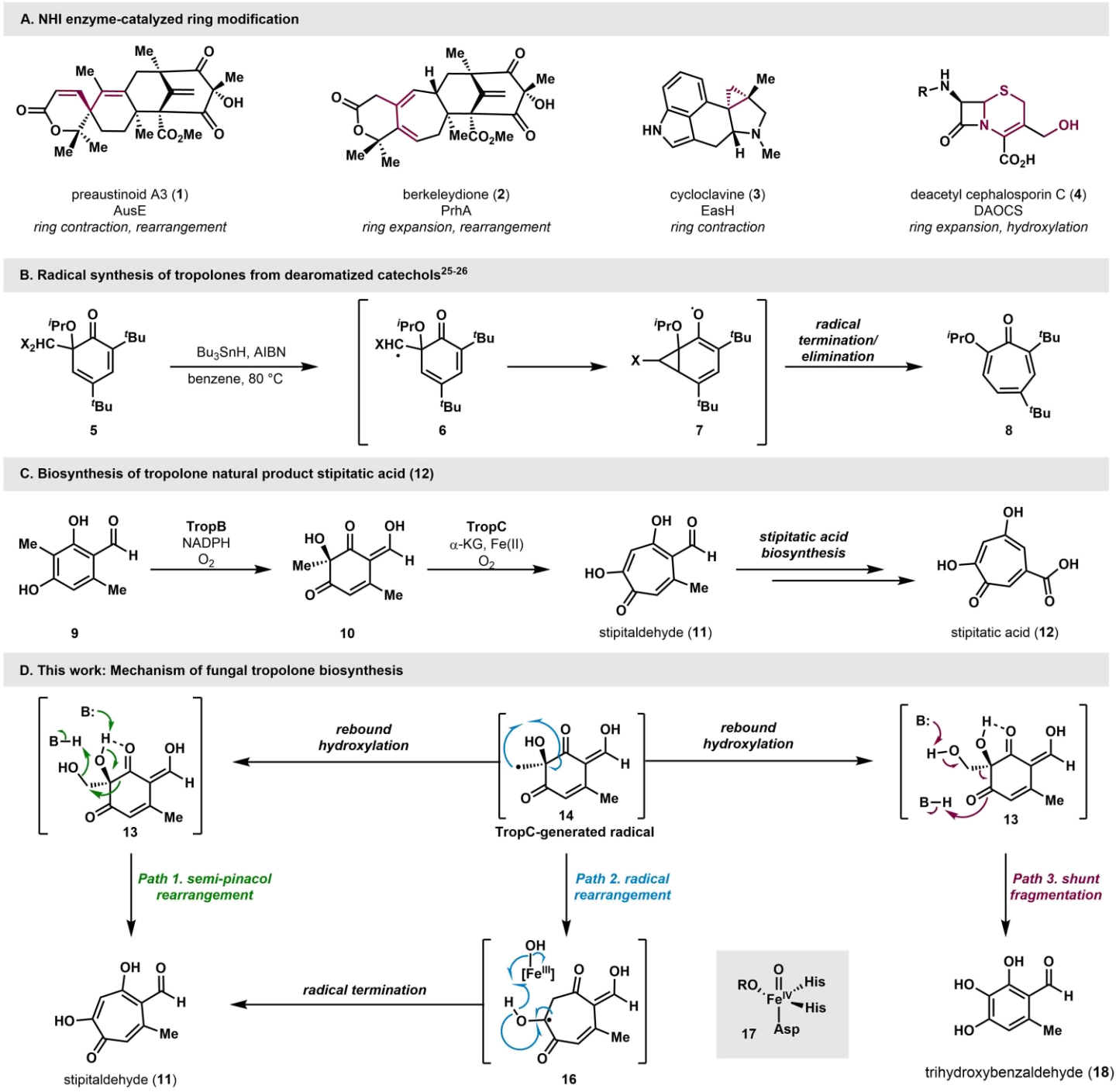

Figure 1. A. Ring rearrangement reactions catalyzed by NHI enzymes. B. Radical tropolone synthesis from dearomatized *ortho*-phenols. C. Biosynthesis of stipitaldehyde (**11**) on path to fungal tropolone natural products. D. This work: Mechanistic studies of ring expansion in NHI enzyme TropC.

Ring-modifying transformations often proceed through an initial C–H atom abstraction, followed by radical rearrangement and termination by single electron oxidation or hydroxylation to yield product.[7-9, 14-17] The NHI active site architecture dictates the reaction outcome by exerting fine control over events downstream from hydrogen atom abstraction, enabling highly selective transformations.[7-9, 14-17] For example, AusE and PrhA are highly related NHI enzymes (78% sequence ID) that catalyze divergent transformations on a common substrate to generate preaustinoid A3 (**1**) and berkeleydione (**2**), respectively.[7-9] Structural and computational studies have shown that minor differences in their active site architecture play a critical role in determining the outcome of the initial enzyme-catalyzed desaturation, ultimately leading to the formation of two distinct natural products through a divergent radical rearrangement process.[7, 9] Similar mechanistic studies found that the NHI-catalyzed biosynthesis of cycloclavine (**3**) and deacetoxy-cephalosporin C (**4**) proceed through a one-electron reaction pathway, suggesting a common mechanistic architype for ring rearrangements catalyzed by NHI enzymes.[14-16, 18]

Natural products often possess medium-sized rings (7-11 atoms) which can be difficult to access using small molecule techniques. One such class of synthetically-challenging targets are tropolones, a structurally-diverse group of bioactive metabolites with an aromatic cycloheptatriene core structure containing an α-hydroxyketone moiety (see Figure 1C, **11**).[19-21] Tropolones have been synthesized through a variety of approaches, typically involving ring expansion.[22] These transformations include classic two-electron rearrangements such as the Büchner reaction,[23] the de Mayo fragmentation[24] and [5+2] cycloadditions.[22] In addition, radical-based approaches have been successful in synthesizing tropolones from *ortho*-dearomatized catechols (**5**) through a selective radical ring expansion mechanism (Figure 1B).[25-26] This approach required pre-functionalization of the arene to ensure that radical initiation occurred at the methyl halide *ipso* to the site of dearomatization, leading to the desired rearrangement (Figure 1B).[25-26] While these methods have been successful in enabling ring expansion, they require arduous synthetic efforts to achieve the desired substitution pattern of the tropolone natural product, preventing facile access to the target compound.[22] In contrast, Nature efficiently assembles complex tropolones using available biosynthetic machinery. In fungi, the identification of the stipitatic acid (**12**) biosynthetic gene cluster in *T. stipitatus* provided a blueprint for the assembly of these aromatic seven-membered rings in Nature (Figure 1C).[21] Fungal tropolone biosynthesis, in the case of stipitatic acid, commences with polyketide synthase production of 3-methylorcinaldehyde (**9**) and subsequent flavin-dependent monooxygenase-mediated oxidative dearomatization.[21, 27] It has been established that the resulting dienone (**10**) undergoes an oxidative ring expansion catalyzed by an α-KG-dependent NHI enzyme, TropC, to afford stipitaldehyde (**11**). Downstream enzymatic modifications of stipitaldehyde (**11**) generate stipitatic acid (**12**).[21] Since the identification and characterization of enzymes involved in stipitatic acid biosynthesis, several other tropolone natural products have been shown to proceed through the same oxidative dearomatization/ring expansion cascade to generate the tropolone core.[28-29] Motivated to understand the chemical steps of this powerful transformation, we initiated our studies on the chemistry and mechanism of the TropC-catalyzed ring expansion. In particular, we sought to investigate two transformations which TropC has been shown to catalyze (1) ring expansion to generate stipitaldehyde (**11**) and (2) a fragmentation reaction which produces trihydroxybenzaldehyde (**18**), a known shunt product in fungal tropolone biosynthesis (Figure 1D).

As the fate of a radical intermediate in NHI dioxygenase-catalyzed transformations is critical to the observed reactivity of the enzyme, we envisioned that TropC-catalyzed ring expansion could occur through several possible mechanistic pathways. Cox and coworkers initially proposed that TropC performs a polar ring expansion to produce stipitaldehyde (**11**, Figure 1D, Path 1).[19-21] Their proposal commences with TropC-mediated C–H atom abstraction on dienone **10** to generate radical species **14**.[19-21] Subsequent rebound hydroxylation would afford diol **13**, which is proposed to undergo a semi-pinacol rearrangement to form stipitaldehyde (**11**). We anticipated that this rearrangement could be assisted by residues in the TropC active site through activation of the alcohol leaving group in diol intermediate **13**.[19-21] The proposed ring expansion mechanism is also consistent with the observed formation of a shunt product in this biosynthetic pathway, **18**, which is anticipated to arise through loss of formaldehyde and concomitant rearomatization to produce trihydroxybenzaldehyde **18** (Figure 1D, Path 3).[21] Based on the radical reaction pathways that have been proposed for other ring modifying enzymes, we envisioned an alternative mechanism to arrive at stipitaldehyde in which radical **14** directly undergoes ring expansion, followed by radical termination via a single electron oxidation involving the iron(III)-hydroxyl species (Figure 1D, Path 2). Under this model, the product generated by the enzyme is determined by the radical termination process which occurs in the active site. If rebound hydroxylation predominates, then trihydroxybenzaldehyde (**18**) will be the major product formed. If radical rearrangement is preferred under the reaction conditions, then stipitaldehyde (**11**) formation will dominate. To decipher the ring expansion mechanism used by TropC, we aimed to investigate the active site architecture of the enzyme, as well as the reactivity of proposed ring expansion intermediate **13**.

Results and discussion

To determine the nature of the TropC-catalyzed ring expansion, we began by performing a computational analysis of the proposed pathways (Figure 1D, Path 1-3). Through these calculations, we aimed to compare the relative barriers of proposed ring expansion pathways to assess the feasibility of a one- or two-electron ring expansion mechanism. Each mechanistic pathway was evaluated using a small molecule NHI mimetic complex (see Supplementary Figure S32). We manually performed tautomerization of reaction pathway products to model stipitaldehyde (**11**) and the trihydroxybenzaldehyde shunt product **18** as protonated, neutral structures, reflecting the enzymatic reaction conditions for TropC-catalyzed ring expansion (pH 7.0). Water molecules were used as proton shuttles to mimic the protonation and deprotonation events that would be facilitated by residues in the enzyme active site.

We began our computational investigations using the radical intermediate **14** (Figure 2), which is the divergence point for each of the pathways along the potential energy surface (PES). We first explored the radical rearrangement (Path 2), which occurs with a barrier of 12.7 kcal/mol (**16**). A subsequent H-atom abstraction by an iron(III)-hydroxyl species to produce the tautomer of stipitaldehyde (**11**) was calculated to be barrierless. This calculation was supported by literature precedent which demonstrated that tropolones could be synthesized from *ortho*-dearomatized radicals (Figure 1B).[22, 26] We then explored the rebound hydroxylation and semi-pinacol rearrangement (Path 1). As expected, rebound hydroxylation to produce diol **13** was found to be a barrierless process in our active site model.[12, 30-31] In an enzyme active site, we anticipate

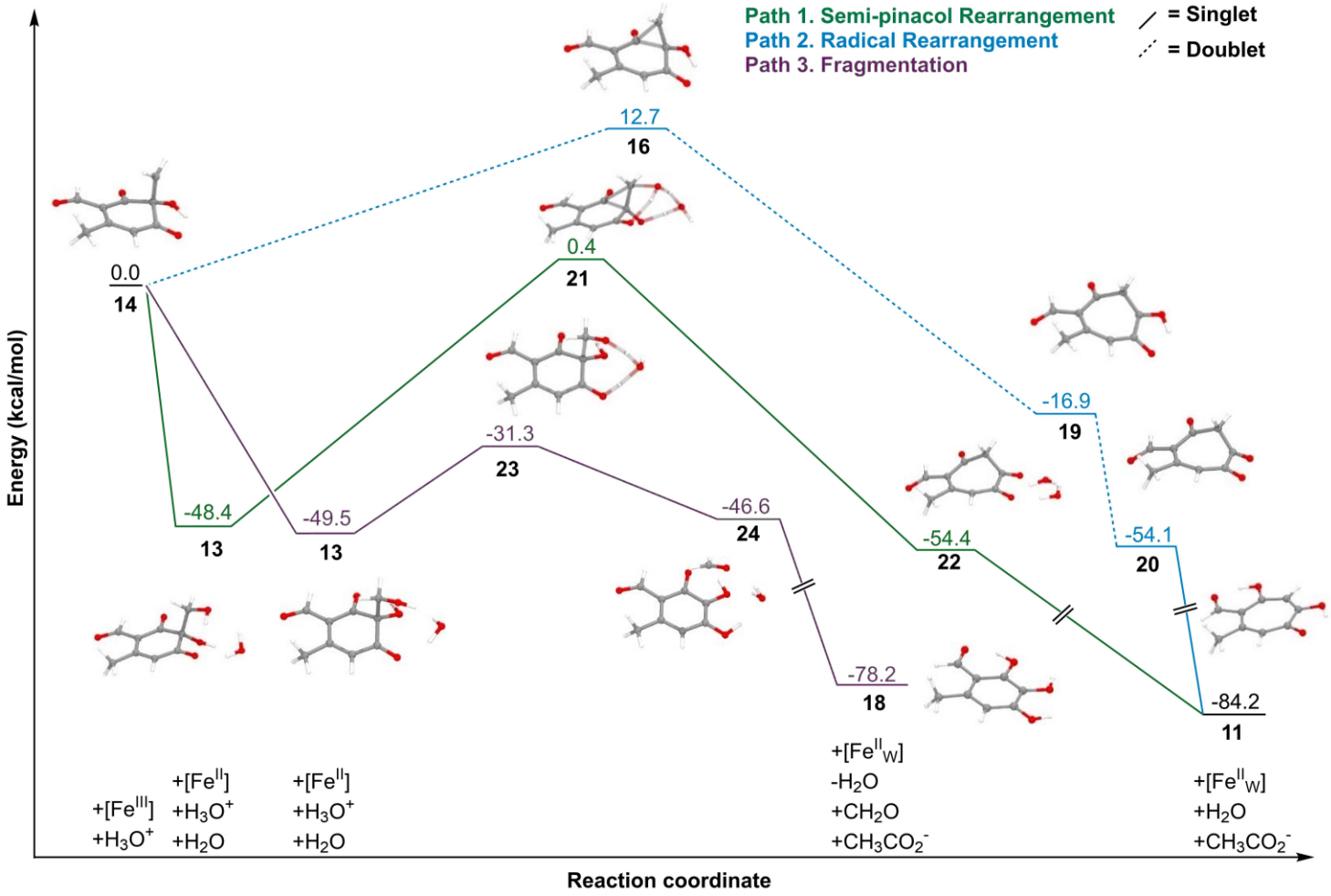

Figure 2. QM calculations for TropC-catalyzed reaction pathways to generate stipitaldehyde (**11**) and trihydroxybenzaldehyde **18**.

that substrate movement and alignment would be restricted by local residues, resulting in thermodynamic barriers to this process.[12, 30-31] The barrier for the proposed semi-pinacol rearrangement was observed to be excessively high at 48.8 kcal/mol (**21**), indicating that this transformation is not likely to occur. These barriers are in agreement with computational analysis by Siegbahn and coworkers examining ring expansion mechanisms of *ortho*-dearomatized phenols, indicating that a semi-pinacol type ring expansion is unlikely to occur in these systems.[32] In comparison, fragmentation to afford an aromatic product from diol **13** (Path 3) to produce formaldehyde and trihydroxybenzaldehyde **18** was found to be a low barrier process at 18.2 kcal/mol (**23**). These calculations suggest that diol **13** favorably undergoes fragmentation and rearomatization (Path 3), rather than the proposed semi-pinacol ring expansion (Path 1). The calculated low barrier for Path 3 is supported by experimental observation of trihydroxybenzaldehyde formation during the TropC-catalyzed reaction. Taken together, the QM simulations support our alternative mechanistic proposal in which the radical rearrangement is a kinetically and thermodynamically accessible route towards tropolone formation (Path 2).

Next, we sought experimental evidence to discriminate between the two reaction pathways under consideration for TropC-catalyzed ring expansion. We aimed to further interrogate the proposed ring expansion mechanisms by performing a detailed mutational analysis of TropC in order to determine if specific active site residues are responsible for catalyzing the ring expansion. To gain structural information to guide this work, we obtained TropC crystals using the sitting drop vapor diffusion method (see supplemental information for details). Following data collection, we found that TropC crystallized in the $P3_121$ space group with two molecules of TropC in the asymmetric unit (PDB ID: 6XJJ). The crystal structure of unliganded TropC was solved at a resolution of 2.7 Å with the molecular replacement method using the structure of thymine-7-hydroxylase (T7H) of *Neurospora crassa* as a search model (Figure 3).[33] Our analysis of the structural data indicated that TropC adopts a similar architecture as other α-KG-dependent NHI dioxygenases [34]. The three-dimensional structure of TropC consists of double-stranded β-helix (DSBH or jelly-roll) fold at the core of the protein [34]. The DSBH core of TropC is comprised of ten anti-parallel β-strands, which form two β-sheets, called major and minor β-sheets. Major β-sheets of TropC include β1-5, β8 and β10, and the minor β-sheet consists of β6, β7 and β9 (Supplementary Figure S29). The exterior of the major β-sheets of the DSBH fold is surrounded by α-helices (α1-3, α5 and α7) to form a compact globular structure.

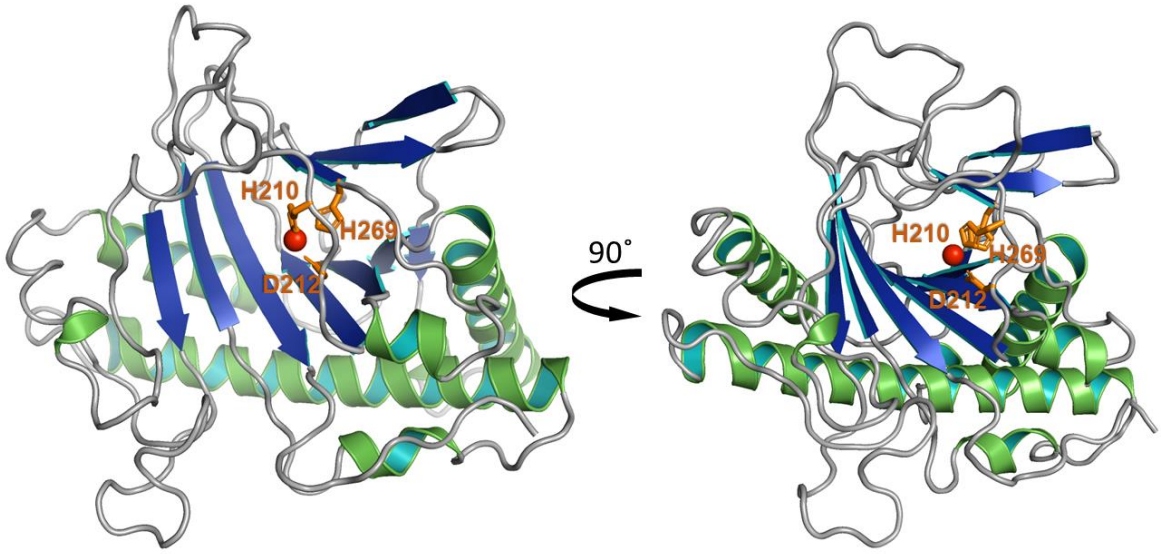

Figure 3. Overall architecture of TropC determined using X-ray crystallography (PDB ID: 6XJJ). (Left) Structure of TropC from *T. stipitatus* in ribbon representation. At the core of TropC, the Fe (III) shown with red sphere and side chain of residues, H210, D212 and H269, are shown in stick representation. (Right) Rotated view of crystal structure of TropC and active site located at the center of the protein.

Structures similar to TropC in the Protein Data Bank (PDB) were explored by using the DALI server (Supplementary Table S2),[35] revealing the highly similar structures of isopenicillin N synthase from *Pseudomonas aeruginosa* PAO1 (*Pal*PNS, PDB ID: 6JYV, Z-score: 32.2)[36] and thymine-7-hydroxylase (T7H, PDB ID: 5C3Q, Z-score: 31.8) of *Neurospora crassa*.[36] An overall structural comparison of TropC with *Pa*IPNS and T7H suggested a putative substrate binding site for TropC (Supplementary Figure S30). Overlaying TropC with T7H revealed several shared residues which define the substrate binding site in the T7H structure (Supplementary Figure S31).[33] Specifically, residues F284 and F213 align well with two conserved aromatic residues in T7H, F292 and Y217, respectively.[33] F292 and Y217 have been demonstrated as critical for substrate binding and alignment in T7H, with F292 providing π-π stacking interactions that align thymine in the enzyme active site for productive catalysis.[33] The conservation of these aromatic residues in homologs of T7H and their alignment with F284 and F213 in TropC suggests that these residues may play an analogous role in substrate alignment.[33] In addition, bound metal ion was observed in the structure of TropC, which was refined to be Fe(III). As has been observed with the active site of other α-KG-dependent NHI dioxygenases, our structure demonstrates that the conserved HxD/E…H metal binding residues are involved in interaction with Fe(II) [33-34, 36]. Specifically, our data showed the coordination of residues H210, D212 and H269 (located at the loop between β4-5 and β9) to the active site Fe(III) atom (Figure 3).

Crystallography experiments yielded vital information on structural features of TropC and enabled further investigation of mechanistic considerations by computational and mutagenic analysis. Toward this goal, we anticipated that an enzyme-substrate complex would provide critical information for determining the active site residues that are involved in ring expansion catalysis. To construct a computational substrate-bound model, we modeled the missing electron density from the C-terminus and used an overlaid structure of T7H to establish the coordinates of critical enzyme cofactors, such as α-KG, ferrous iron and substrate (see Supplemental Information for model construction and simulation details). To prepare the model for substrate binding studies, we performed a molecular mechanics (MM) minimization over 5000 steps. The system was then prepared for a combined quantum mechanics and molecular dynamics (QM/MD) simulation. The system was subjected to three phases of MD simulations in which the system was heated, equilibrated, and sampled for a total of 12 ns to generate an enzyme-substrate-cosubstrate complex with the appropriate geometry and alignment for C–H atom abstraction (see Supplemental Information for details).

Our analysis of the substrate-bound TropC model revealed that substrate **10** was flanked by numerous active site residues that could potentially be involved in substrate binding or catalysis (Figure 4C). Residues from the TropC substrate pocket were identified and selected for alanine screening to determine if specific amino acids are critical for the ring expansion process. We anticipated that a TropC variant, without the required residue for a polar, semi-pinacol-type ring expansion, would be unable to generate stipitaldehyde, resulting in a change to the ratio of observed enzyme products toward formation of the shunt product, **18** (Figure 4A). We carried out mutagenesis of twelve active site residues, generating the corresponding alanine variants (Figure 4B and Supplementary Figure S2) as well as variants with isosteric and isoelectronic residues at the same position. These residues were chosen using the substrate-bound TropC model as a guide and were selected for their proximity to the substrate as well as their ability to participate in the proposed reaction pathways. Many of the resulting variants were soluble, but catalytically inactive, suggesting that the structural changes in

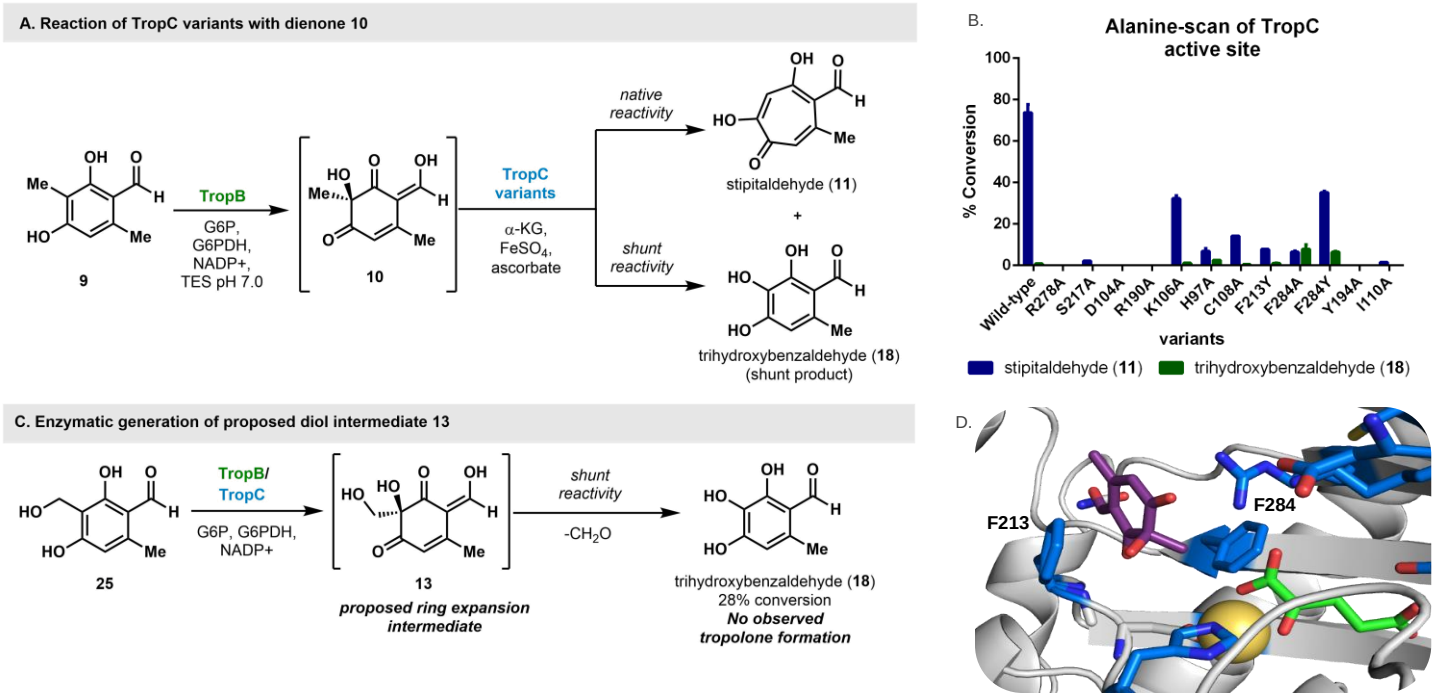

Figure 4. A. Oxidative dearomatization and ring expansion cascade to generate stipitaldehyde (**11**) and trihydroxybenzaldehyde (**18**). B. Product profiles observed in alanine-scanning of TropC active site residues. C. Enzymatic synthesis of proposed ring expansion intermediate, diol **10**. D. Close-up view of substrate-bound model of TropC with select targeted alanine-scanning residues highlighted in blue, α-KG highlighted in green and the substrate shown in purple.

some variants prevented productive catalysis. Catalytically active variants exhibited reduced enzymatic conversion to products, but the product profiles were largely unaltered, and stipitaldehyde (**11**) remained the major product under the reaction conditions, suggesting that most of the substrate-flanking residues were not involved in catalysis. However, the F284A variant uniquely demonstrated a shift in the product profile to produce nearly equimolar amounts of stipitaldehyde (**11**) and trihydroxybenzaldehyde (**18**). Analysis of the substrate-bound TropC model suggests that this residue could be important for positioning of the substrate in the active site. This proposed role is analogous to the function of residue F292 in T7H, which has been shown to be critical for binding and alignment of substrate for productive catalysis. The binding mode of substrate **10** in the TropC MD simulation demonstrates that F284 and F213 flank the substrate in the active site, potentially guiding the proper alignment for C–H atom abstraction. This proposal is likewise analogous to the reported role of F292 and Y217 in T7H, suggesting a similar function in aligning the TropC substrate to achieve catalysis.[33] To further investigate this hypothesis, we generated the isosteric variant TropC F284Y which reconstituted the ring expansion activity of the enzyme, providing further evidence that F284 is a critical residue for determining the product mixtures generated by TropC. We aimed to further analyze this reaction by generating a TropC F213A variant but were unable to produce soluble protein with this construct. Despite this challenge, the data generated through alanine scanning of the TropC active site suggested that substrate alignment plays a role in determining the product profile of the enzyme. Perturbations of this alignment often result in a change to the products generated by the enzyme, providing clues about the mechanism of the transformation.[7, 9] In particular, substrate alignment relative to the iron(III)-hydroxyl species is key in discriminating whether rebound hydroxylation occurs over other NHI-catalyzed reactivity, such as halogenation.[37] In the context of our TropC model, these observations support the proposed mechanistic pathway for radical ring expansion (Path 1) in which the fate of the radical (rearrangement versus rebound hydroxylation) determines which product is generated by the enzyme. In addition, mutagenic changes to polar residues did not produce a corresponding shift in the product profile to the production of trihydroxybenzaldehyde **18**, suggesting that local acid or base catalysis does not drive a ring expansion mechanism (Figure 1D, Path 1).

We aimed to further interrogate the proposed semi-pinacol rearrangement (Figure 1D, Path 1) by evaluating the reactivity of the proposed diol intermediate **13**. To generate the target diol in the absence of TropC, a biocatalytic approach was employed using CitB and TropB.[21, 27, 38-40] We aimed to directly synthesize diol **13** through oxidative dearomatization of benzylic alcohol **25** using TropB. Notably, trihydroxybenzaldehyde **18** was detected in these reactions, but diol intermediate **13** was not observed, suggesting that the fragmentation reaction described in Path 3 (Figure 1D) occurs spontaneously under the reaction conditions. To further probe whether diol **13** is a ring expansion intermediate in TropC catalysis, we again performed a TropB-catalyzed oxidative dearomatization of benzylic alcohol **25** and included TropC in this reaction. We envisioned that diol **13**, when generated *in situ*, could enter the active site of TropC and undergo a ring expansion reaction

as proposed in reaction Path 2 (Figure 1D). In this reaction, exclusive formation of trihydroxybenzaldehyde (**18**) was observed with no stipitaldehyde (**11**) detected, suggesting that fragmentation and rearomatization of diol **13** is the predominant mode of reactivity observed for this putative intermediate (Figure 4D). In support of this finding, Riess and coworkers noted this same fragmentation and rearomatization reactivity in their attempts to perform ring expansion reactions on *ortho*-dearomatized phenols to produce tropolones (Supplementary Figure S29).[41] These observations also agree with the computational modelling which suggests that fragmentation and rearomatization is a low-barrier process (18.2 kcal/mol). Taken together, these data indicate that diol intermediate **13** is unlikely to be the correct ring expansion intermediate in the TropC-catalyzed reaction, further suggesting that a radical mechanism (Path 2) leads to tropolone formation in this NHI system.

Conclusions

These experimental observations and QM calculations suggest that TropC-catalyzed ring expansion occurs through a radical-based process (Path 2), rather than the previously proposed rebound hydroxylation/semi-pinacol sequence (Path 1). This mechanistic proposal is supported by structural characterization, modelling and mutagenic analysis of the TropC active site, demonstrating that modification of a residue involved in substrate positioning altered the products generated by the enzyme. These data suggest that substrate positioning in TropC determines which radical termination step predominates: rebound hydroxylation or radical rearrangement followed by single electron transfer. Furthermore, we have demonstrated that rebound hydroxylation generates an intermediate (**13**) which does not undergo ring expansion, but rather a fragmentation and rearomatization process to produce trihydroxybenzaldehyde **18**. The observed reactivity of intermediate **13** illustrates the thermodynamic favorability for rearomatization over ring expansion in *ortho*-dearomatized phenols, as has been documented in previous studies.[32, 41] This revised proposal of radical-based ring expansion is also supported by literature precedent, demonstrating that tropolones can be synthesized from *ortho*-dearomatized radicals. These findings provide strong evidence of a radical-based mechanism for fungal tropolone biosynthesis, representing a major shift in the current understanding of the role of NHI enzymes in this process. In addition, our observations provide new insight into the mechanistic processes harnessed by NHI enzymes for the selective synthesis of complex molecules. We anticipate that computational studies that consider active site geometries could provide additional insight into these transformations and the observed behavior of TropC variants. Furthermore, we envision that the molecular details of NHI-catalyzed ring expansion can be leveraged to address current challenges in the synthesis of tropolone natural product scaffolds.

Acknowledgements

This work was supported by funds from the University of Michigan Life Sciences Institute and Department of Chemistry. T.J.D. thanks the National Science Foundation for a Graduate Research Fellowship. K.C.S acknowledges a Rackham Merit Fellowship from the University of Michigan Rackham Graduate School. P.M.Z. acknowledges partial support from NIH R35GM128830.

References

1. Walsh, C. T.; Moore, B. S., Enzymatic Cascade Reactions in Biosynthesis. *Angew. Chem. Intl. Ed.* **2019,** *58* (21), 6846-6879.
2. Klas, K.; Tsukamoto, S.; Sherman, D. H.; Williams, R. M., Natural Diels–Alderases: Elusive and Irresistable. *J. Org. Chem.* **2015,** *80* (23), 11672-11685.
3. Christianson, D. W., Structural and Chemical Biology of Terpenoid Cyclases. *Chem. Rev.* **2017,** *117* (17), 11570-11648.
4. Herr, C. Q.; Hausinger, R. P., Amazing Diversity in Biochemical Roles of Fe(II)/2-Oxoglutarate Oxygenases. *Trends. Biochem. Sci.* **2018,** *43* (7), 517-532.
5. Dowd, P.; Zhang, W., Free radical-mediated ring expansion and related annulations. *Chem. Rev.* **1993,** *93* (6), 2091-2115.
6. Donald, J. R.; Unsworth, W. P., Ring-Expansion Reactions in the Synthesis of Macrocycles and Medium-Sized Rings. *Chem. Eur. J.* **2017,** *23* (37), 8780-8799.
7. Bai, J.; Yan, L.; Liu, Y., Catalytic mechanism of the PrhA (V150L/A232S) double mutant involved in the fungal meroterpenoid biosynthetic pathway: a QM/MM study. *Phys. Chem. Chem. Phys.* **2019,** *21* (46), 25658-25668.
8. Matsuda, Y.; Iwabuchi, T.; Fujimoto, T.; Awakawa, T.; Nakashima, Y.; Mori, T.; Zhang, H.; Hayashi, F.; Abe, I., Discovery of Key Dioxygenases that Diverged the Paraherquonin and Acetoxydehydroaustin Pathways in Penicillium brasilianum. *J. Am. Chem. Soc.* **2016,** *138* (38), 12671-7.
9. Nakashima, Y.; Mori, T.; Nakamura, H.; Awakawa, T.; Hoshino, S.; Senda, M.; Senda, T.; Abe, I., Structure function and engineering of multifunctional non-heme iron dependent oxygenases in fungal meroterpenoid biosynthesis. *Nat. Commun.* **2018,** *9* (1), 104.

10. Nakamura, H.; Matsuda, Y.; Abe, I., Unique chemistry of non-heme iron enzymes in fungal biosynthetic pathways. *Nat. Prod. Rep.* **2018,** *35* (7), 633-645.
11. Kovaleva, E. G.; Lipscomb, J. D., Versatility of biological non-heme Fe(II) centers in oxygen activation reactions. *Nat. Chem. Biol.* **2008,** *4* (3), 186-93.
12. Timmins, A.; Visser, S. P. d., A Comparative Review on the Catalytic Mechanism of Nonheme Iron Hydroxylases and Halogenases. *Catalysts* **2018,** *8* (8).
13. Martinez, S.; Hausinger, R. P., Catalytic Mechanisms of Fe(II)- and 2-Oxoglutarate-dependent Oxygenases. *J. Biol. Chem.* **2015,** *290* (34), 20702-11.
14. Yan, L.; Liu, Y., Insights into the Mechanism and Enantioselectivity in the Biosynthesis of Ergot Alkaloid Cycloclavine Catalyzed by Aj_EasH from Aspergillus japonicus. *Inorg. Chem.* **2019,** *58* (20), 13771-13781.
15. Jakubczyk, D.; Caputi, L.; Stevenson, C. E. M.; Lawson, D. M.; O'Connor, S. E., Structural characterization of EasH (Aspergillus japonicus) – an oxidase involved in cycloclavine biosynthesis. *Chem. Commun.* **2016,** *52* (99), 14306-14309.
16. Tarhonskaya, H.; Szöllössi, A.; Leung, I. K. H.; Bush, J. T.; Henry, L.; Chowdhury, R.; Iqbal, A.; Claridge, T. D. W.; Schofield, C. J.; Flashman, E., Studies on Deacetoxycephalosporin C Synthase Support a Consensus Mechanism for 2-Oxoglutarate Dependent Oxygenases. *Biochemistry* **2014,** *53* (15), 2483-2493.
17. Valegard, K.; Terwisscha van Scheltinga, A. C.; Dubus, A.; Ranghino, G.; Oster, L. M.; Hajdu, J.; Andersson, I., The structural basis of cephalosporin formation in a mononuclear ferrous enzyme. *Nat. Struct. Mol. Biol.* **2004,** *11* (1), 95-101.
18. Jakubczyk, D.; Caputi, L.; Hatsch, A.; Nielsen, C. A.; Diefenbacher, M.; Klein, J.; Molt, A.; Schroder, H.; Cheng, J. Z.; Naesby, M.; O'Connor, S. E., Discovery and reconstitution of the cycloclavine biosynthetic pathway--enzymatic formation of a cyclopropyl group. *Angew. Chem. Int. Ed. Engl.* **2015,** *54* (17), 5117-21.
19. Cox, R., Oxidative rearrangements during fungal biosynthesis. *Nat. Prod. Rep.* **2014,** *31* (10), 1405-24.
20. Cox, R. J.; Al-Fahad, A., Chemical mechanisms involved during the biosynthesis of tropolones. *Curr. Opin. Chem. Biol.* **2013,** *17* (4), 532-6.
21. Davison, J.; al Fahad, A.; Cai, M.; Song, Z.; Yehia, S. Y.; Lazarus, C. M.; Bailey, A. M.; Simpson, T. J.; Cox, R. J., Genetic, molecular, and biochemical basis of fungal tropolone biosynthesis. *Proc. Natl. Acad. Sci. U. S. A.* **2012,** *109* (20), 7642-7.
22. Liu, N.; Song, W.; Schienebeck, C. M.; Zhang, M.; Tang, W., Synthesis of Naturally Occurring Tropones and Tropolones. *Tetrahedron* **2014,** *70* (49), 9281-9305.
23. Reisman, S. E.; Nani, R. R.; Levin, S., Buchner and Beyond: Arene Cyclopropanation as Applied to Natural Product Total Synthesis. *Synlett* **2011,** *2011* (17), 2437-2442.
24. Stevens, H. C.; Reich, D. A.; Brandt, D. R.; Fountain, K. R.; Gaughan, E. J., A New Tropolone Synthesis via Dichloroketene. *Journal of the American Chemical Society* **1965,** *87* (22), 5257-5259.
25. Barbier, M.; Barton, D. H. R.; Devys, M.; Topgi, R. S., A simple synthesis of tropones and related compounds. *Tetrahedron* **1987,** *43* (21), 5031-5038.
26. Barbier, M.; Barton, D. H. R.; Devys, M.; Topgi, R. S., A simple synthesis of the tropone nucleus. *J. Chem. Soc. Chem. Commun.* **1984,** (12), 743-744.
27. Abood, A.; Al-Fahad, A.; Scott, A.; Hosny, A. E.-D. M. S.; Hashem, A. M.; Fattah, A. M. A.; Race, P. R.; Simpson, T. J.; Cox, R. J., Kinetic characterisation of the FAD dependent monooxygenase TropB and investigation of its biotransformation potential. *RSC Adv.* **2015,** *5* (62), 49987-49995.
28. Schor, R.; Schotte, C.; Wibberg, D.; Kalinowski, J.; Cox, R. J., Three previously unrecognised classes of biosynthetic enzymes revealed during the production of xenovulene A. *Nat. Commun.* **2018,** *9* (1), 1963.
29. Zhai, Y.; Li, Y.; Zhang, J.; Zhang, Y.; Ren, F.; Zhang, X.; Liu, G.; Liu, X.; Che, Y., Identification of the gene cluster for bistropolone-humulene meroterpenoid biosynthesis in Phoma sp. *Fungal Genet. Biol.* **2019,** *129*, 7-15.
30. Cho, K.-B.; Hirao, H.; Shaik, S.; Nam, W., To rebound or dissociate? This is the mechanistic question in C–H hydroxylation by heme and nonheme metal–oxo complexes. *Chem. Soc. Rev.* **2016,** *45* (5), 1197-1210.
31. Timmins, A.; Fowler, N. J.; Warwicker, J.; Straganz, G. D.; de Visser, S. P., Does Substrate Positioning Affect the Selectivity and Reactivity in the Hectochlorin Biosynthesis Halogenase? *Front. Chem.* **2018,** *6* (513).
32. Borowski, T.; Wójcik, A.; Miłaczewska, A.; Georgiev, V.; Blomberg, M. R. A.; Siegbahn, P. E. M., The alkenyl migration mechanism catalyzed by extradiol dioxygenases: a hybrid DFT study. *J. Biol. Inorg. Chem.* **2012,** *17* (6), 881-890.
33. Li, W.; Zhang, T.; Ding, J., Molecular basis for the substrate specificity and catalytic mechanism of thymine-7-hydroxylase in fungi. *Nucleic Acids Res.* **2015,** *43* (20), 10026-10038.
34. Aik, W.; McDonough, M. A.; Thalhammer, A.; Chowdhury, R.; Schofield, C. J., Role of the jelly-roll fold in substrate binding by 2-oxoglutarate oxygenases. *Curr. Opin. Struct. Biol.* **2012,** *22* (6), 691-700.
35. Holm, L.; Rosenstrom, P., Dali server: conservation mapping in 3D. *Nucleic Acids Res* **2010,** *38* (Web Server issue), W545-9.
36. Zhang, H.; Che, S.; Wang, R.; Liu, R.; Zhang, Q.; Bartlam, M., Structural characterization of an isopenicillin N synthase family oxygenase from Pseudomonas aeruginosa PAO1. *Biochem. Biophys. Res. Commun.* **2019,** *514* (4), 1031-1036.

37. Mitchell, A. J.; Dunham, N. P.; Bergman, J. A.; Wang, B.; Zhu, Q.; Chang, W. C.; Liu, X.; Boal, A. K., Structure-Guided Reprogramming of a Hydroxylase To Halogenate Its Small Molecule Substrate. *Biochemistry* **2017,** *56* (3), 441-444.
38. Doyon, T. J.; Perkins, J. C.; Baker Dockrey, S. A.; Romero, E. O.; Skinner, K. C.; Zimmerman, P. M.; Narayan, A. R. H., Chemoenzymatic o-Quinone Methide Formation. *J. Am. Chem. Soc.* **2019,** *141* (51), 20269-20277.
39. Baker Dockrey, S. A.; Lukowski, A. L.; Becker, M. R.; Narayan, A. R. H., Biocatalytic site- and enantioselective oxidative dearomatization of phenols. *Nat. Chem.* **2018,** *10* (2), 119-125.
40. He, Y.; Cox, R. J., The molecular steps of citrinin biosynthesis in fungi. *Chem. Sci.* **2016,** *7* (3), 2119-2127.
41. Cacioli, P.; Reiss, J., Reactions of 1-Oxaspiro[2.5]octa-5,7-dien-4-ones with nucleophiles. *Aust. J. Chem.* **1984,** *37* (12), 2525-2535.

Radical tropolone biosynthesis

Supplemental Information

Tyler J. Doyon,[1,2] Kevin C. Skinner,[1,3] Di Yang,[1,3] Leena Mallik,[2,3] Troy Wymore,[3] Markos Koutmos,[2,3] Paul M. Zimmerman,[3] Alison R. H. Narayan[1,2,3]*

[1]Life Sciences Institute, University of Michigan, Ann Arbor, Michigan 48109, USA. [2]Program in Chemical Biology, University of Michigan, Ann Arbor, Michigan 48109, USA. [3]Department of Chemistry, University of Michigan, Ann Arbor, Michigan 48109, USA.

[*]Corresponding author, email: arhardin@umich.edu

Table of Contents

Part I. Substrate synthesis information

General Information: All reagents were used as received unless otherwise noted. Reactions were carried out under a nitrogen atmosphere using standard Schlenk techniques unless otherwise noted. Solvents were degassed and dried over aluminum columns on an MBraun solvent system (Innovative Technology, inc., Model PS-00-3). Reactions were monitored by thin layer chromatography using Millipore 60 F254 pre-coated silica TLC plates (0.25 mm) which were visualized using UV, *p*-anisaldehyde, CAM, DNP, or bromocresol green stains. Flash column chromatography was performed using Machery-Nagel 60 µm (230-400 mesh) silica gel. All compounds purified by column chromatography were sufficiently pure for use in further experiments unless otherwise indicated. ^{1}H and ^{13}C NMR spectra were obtained in $CDCl_3$ at rt (25 °C), unless otherwise noted, on Varian 400 MHz or Varian 600 MHz spectrometers. Chemical shifts of ^{1}H NMR spectra were recorded in parts per million (ppm) on the δ scale. High resolution electrospray mass spectra were obtained on an Agilent 1290 Series Infinity II HPLC with a 6230 Series Time-of-Flight mass spectrometer or an Agilent 1290 Series Infinity HPLC with a 6545 Series Quadrupole-Time-of-Flight mass spectrometer. UPLC-PDA spectrometric traces were obtained on a Waters Aquity H-class instrument. IR spectra were recorded on a Perkin-Elmer Spectrum BX FT-IR spectrometer.

Compound **9** was prepared and characterized by our lab previously.[1] Details of this characterization can be found in the Supplementary Information of the provided reference.

Part II. Plasmid and protein information

Plasmid: The genes encoding *tropC* (DAA64706.1), *citB* (KT781075.1), and *tropB* (DAA64700.1) were codon-optimized for overexpression in *E. coli* and synthesized by GeneArt (ThermoFisher). The synthesized sequence was cloned by GeneArt into a pET-151 vector containing the T7 expression system, ampicillin resistance, and N-terminal 6xHis-tag encoded upstream from the insert gene. No further modifications to this plasmid construct were necessary.

Codon-Optimized *tropC* Sequence (including 6 x His Tag)

```
ATGCATCATCACCATCACCATGGTAAGCCTATCCCTAACCCTCTCCTCGGTCTCGATTCTACGGAAAACCTGTATTT
TCAGGGAATTGATCCCTTCACCATGAGCATTGGTGATGAAGTTATTCCGACCGTTGATATTAGCGCATGGCTGAGCA
GCACCGCAAGTCCGGAAAGCAAAAACAAAGTTGTTGAAGAAGTTCGTAGCGCCTGCAACAAATATGGCTTTTTTAAC
CTGGTTGGTCATGGTATTCCGGCAGAAGCACGCGAAAAAATCTTTGGTTGTACCAAAAAATTCTTCGACCTGCCGCT
GGAAGAGAAAATGAAAATTTCAGTTGATAAAAGCCTGGGCAAAAGCTTTCGTGGTTATGAACCGAGCCTGATTCAGA
CCCATCAGGATGGTCTGCTGCCGGATACAAAAGAATGTTTTATTACCGGTGCAGAAATCCCTGCAGATCATCCAGAT
GCAGGTAAATTTAGCACCGGTCCGAATCTGTGGCCTGAAGGTCTGAGCGATAAAGAATTTCGTCAGCCGGTTATGGA
ATATCGTGCACTGATGCTGGATCTGGTTAGCACCATTGTTCGTATTCTGGGTCAGGGTATTCATAAAGCATTTGGTC
ATCCGAGTGATGTGCTGAACGATATTCTGATTAATCCGAGCATTCCGATGCGCCTGCTGCATTATGCTCCGCAAGAA
AATCCGGATCCGCGTCAGTTTGGTGTTGGTGATCACACCGATTTTGGTTGTGTTAGCATTCTGCTGCAACAGAAAGG
CACCAAAGGTCTGGAAGTTTGGTATCCGCCTAAAGAAACCTGGATTCCGGTTCCGGTTATTGAAGATGCATTTGTGA
TTAATATGGGCGATACCATGCATCGTTGGACCGGTGGTTATTATCGTAGCGCACGTCATCGTGTGTATATTACAGGT
GAACGTCGTTATAGCGTTGCCTTTTTTCTGAATGGTAACCTGAACCTGAAAATCAAACCGCTGGATGGTAGCGGTGG
TGAAGCAAGCGTTGGTGAACATATTAACAGCCGTCTGGCACATACCCTGGGTGATAATGCAAAATATCTGCGC
```

TropC Protein Sequence (including 6 x His Tag)

```
MHHHHHHGKPIPNPLLGLDSTENLYFQGIDPFTMSIGDEVIPTVDISAWLSSTASPESKNKVVEEVRSACNKYGFFN
LVGHGIPAEAREKIFGCTKKFFDLPLEEKMKISVDKSLGKSFRGYEPSLIQTHQDGLLPDTKECFITGAEIPADHPD
AGKFSTGPNLWPEGLSDKEFRQPVMEYRALMLDLVSTIVRILGQGIHKAFGHPSDVLNDILINPSIPMRLLHYAPQE
NPDPRQFGVGDHTDFGCVSILLQQKGTKGLEVWYPPKETWIPVPVIEDAFVINMGDTMHRWTGGYYRSARHRVYITG
ERRYSVAFFLNGNLNLKIKPLDGSGGEASVGEHINSRLAHTLGDNAKYLR
```

Codon-Optimized *citB* Sequence (including 6 x His Tag)

```
ATGCATCATCACCATCACCATGGTAAGCCTATCCCTAACCCTCTCCTCGGTCTCGATTCTACGGAAAACCTGTATTT
TCAGGGAATTGATCCCTTCACCATGCCGATTAGCACCAAAAGCAGCTTTTATCTGCCTGCAGTTGATATTAGCCCGT
```

ATCTGCAGGATCCGAATAGTGATGCAGCACGTAAAGTTATTGATGATGTTCGTGCAGCATGTACCAGCACCGGTTTT
TTTCAGCTGTTAGGTCATGGTATTAGTCCGGCACTGCAGCAGAGCGTTTTTGCAGCAGCAGCAAAATTCTTTGCACT
GCCGAGTGATGTTAAAAGCCGTTGTCGTAATGTTGGTTTTCGTGGTTATGATCCGATGGCAAGCCAGAGCTATGAAC
TGGGTGTTCTGCCGGATCTGAAAGAAGGTTTTATTGCCGGTAAAGATATTCCGCTGGATGATCCGCGTGTTGCAAGC
CAGCGCTTTTTTATGGGTCAGAATGCATGGCCTCCGAGCGAACTGCTGCCGGAAGCAAATTTTCGTCGTCCGATTGA
AGAATATTATCAGGCAATGCTGAAACTGTGTTGGGTTGTTCTGGATCTGGTTGCAGCAACCCTGCCGTATGGTCCGC
ATGTTTTTGATGAATTCAAAGAAAATGATCCGGCATGTCCGCTGCGTCTGCTGCATTATCCGCCTGCACCGGCACCG
GATGTTGCAAAAGGTCGTCAGCTGGGTAGCAGCGCACATACCGATTTTGGTGCAATTACCCTGCTGTTACAGGATGA
TCATAGCGGTCTGGAAGTTCAGGATTGTGAAACCGGTGAATGGATTGGTGTTCCGCCTAATAAAGATGCCTATGTTG
TTAATCTGGGCGATATGATGAGCCGTATTACCCGTGGTCACTATAAAAGCAGCATTCATCGTGTGATTAACCAGAAT
CTGACCGATCGTTATAGCGTGGTGTTTTTTTTCGATGGCAATCTGGATTATCGTCTGCGTCCTCTGGATCGTGTTGG
TCAGAATTGGGATGAAGAAGATACCCTGACCGTTGAAGAACATATGCTGGAACGTACCACCACCACCTATAATCTGA
AAGTGAAATAA

CitB Protein Sequence (including 6 x His Tag)

MHHHHHHGKPIPNPLLGLDSTENLYFQGIDPFTMPISTKSSFYLPAVDISPYLQDPNSDAARKVIDDVRAACTSTGF
FQLLGHGISPALQQSVFAAAAKFFALPSDVKSRCRNVGFRGYDPMASQSYELGVLPDLKEGFIAGKDIPLDDPRVAS
QRFFMGQNAWPPSELLPEANFRRPIEEYYQAMLKLCWVVLDLVAATLPYGPHVFDEFKENDPACPLRLLHYPPAPAP
DVAKGRQLGSSAHTDFGAITLLLQDDHSGLEVQDCETGEWIGVPPNKDAYVVNLGDMMSRITRGHYKSSIHRVINQN
LTDRYSVVFFFDGNLDYRLRPLDRVGQNWDEEDTLTVEEHMLERTTTTYNLKVK

Codon-Optimized *tropB* Sequence

ATGCCTGGTAGCCTGATTGATACCCGTCAGCAGCCGCTGAGCGTTGGTATTGTTGGTGGTGGTATTATTG
GCGTTATTCTGGCAGCAGGTCTGGTTCGTCGTGGTATTGATGTTAAAGTTTTTGAACAGGCACGTGGCTT
TCGTGAAATTGGTGCAGGTATGGCATTTACCGCAAATGCAGTTCGTTGTATGGAAATGCTGGATCCGGCA
ATTGTTTGGGCACTGCGTAGCAGCGGTGCAGTTCCGATTAGCATTGGTGATCATCAGGCCGAAGCACGTG
ATTATCTGCGTTGGGTTGATGGTTATCATGAAAGCAGCAAACGTCTGTATCAGCTGGATGCAGGTATTCG
TGGTTTTGAAGCATGTCGTCGTGATCAGTTTCTGGAAGCACTGGTTAAAGTTCTGCCGGAAGGTATTGTG
GAATGTCAGAAACGTCTGCAGAAAATCCACGAAAAAAACGAAACCGAAAAAGTGACCCTGGAATTTGCAG
ATGGCACCTTTGCACATGTTGATTGTGTTATTGGTGCCGATGGTATTCGTAGCCGTGTTCGTCAGCACCT
GTTTGGTGAAGATAGCCCGTATAGCCATCCGCATTATAGCCATAAATTTGCATTTCGTGGTCTGATCACC
ATGGAAAATGCAATTAGCGCACTGGGCGAAGATAAAGCACGTACCCTGAATATGCATGTTGGTCCGAATG
CACATCTGATTCATTATCCGGTTGCAAATGAAACCATGGTGAATATTGCAGCCTTTGTTAGCGATCCGGA
AGAATGGCCTGATAAACTGAGCCTGGTTGGTCCGGCAACCCGTGAAGAAGCAATGGGTTATTTTGCAAAT
TGGAATCCGGGTCTGCGTGCAGTTCTGGGTTTTATGCCGGAAAATATTGATCGTTGGGCAATGTTCGATA
CCTATGATTATCCGGCACCGTTTTTTAGCCGTGGTAAAATTTGTCTGGTTGGTGATGCAGCACATGCAGC
AGTTCCGCATCATGGTGCCGGTGCATGTATTGGTATTGAAGATGCACTGTGTGCAACCGTTCTGCTGGCA
GAAGTTTTTGTTAGCACCCGTGGCAAAAGCAGCATTGTTCGTAATCGTGCAATTGCCGCAGCATTTGGTA
GCTTTAATGCAGTGCGTCGTGTTCGTGCACAGTGGTTTGTTGATAGCAGCCGTCGTGTTTGTGATCTGTA
TCAACAGCCGGAATGGGCAGATCCGCAGAAACGTATTAAAGCCGAAAATTGCTTCGAAGAGATTAAAGAT
CGCAGCCATAAAATCTGGCACTTCGATTATAACTCCATGCTGCAAGAAGCCATCGAAAAATATCGTCATA
ATATGGGCAGCTAA

TropB Protein Sequence

MPGSLIDTRQQPLSVGIVGGGIIGVILAAGLVRRGIDVKVFEQARGFREIGAGMAFTANAVRCMEMLDPA
IVWALRSSGAVPISIGDHQAEARDYLRWVDGYHESSKRLYQLDAGIRGFEACRRDQFLEALVKVLPEGIV
ECQKRLQKIHEKNETEKVTLEFADGTFAHVDCVIGADGIRSRVRQHLFGEDSPYSHPHYSHKFAFRGLIT
MENAISALGEDKARTLNMHVGPNAHLIHYPVANETMVNIAAFVSDPEEWPDKLSLVGPATREEAMGYFAN
WNPGLRAVLGFMPENIDRWAMFDTYDYPAPFFSRGKICLVGDAAHAAVPHHGAGACIGIEDALCATVLLA
EVFVSTRGKSSIVRNRAIAAAFGSFNAVRRVRAQWFVDSSRRVCDLYQQPEWADPQKRIKAENCFEEIKD
RSHKIWHFDYNSMLQEAIEKYRHNMGS

Protein Overexpression and Purification: The plasmids containing *tropC, tropB,* and *citB* were transformed using standard heat-shock protocols for chemically competent *E. coli* into BL21(DE3) cells. Overexpression of these enzymes was achieved using 4% glycerol (v/v) Terrific Broth (TB) in 2.8 L flasks. 500 mL portions of autoclaved media were inoculated with 5 mL of overnight culture prepared from a single colony in Luria Broth (LB) and 100 µg/mL ampicillin (Gold Biotechnology). Cultures were grown at 37 °C and 200 rpm until the optical density (at 600 nm) reached 0.8. The cultures were then cooled to 20 °C for 1 h and protein expression was induced with 0.2 mM isopropyl-β-D-1-thiogalactopyranoside (IPTG, Gold Biotechnology). Expression was continued at 20 °C overnight (approx. 18 h) at 200 rpm. The typical yield for one 500 mL culture cell pellet (wet cell pellet) was ~25-30 g.

General Considerations: HisPur nickel-nitrilotriacetic acid resin (Ni-NTA resin) was purchased from Thermo Scientific. Fast protein liquid chromatography (FPLC) purification was conducted on an ÄTKA Pure FPLC system (GE Healthcare) equipped with a HiPrep 16/60 Sephacryl S-200 HR column purchased from GE Healthcare. Proteins were concentrated at 4,500 x g at 4 °C using Amicon centrifuge filters purchased from EMD Millipore.

General Purification Procedure (for biocatalytic reactions): 50-60 g of cell pellet was resuspended in 250 mL of lysis buffer containing 50 mM Tris HCl (pH 7.4), 300 mM NaCl, 10 mM imidazole and 10% glycerol. The mixture was homogenized using a handheld dounce homogenizer. Approximately 1 mg/mL lysozyme (Gold Biotechnology) was added prior to 1 h incubation on a rocker held at 4 °C. Cells were lysed by sonication of the total cell lysate in 100 mL batches on ice. Each cycle of sonication was 10 s sonication, followed by a 20 s rest period, for a total of 6 min at 60% power. The total cell lysate was centrifuged at 45,000 x g for 30 min and the supernatant was removed. The cell lysate was then batch-bound to 3 mL of Ni-NTA resin (Thermo) for 1 h at 4 °C with gentle rocking. The supernatant was filtered through a fritted 50 mL plastic column (Gold Biotechnologies) to isolate the Ni-NTA resin. The resin was washed with 100 mL of wash buffer containing 50 mM Tris HCl (pH 7.4), 300 mM NaCl, 25 mM imidazole and 10% glycerol. The protein was then eluted using 15 mL of an elution buffer containing 50 mM Tris HCl (pH 7.4), 300 mM NaCl, 250 mM imidazole and 10% glycerol. The eluted protein was concentrated to a volume of 2.5 mL using a 30 KDa molecular weight cutoff ultrafiltration device (Amicon). The concentrated protein was desalted using a PD-10 desalting column that was pre-equilibrated with a storage buffer containing 50 mM Tris HCl (pH 7.4), 300 mM NaCl, and 10% glycerol. The protein was eluted from the column with 3.5 mL of storage buffer, before flash freezing in liquid nitrogen and storage at -80 °C. Protein concentration was determined by the A280 absorbance method using a Nanodrop spectrophotometer. The concentration was corrected using the estimated extinction coefficient from the ProtParam tool on the Expasy server (ε = 1.128). **Average yield:** 60-70 mg/L of TropC. 40-50 mg/L of TropB. 60-70 mg/L of CitB.

Purification protocols for TropC crystallography: Initial purification steps are identical to those outlined above. Following purification by Ni-NTA column, the volume of the resulting protein solution was reduced by ultrafiltration (Amicon, 30 KDa weight cutoff) to a volume of 2 mL. The concentrated protein solution was loaded onto a 16/60 Sephacryl S200 HR column at 0.5 mL/min from a 2 mL sample loop using the ÄTKA Pure FPLC system with the size exclusion buffer containing 20 mM Tris HCl (pH 7.4), 1 mM tris(2-carboxyethyl)phosphine (TCEP), and eluted at 0.5 mL/min. Fractions containing TropC were diluted to 1 mg/mL and placed in a dialysis bag containing 0.1 mg/mL of TEV protease. The TEV protease digestion was allowed to incubate for 18 h at 4 °C in TEV protease dialysis buffer (50 mM TrisHCl, 50 mM NaCl, 0.5 mM EDTA, 1 mM DTT). After completion of the TEV digestion, the protein solution was incubated for 1 h with 1 mL of Ni-NTA resin at 4 °C. The reaction mixture was loaded onto a 50 mL fritted column and the flow through was collected and concentrated to 12 mg/mL. The resulting protein solution was briefly stored at 4 °C and used within 48 h for crystallization procedures (see Part VIII for details).

Supplementary Figure S1. SDS-PAGE gels of purified wild-type TropC and TropC variants (39.95 kDa with 6x His tag)

Wild-type TropC purified for X-ray crystallography

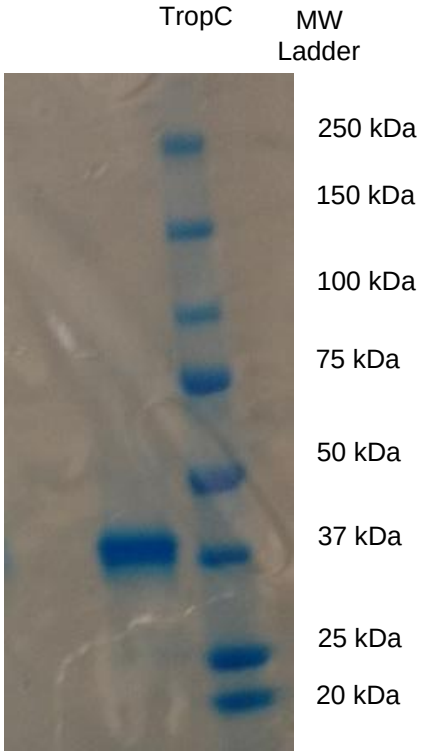

TropC variants purified for biocatalytic experiments

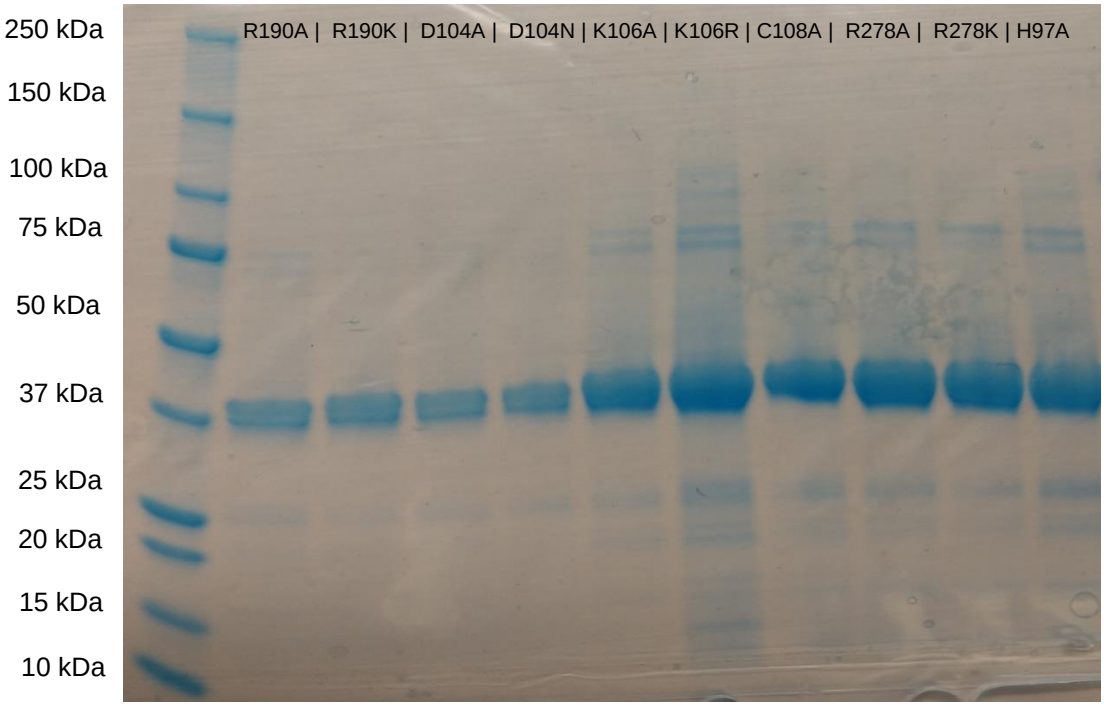

TropC variants purified for biocatalytic reactions

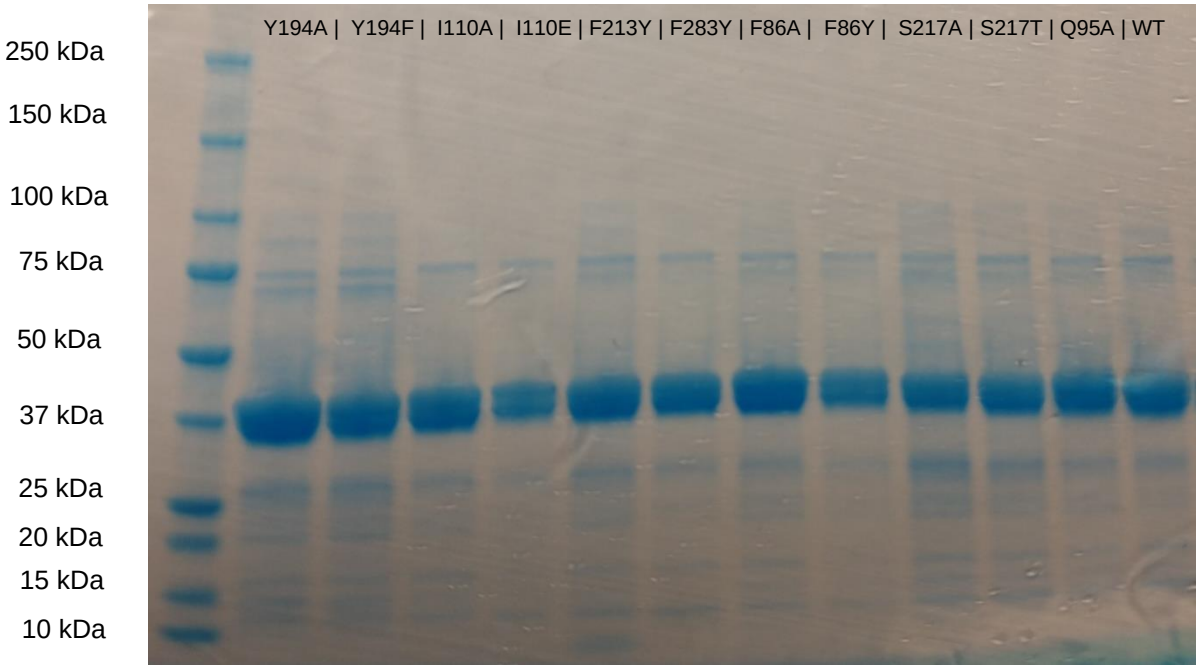

Part III. Site-directed mutagenesis of TropC

TropC variant	Vector	Primer sequence
TropC Y194A	pET-151	CGCCTGCTGCAT**GCG**GCTCCGCAAG
TropC Y194F	pET-151	CGCCTGCTGCAT**TTT**GCTCCGCAAGAAAAT
TropC R278A	pET-151	GTATATTACAGGTGAACGT**GCG**TATAGCGTTGCC
TropC R278K	pET-151	GTATATTACAGGTGAACGT**AAA**TATAGCGTTGCC
TropC F284A	pET-151	CGTCGTTATAGCGTTGCC**GCG**TTTCTGAATGGTAAC
TropC F284Y	pET-151	CGTCGTTATAGCGTTGCC**TAT**TTTCTGAATGGTAAC
TropC R190A	pET-151	GAGCATTCCGATG**GCG**CTGCTGCATTATG
TropC R190K	pET-151	CCGAGCATTCCGATG**AAA**CTGCTGCATTATG
TropC C108A	pET-151	CCGGATACAAAAGAA**GCG**TTTATTACCGGTGC
TropC H97A	pET-151	CTGATTCAGACC**GCG**CAGGATGGTCTG
TropC K106A	pET-151	CTGCTGCCGGATACA**GCG**GAATGTTTTATTAC
TropC K106R	pET-151	CTGCTGCCGGATACA**CGT**GAATGTTTTATTACC
TropC D104A	pET-151	GATGGTCTGCTGCCG**GCG**ACAAAAGAATG
TropC D104N	pET-151	GATGGTCTGCTGCCG**AAC**ACAAAAGAATG
TropC I110A	pET-151	CAAAAGAATGTTTT**GCG**ACCGGTGCAGAAATC
TropC F86A	pET-151	GCCTGGGCAAAAGC**GCG**CGTGGTTATGAAC
TropC F86Y	pET-151	GCCTGGGCAAAAGC**TAT**CGTGGTTATGAACCG
TropC F213Y	pET-151	GTTGGTGATCACACCGAT**TAT**GGTTGTGTTAGCATTC
TropC Q95A	pET-151	GAACCGAGCCTGATT**GCG**ACCCATCAGGATGG
TropC S217A	pET-151	CGATTTTGGTTGTGTT**GCG**ATTCTGCTGCAACAG
TropC S217T	pET-151	CGATTTTGGTTGTGTT**ACC**ATTCTGCTGCAACAG
TropC-5N (5 residue N-terminal truncation)	pET-151	GAATTGATCCCTTCACCGAAGTTATTCCGACC

Supplementary Table S1. Primers used in the generation of TropC variants.

Whole plasmid mutagenesis procedure: Variants of TropC were generated via polymerase chain reaction (PCR) using the primers listed above. Substitutions were generated by site-directed mutagenesis of the pET-151-*tropC* parent plasmid. 25 µL PCR reaction mixtures contained 5 x Phusion HF buffer (NEB), 1 ng/µL parent plasmid, 500 nM primer, 200 µM dNTPs, 1% DMSO, and 1 U/µL Phusion HF DNA polymerase (NEB). Mutant plasmid amplification was accomplished using the following procedure. 98 °C (30 s) then a repeating cycle (30 cycles) of the following temperatures: 98 °C (30 s), T_m – 5 °C (30 s), 72 °C (3 min), followed by a final extension at 72 °C for 10 min. Parent plasmid DNA was digested in a 10 µL reaction containing 8 µL PCR product mixture, 1 µL CutSmart buffer (NEB), and 20 U (1 µL) DpnI endonuclease (NEB). The reaction was incubated at 37 °C for 3 h and transformed into chemically competent DH5-α *E. coli* cells.

Part IV. Biocatalytic reaction conditions and products

Stock solutions: Stock solutions of each substrate (50 mM) were prepared by dissolving the substrate in DMSO (analytical grade). Stock solutions of α-ketoglutaric acid (125 mM), ferrous sulfate (10 mM) and sodium ascorbate (50 mM) were freshly prepared in MQ water before each use, stored on ice, and used within 3 h. Aliquots of glucose-6-phosphate (G6P, 500 mM), glucose-6-phosphate dehydrogenase (G6PDH, 100 U/mL), and nicotinamide adenine dinucleotide (NADP+, 100 mM) were prepared and stored at -20 °C before use. Aliquots of WT TropC and variants were stored at -80 °C.

***In vitro* analytical-scale TropB/TropC cascade reactions:** Cascade oxidative dearomatization/ring-expansion reactions were performed as follows. Each reaction contained 50 mM TES buffer pH 7.5 (2.5 µL, 1 M), 2.5 mM substrate (2.5 µL, 50 mM), 5 µM TropB, 10 µM TropC, 5 mM glucose-6-phosphate (G6P, 0.5 µL, 500 mM), 1 mM nicotinamide adenine dinucleotide phosphate disodium salt (NADP+, 0.5 µL, 100 mM), 1 U/mL glucose-6-phosphate dehydrogenase (G6PDH, 0.5 µL, 100 U/mL), 5 mM α-ketoglutaric acid (α-KG, 2 µL, 125 mM), 0.1 mM ferrous sulfate ($FeSO_4$, 0.5 µL, 10 mM), 8 mM sodium ascorbate (8 µL, 50 mM) and Milli-Q water to a final volume of 50 µL. Reactions were carried out at 30 °C for 3 h and quenched by the addition of 3 volumes of methanol containing 3.5 mM pentamethyl benzene as an internal standard. Precipitated biomolecules were pelleted by centrifugation (17,000 x g, 20 min). The supernatant was analyzed by UPLC-DAD and conversion obtained by comparison to calibration curves of each product.

***In vitro* analytical-scale TropB reactions:** Analytical-scale oxidative dearomatization reactions were performed as follows. Each reaction contained 50 mM TES buffer pH 7.5 (2.5 µL, 1 M), 2.5 mM substrate (2.5 µL, 50 mM), 5 µM TropB, 5 mM glucose-6-phosphate (G6P, 0.5 µL, 500 mM), 1 mM nicotinamide adenine dinucleotide phosphate disodium salt (NADP+, 0.5 µL, 100 mM), 1 U/mL glucose-6-phosphate dehydrogenase (G6PDH, 0.5 µL, 100 U/mL) and Milli-Q water to a final volume of 50 µL. Reactions were carried out at 30 °C for 3 h and quenched by the addition of 3 volumes of methanol containing 3.5 mM pentamethyl benzene as an internal standard. Precipitated biomolecules were pelleted by centrifugation (17,000 x g, 20 min). The supernatant was analyzed by UPLC-DAD and conversion obtained by comparison to calibration curve of the product.

Determination of percent yield: Percent yield of product was determined by analysis of each reaction after 3 h. PDA spectrometric analysis was performed on a Waters Aquity H-Class instrument, using a Phenomenex Kinetex (1.7 µm C18, 2.1 x 150 mm) column under the following conditions: mobile phase (Solvent A: deionized water + 0.1% formic acid; Solvent B: acetonitrile + 0.1% formic acid) 5% to 100% solvent B over 2 min, 100% solvent B for 1 min; flow rate: 0.5 mL/min. Based on the calibration curves of isolated products, the percent yield of stipitaldehyde (**11**) was calculated with $AUC_{product}$ (360 nm)/$AUC_{internal\ standard}$ (270 nm). The percent yield of trihydroxybenzaldehyde **18** was calculated with $AUC_{product}$ (360 nm)/$AUC_{internal\ standard}$ (270 nm). *In vitro* reactions were performed and analyzed in duplicate, with reported conversions as an average of those trials.

Procedure for *in vitro* milligram-scale TropB/TropC reactions: Preparative-scale cascade oxidative dearomatization/ring-expansion reactions were performed on 50 mg scale. Each reaction contained 50 mM TES buffer pH 7.5, 2.5 mM substrate, 5 µM TropB, 10 µM TropC, 5 mM G6P, 1 mM NADP+, 1 U/mL G6PDH, 5 mM α-KG, 0.1 mM $FeSO_4$, 8 mM sodium ascorbate. TropB-catalyzed oxidative dearomatization was carried out at 30 °C and allowed to proceed to completion (~1 h) before the addition of TropC, α-KG, ascorbate and $FeSO_4$. The reaction was then further incubated at 30 °C for an additional 2 h before workup. Reaction progress was monitored by UPLC-DAD analysis of 50 µL samples, quenched by the addition of 3 volumes of methanol containing 3.5 mM pentamethyl benzene as an internal standard. Precipitated biomolecules were pelleted by centrifugation (17,000 x g, 20 min). The supernatant was analyzed by UPLC-DAD and conversion obtained by comparison to calibration curves of each product. **Isolation procedure:** The reaction mixture was transferred to a separatory funnel and acidified to pH 2.0 with 0.1 M HCl. The organic materials were extracted from the aqueous layer with ethyl acetate (3 x 50 mL). The organic fractions were pooled and concentrated under reduced pressure to yield a crude mixture. This mixture was purified using preparative HPLC according to the procedure listed below.

Purification by preparative HPLC: For purification of milligram-scale reactions, the resulting crude mixture was taken up in a 50:50 mixture of milli-Q water:acetonitrile (4 mL). The product(s) were purified from this mixture by preparative HPLC using a Phenomenex Kinetex 5 µm C18, 150 x 21.2 mm column under the following conditions: mobile phase (Solvent A: deionized water + 0.1% formic acid; Solvent B: acetonitrile + 0.1% formic acid) 5% to 100% solvent B over 10 min, 100% solvent B for 4 min; flow rate: 11.5 mL/min. Product elution was monitored at wavelengths corresponding to maximal absorbances for each product: stipitaldehyde (**11**) at 360 nm, trihydroxybenzaldehyde (**18**) at 300 nm.

Procedure for *in vitro* milligram-scale CitB reaction: Preparative-scale enzymatic reactions were conducted on 200 mg scale under the following conditions: 2.5 mM substrate, 50 mM TES buffer pH 7.5, 5 mM α-ketoglutaric acid, 0.1 mM ferrous sulfate, 8 mM sodium ascorbate, 45 mg/mL CitB wet cell pellet. Reactions were performed in Erlenmeyer flasks of appropriate volume to achieve proper oxygenation (at least 3 times reaction volume) and shaken at 100 rpm at 30 °C. Reaction progress was monitored at hourly intervals by analysis of a 50 µL aliquot by UPLC-DAD as described previously.[2] Upon satisfactory conversion of the substrate, the product(s) were isolated in the following manner. **Isolation procedure:** The reaction mixture was transferred to a 50 mL falcon tube and 2 volumes of acetone were added. The mixture was centrifuged at 4,500 x g for 10 min to separate the biomolecule components from the aqueous reaction mixture. The supernatant was removed and acetone removed under reduced pressure. The supernatant was acidified to pH 2.0 with 0.1 M HCl. The organic materials were extracted from the aqueous layer with ethyl acetate (3 x 50 mL). The organic fractions were pooled and concentrated under reduced pressure to yield a crude mixture, which was purified by silica gel chromatography to yield the hydroxylated product.

Supplementary Figure S2. Products generated in the reaction of TropC variants with TropB-generated dienone **10**.

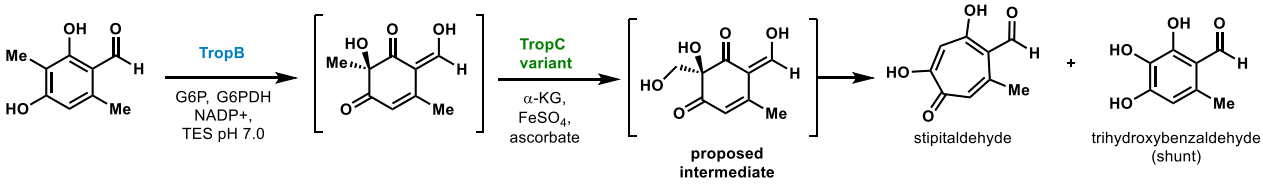

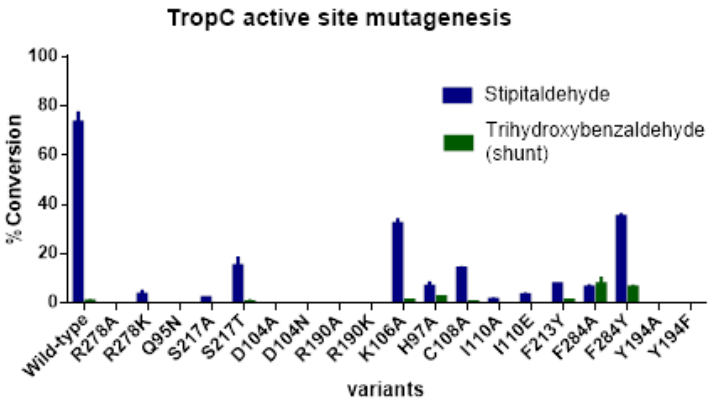

Biocatalytic reaction products

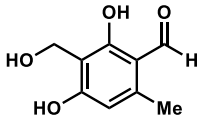

25

2,4-dihydroxy-3-(hydroxymethyl)-6-methylbenzaldehyde (25)
The title compound was synthesized and characterized previously by our group using a procedure for preparative-scale benzylic hydroxylation reactions with CitB.[2] Purification by flash chromatography afforded 460 mg (84% yield) of the title compound as a white solid. **^{1}H NMR** (400 MHz, MeOD) δ 10.07 (s, 1H), 6.26 (s, 1H), 4.68 (s, 2H), 2.50 (s, 3H); **HR-ESI-MS**: m/z calcd for $C_9H_{11}O_4^+$ $[M+H-H_2O]^+$: 165.0546, found: 165.0544.

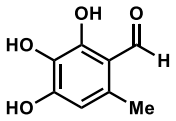

18

2,3,4-trihydroxy-6-methylbenzaldehyde (trihydroxybenzaldehyde 18)
The title compound was synthesized according to the procedure for preparative-scale TropB/TropC reactions. Full characterization for this compound has been reported previously.[3] Purification by preparative HPLC afforded 10.2 mg (20% yield) of the title compound as a yellow solid. **^{1}H NMR** (400 MHz, $CDCl_3$) δ 10.08 (s, 1H), 6.35 (s, 1H), 2.90 (s, 3H). **HR-ESI-MS**: m/z calcd for $C_8H_8O_4^+$ $[M+H]^+$: 169.0495, found: 169.0494.

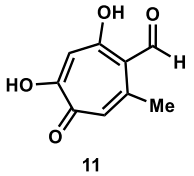

11

2,4-dihydroxy-7-methyl-5-oxocyclohepta-1,3,6-triene-1-carbaldehyde (stipitaldehyde, 11)
The title compound was synthesized according to the procedure for preparative-scale TropB/TropC reactions. Full characterization for this compound has been reported previously.[3] Purification by preparative HPLC afforded 8 mg (16% yield) of the title compound as an orange solid. **^{1}H NMR** (600 MHz, MeOD) δ 10.13 (s, 1H), 6.83 (s, 1H), 6.82 (s, 1H), 2.65 (s, 3H). **HR-ESI-MS**: m/z calcd for $C_9H_8O_4^+$ $[M+H]^+$: 181.0495, found 181.0497.

Part V. Product standard curves

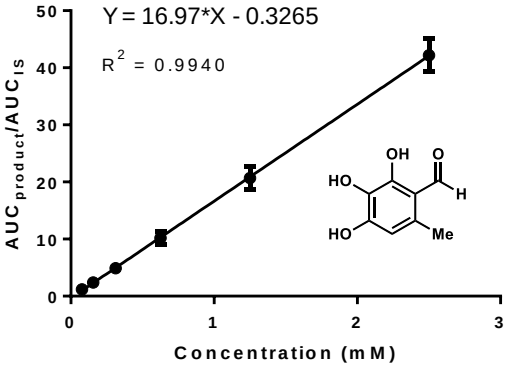

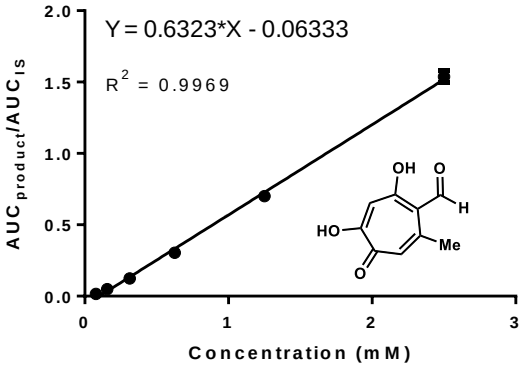

Part VI. UPLC traces of biocatalytic reactions

Supplementary Figure S3. Reaction of wild-type TropC with TropB-generated dienone **10**. PDA traces of enzymatic reaction analyzed at 360 nm.

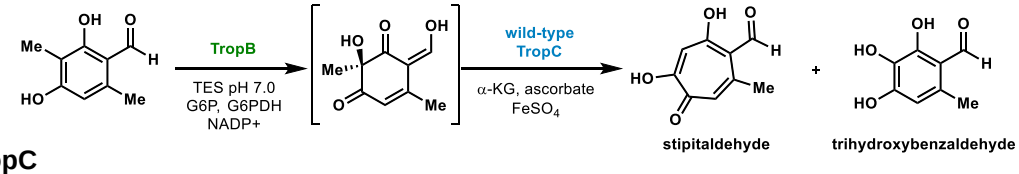

With TropC

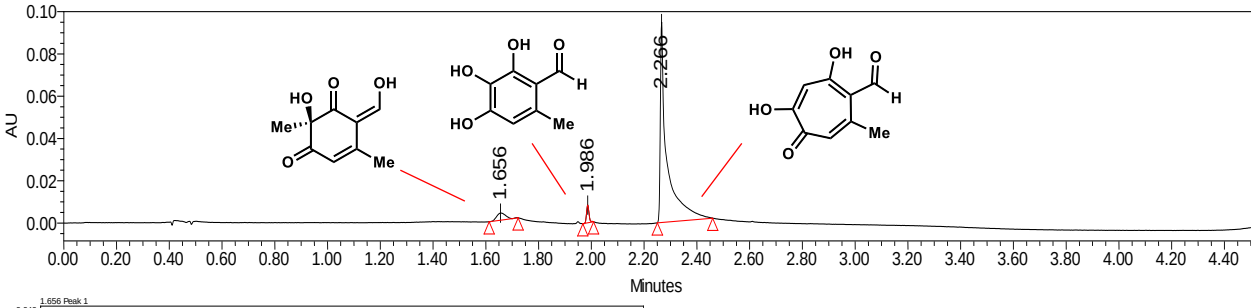

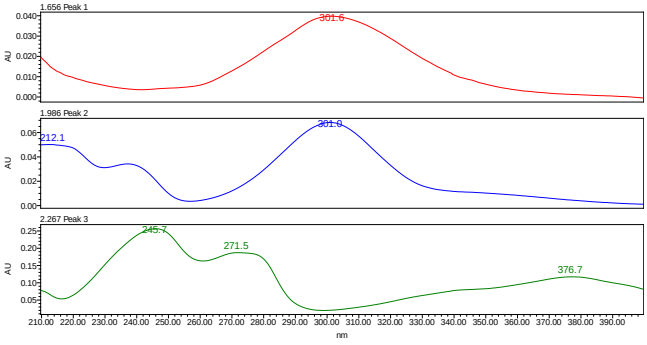

	Retention Time	Area	% Area	Height
1	1.656	8022	4.49	3380
2	1.986	5527	3.09	8463
3	2.266	165108	92.42	95011

TropB only

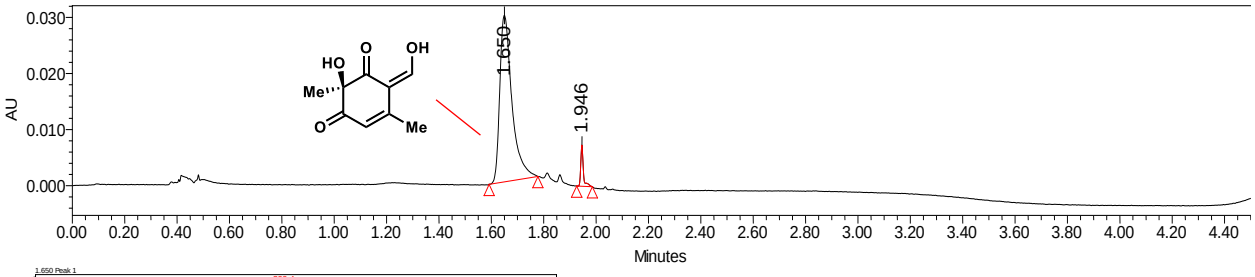

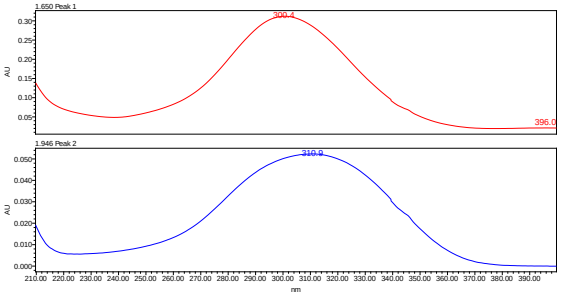

	Retention Time	Area	% Area	Height
1	1.650	96047	95.01	29701
2	1.946	5046	4.99	7337

Stipitaldehyde (11) product standard

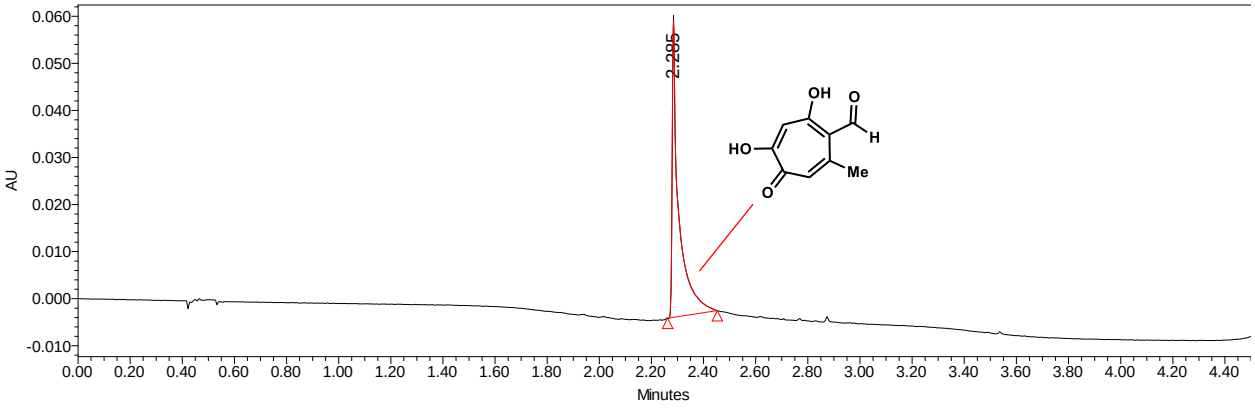

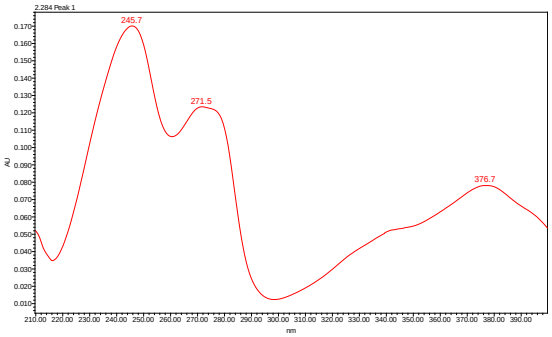

	Retention Time	Area	% Area	Height
1	2.285	110190	100.00	63128

Trihydroxybenzaldehyde (18) product standard

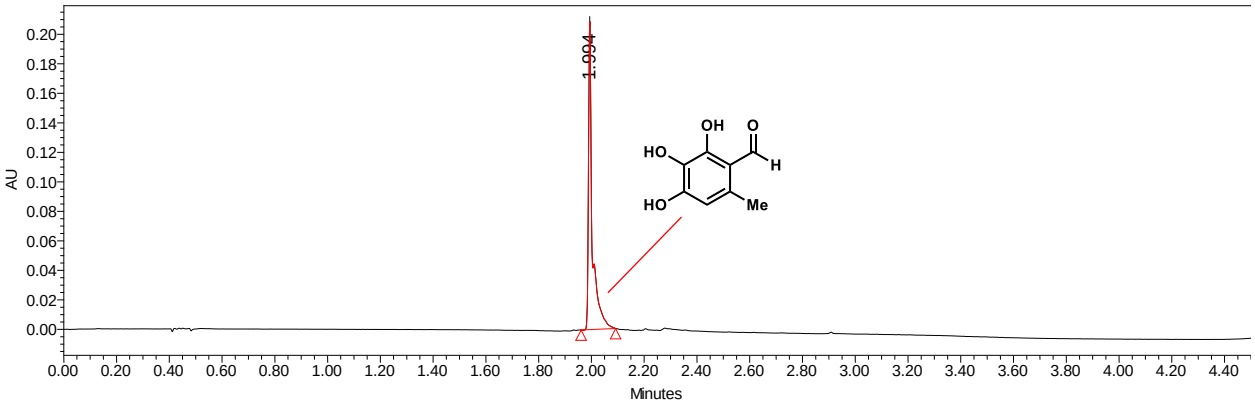

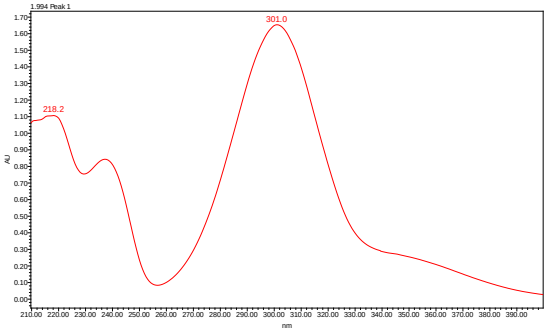

	Retention Time	Area	% Area	Height
1	1.994	209222	100.00	209461

Supplementary Figure S4. Reaction of TropC R190A with TropB-generated dienone **10**. PDA traces of enzymatic reaction analyzed at 360 nm.

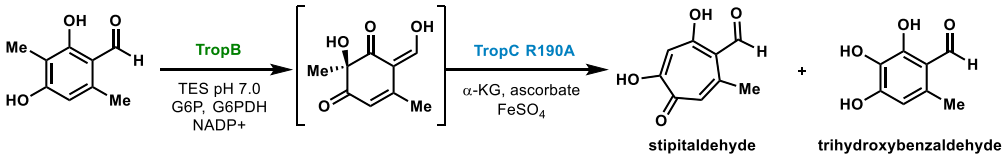

With TropC

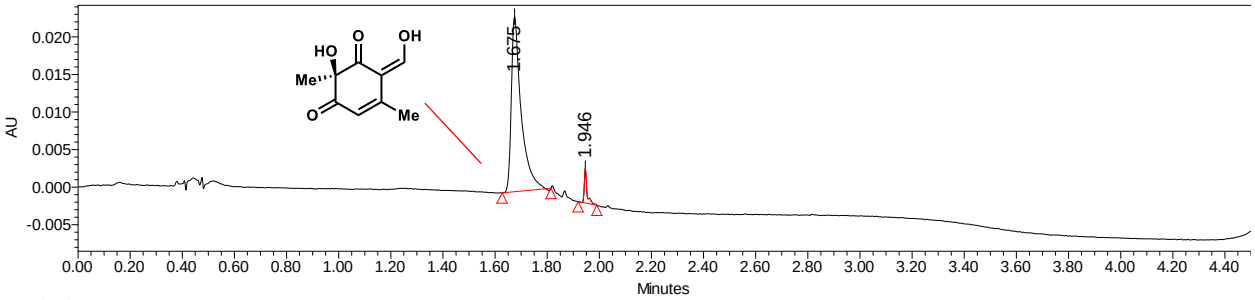

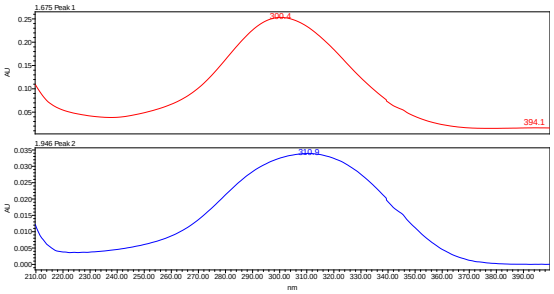

	Retention Time	Area	% Area	Height
1	1.675	61537	94.92	23309
2	1.946	3294	5.08	4602

TropB only

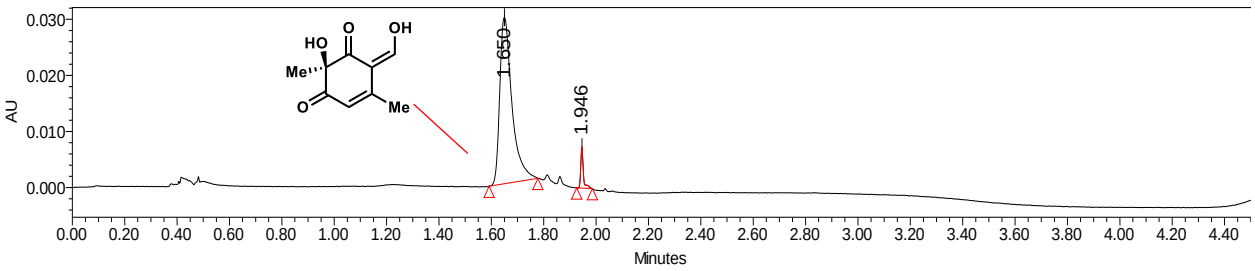

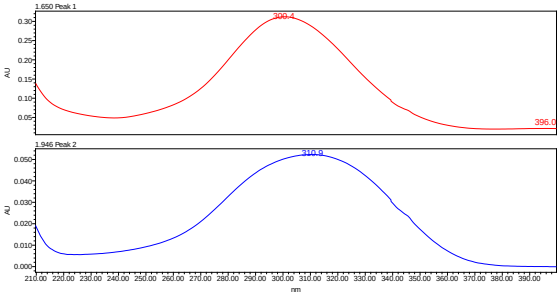

	Retention Time	Area	% Area	Height
1	1.650	96047	95.01	29701
2	1.946	5046	4.99	7337

Supplementary Figure S5. Reaction of TropC R190K with TropB-generated dienone **10**. PDA traces of enzymatic reaction analyzed at 360 nm.

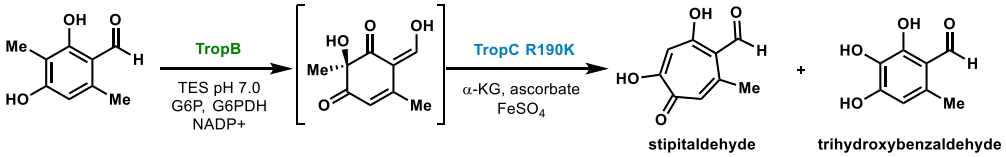

With TropC

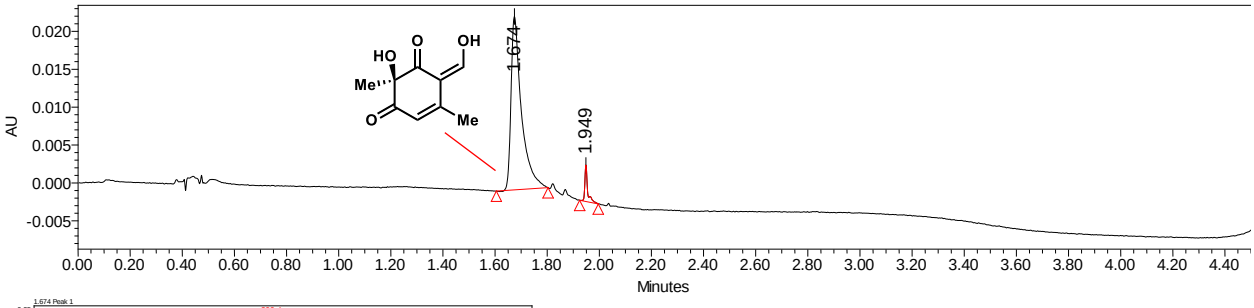

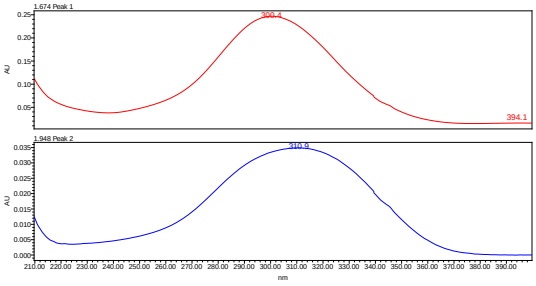

	Retention Time	Area	% Area	Height
1	1.674	63799	94.66	22880
2	1.949	3601	5.34	4825

TropB only

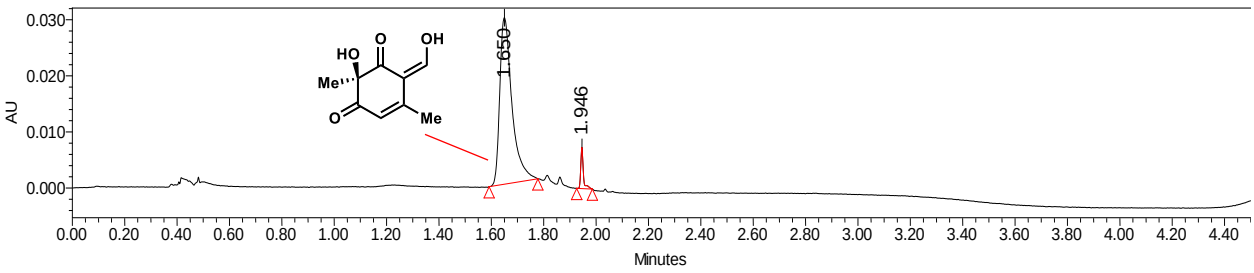

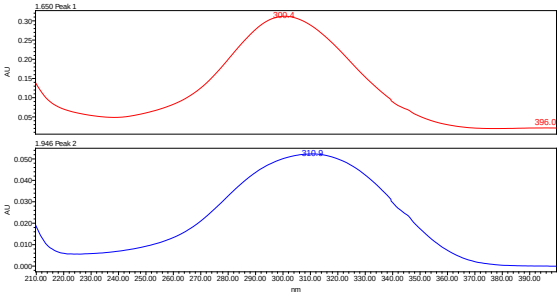

	Retention Time	Area	% Area	Height
1	1.650	96047	95.01	29701
2	1.946	5046	4.99	7337

Supplementary Figure S6. Reaction of TropC D104A with TropB-generated dienone **10**. PDA traces of enzymatic reaction analyzed at 360 nm.

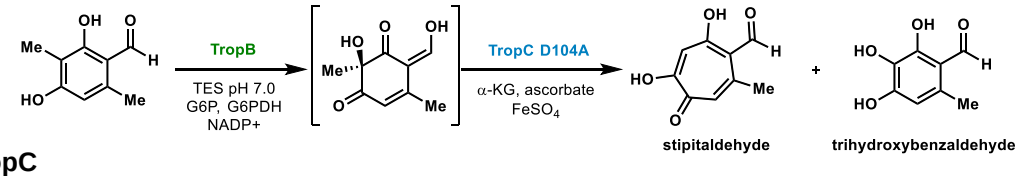

With TropC

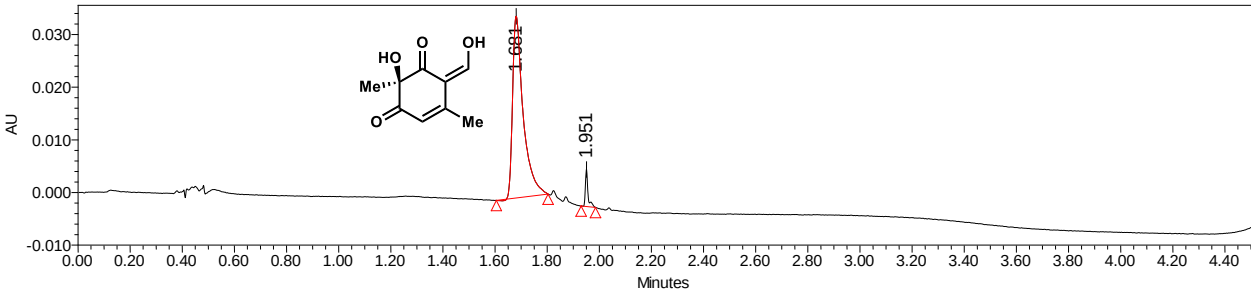

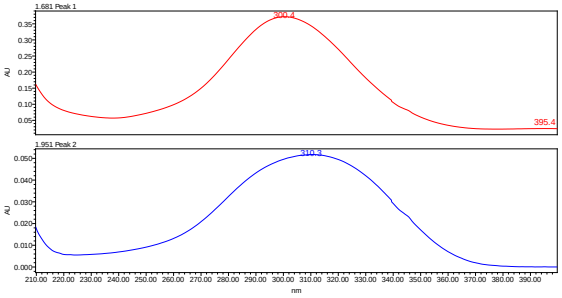

	Retention Time	Area	% Area	Height
1	1.681	98240	95.26	34505
2	1.951	4891	4.74	7063

TropB only

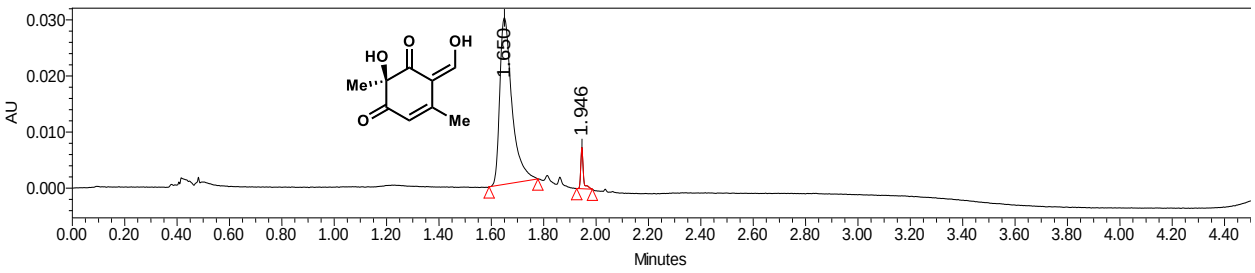

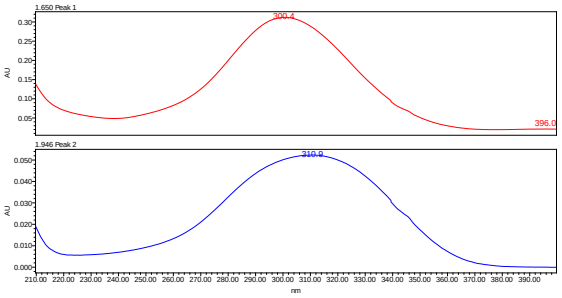

	Retention Time	Area	% Area	Height
1	1.650	96047	95.01	29701
2	1.946	5046	4.99	7337

Supplementary Figure S7. Reaction of TropC D104N with TropB-generated dienone **10**. PDA traces of enzymatic reaction analyzed at 360 nm.

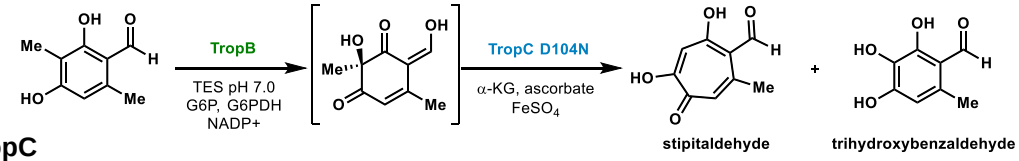

With TropC

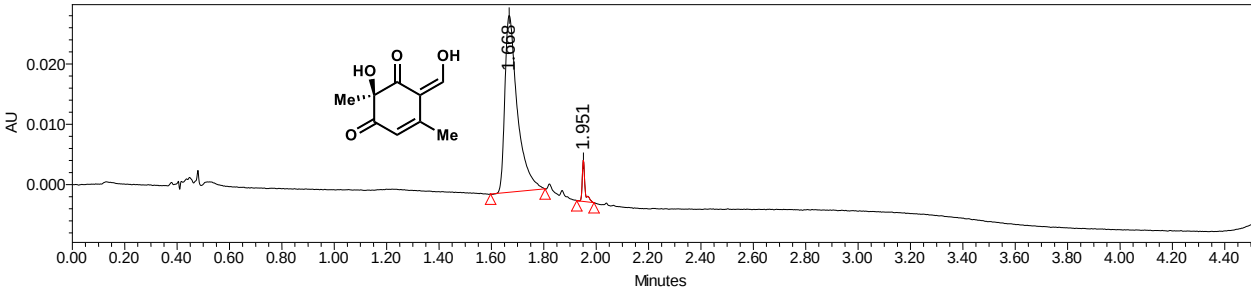

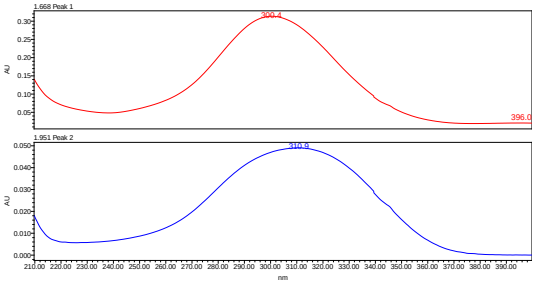

	Retention Time	Area	% Area	Height
1	1.668	97336	95.10	29302
2	1.951	5013	4.90	6842

TropB only

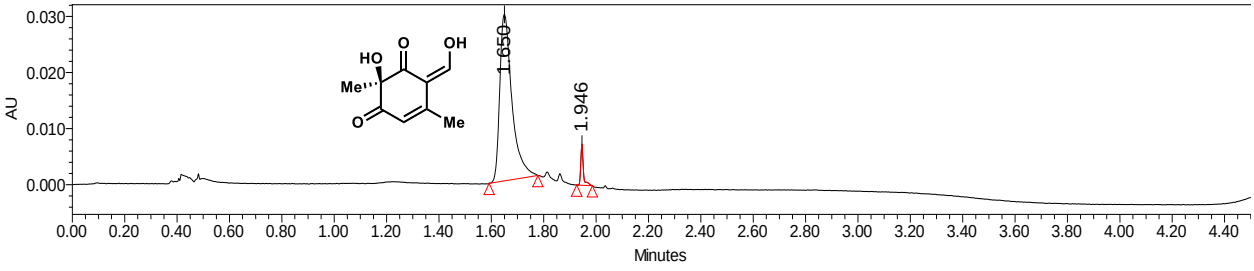

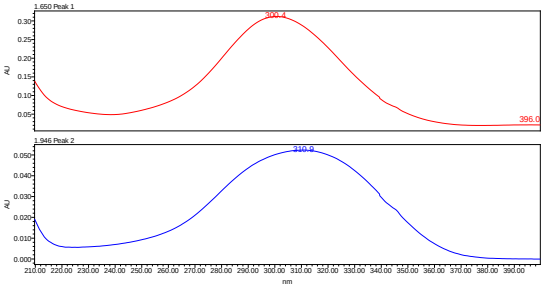

	Retention Time	Area	% Area	Height
1	1.650	96047	95.01	29701
2	1.946	5046	4.99	7337

Supplementary Figure S8. Reaction of TropC Y194A with TropB-generated dienone **10**. PDA traces of enzymatic reaction analyzed at 360 nm.

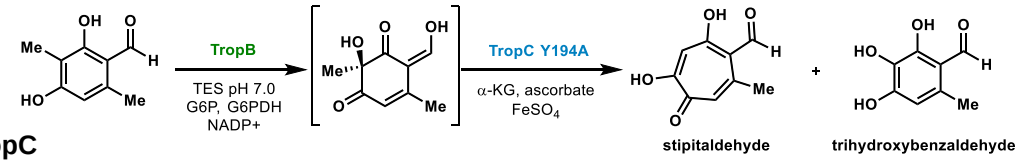

With TropC

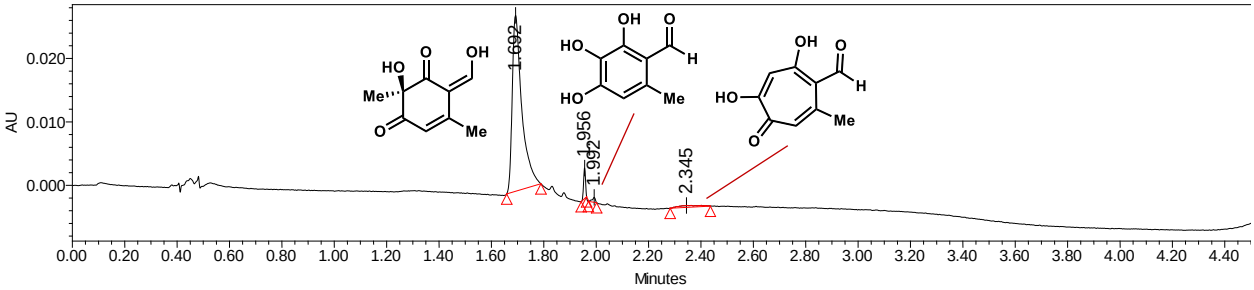

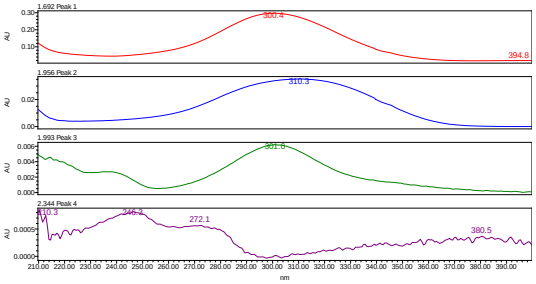

	Retention Time	Area	% Area	Height
1	1.692	70681	93.73	27731
2	1.956	2433	3.23	4819
3	1.992	638	0.85	777
4	2.345	1653	2.19	307

TropB only

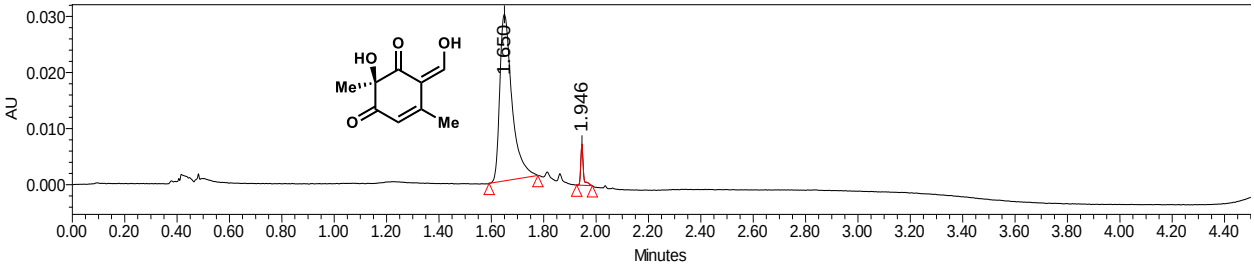

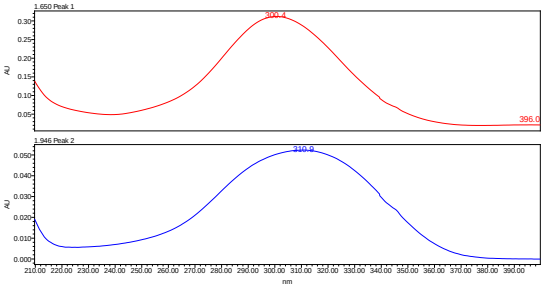

	Retention Time	Area	% Area	Height
1	1.650	96047	95.01	29701
2	1.946	5046	4.99	7337

Supplementary Figure S9. Reaction of TropC Y194F with TropB-generated dienone **10**. PDA traces of enzymatic reaction analyzed at 360 nm.

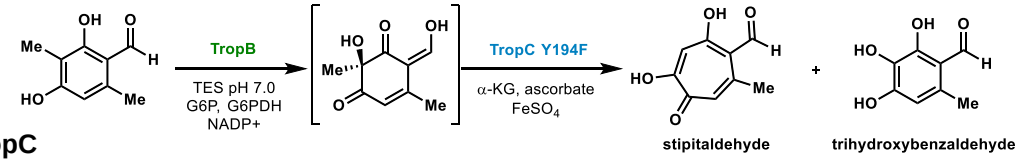

With TropC

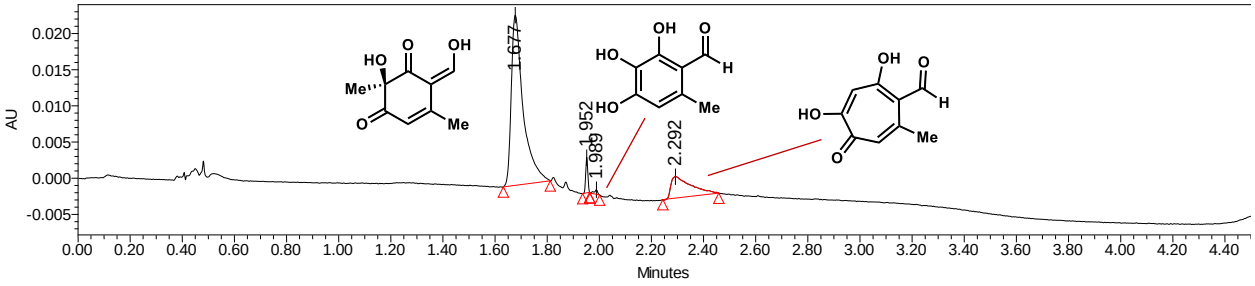

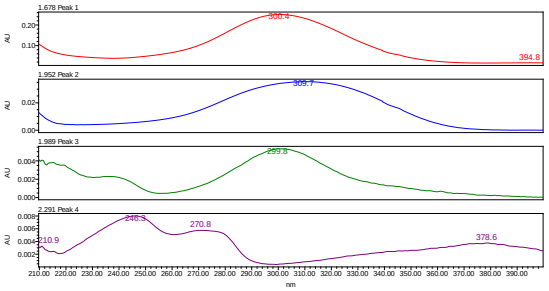

	Retention Time	Area	% Area	Height
1	1.677	74618	79.52	23525
2	1.952	2759	2.94	4890
3	1.989	583	0.62	640
4	2.292	15872	16.92	2962

TropB only

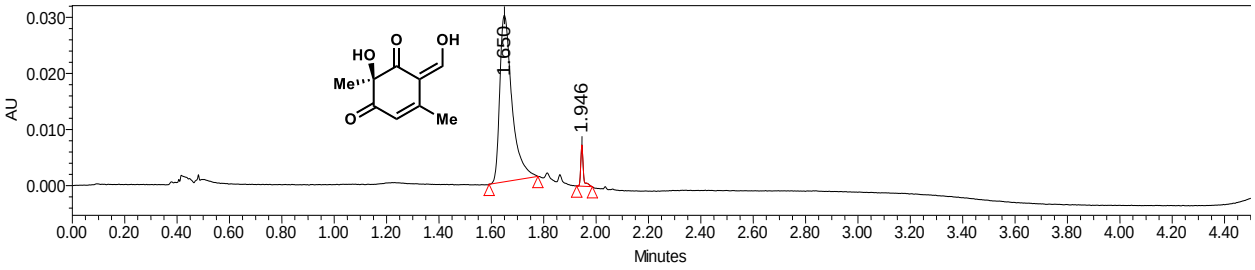

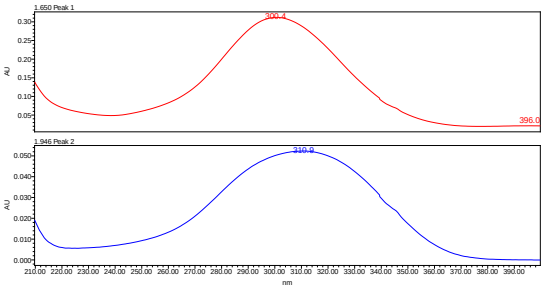

	Retention Time	Area	% Area	Height
1	1.650	96047	95.01	29701
2	1.946	5046	4.99	7337

Supplementary Figure S10. Reaction of TropC K106A with TropB-generated dienone **10**. PDA traces of enzymatic reaction analyzed at 360 nm.

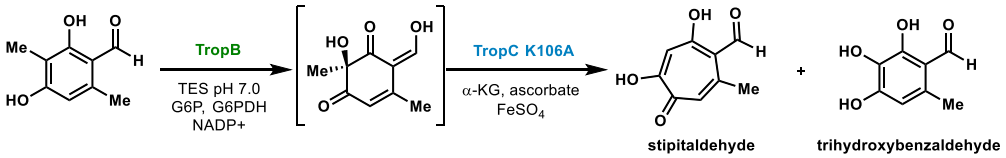

With TropC

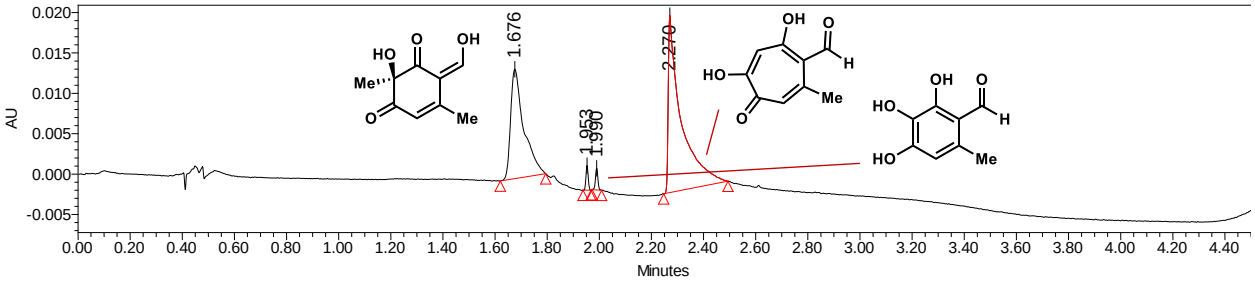

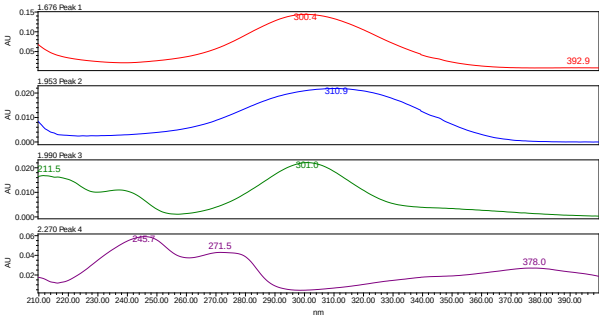

	Retention Time	Area	% Area	Height
1	1.676	47508	37.52	13538
2	1.953	1816	1.43	3056
3	1.990	1741	1.38	2689
4	2.270	75547	59.67	21945

TropB only

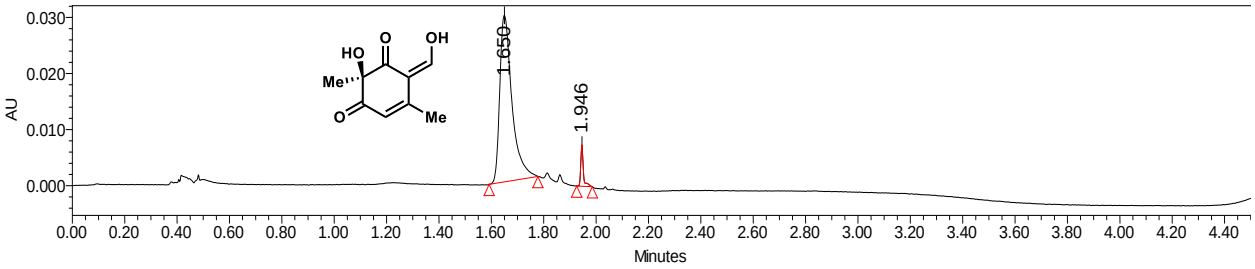

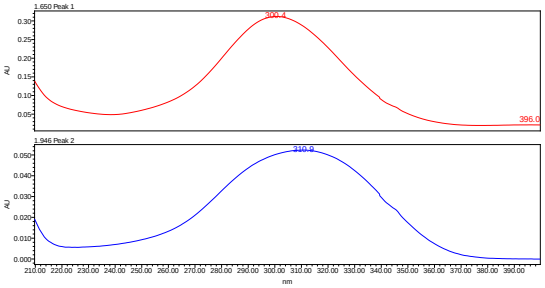

	Retention Time	Area	% Area	Height
1	1.650	96047	95.01	29701
2	1.946	5046	4.99	7337

Supplementary Figure S11. Reaction of TropC K106R with TropB-generated dienone **10**. PDA traces of enzymatic reaction analyzed at 360 nm.

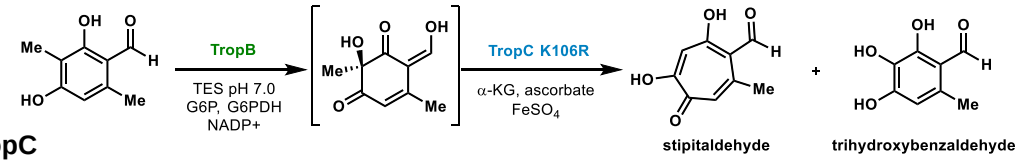

With TropC

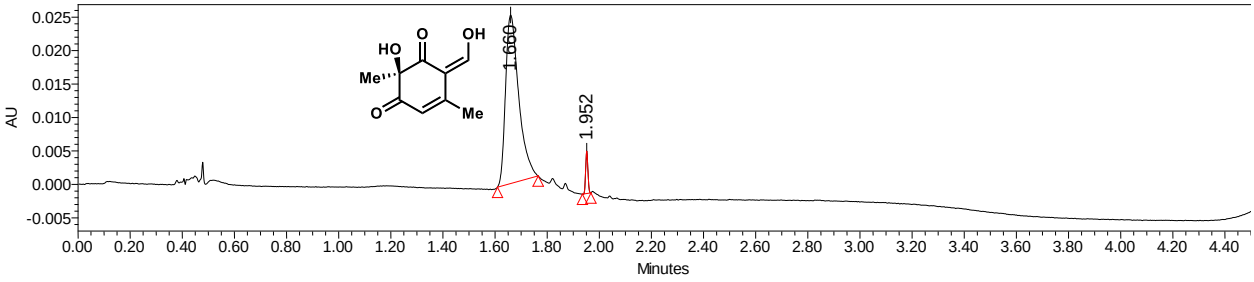

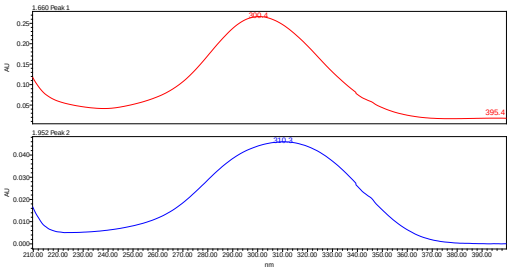

	Retention Time	Area	% Area	Height
1	1.660	88528	95.85	25190
2	1.952	3835	4.15	6351

TropB only

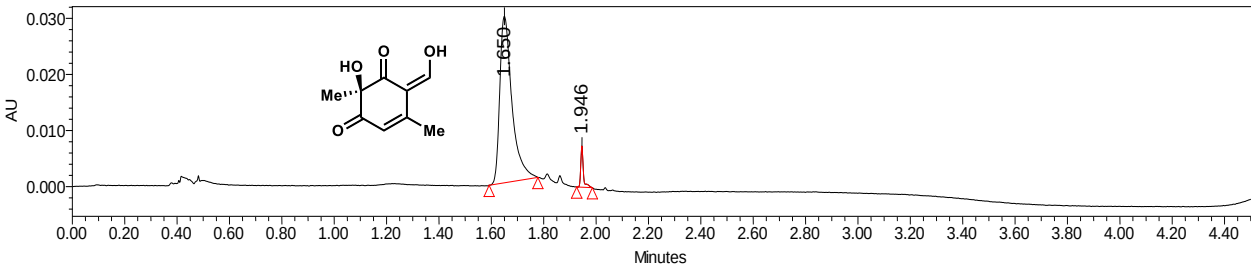

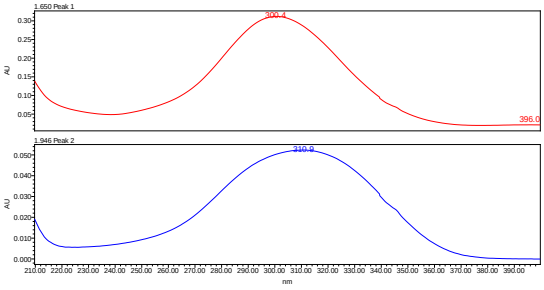

	Retention Time	Area	% Area	Height
1	1.650	96047	95.01	29701
2	1.946	5046	4.99	7337

Supplementary Figure S12. Reaction of TropC H97A with TropB-generated dienone **10**. PDA traces of enzymatic reaction analyzed at 360 nm.

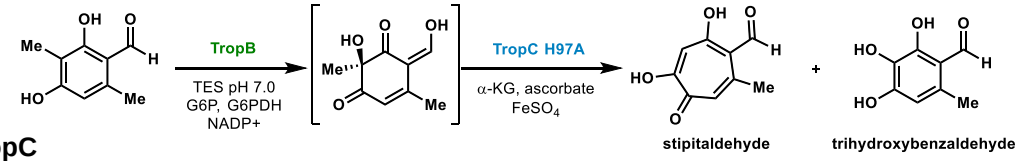

With TropC

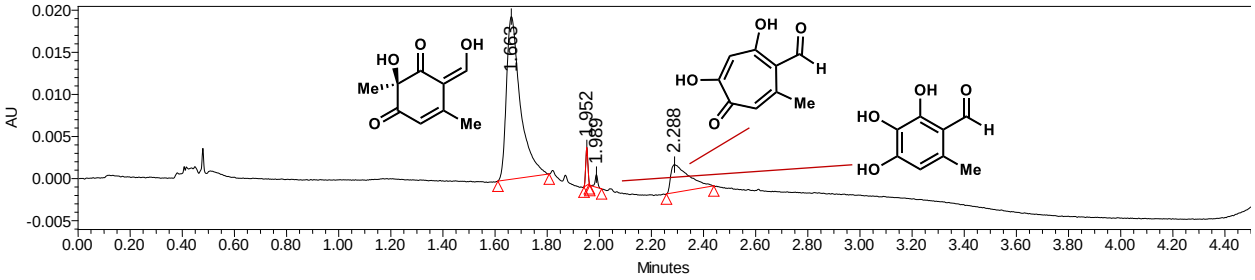

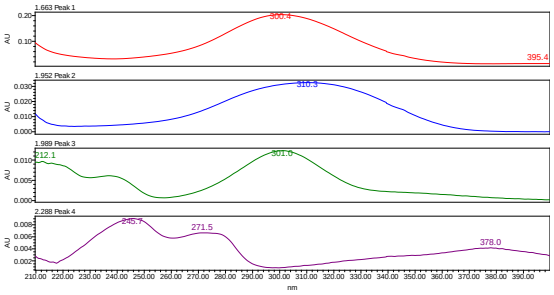

	Retention Time	Area	% Area	Height
1	1.663	71366	78.57	19312
2	1.952	2552	2.81	4487
3	1.989	1065	1.17	1516
4	2.288	15843	17.44	3331

TropB only

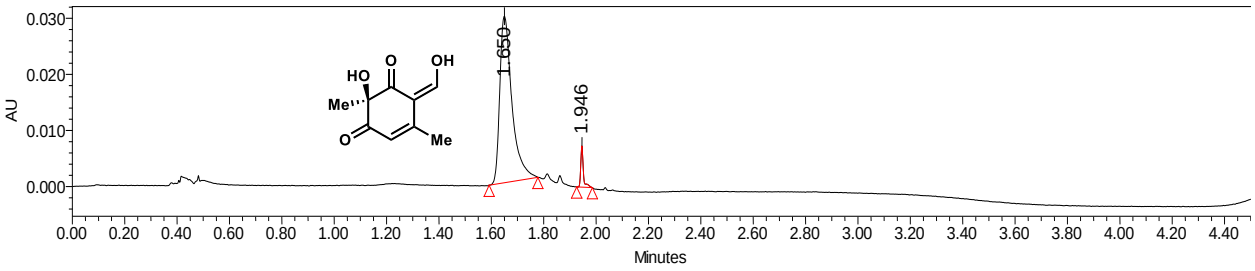

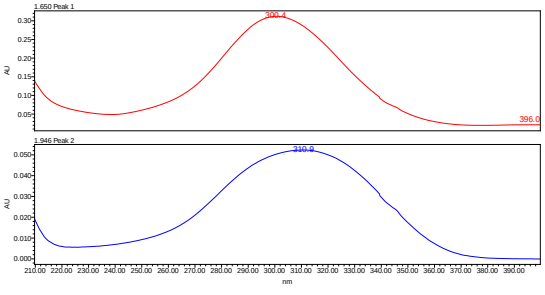

	Retention Time	Area	% Area	Height
1	1.650	96047	95.01	29701
2	1.946	5046	4.99	7337

Supplementary Figure S13. Reaction of TropC I110A with TropB-generated dienone **10**. PDA traces of enzymatic reaction analyzed at 360 nm.

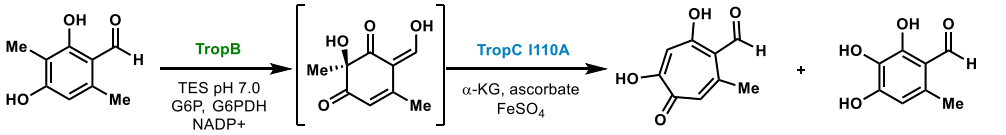

With TropC

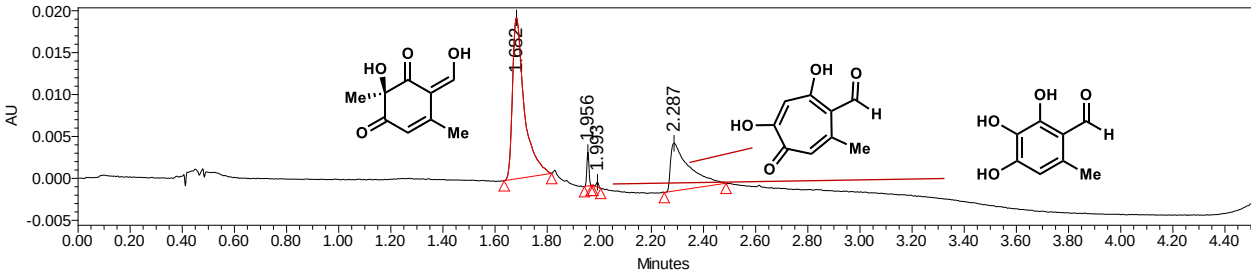

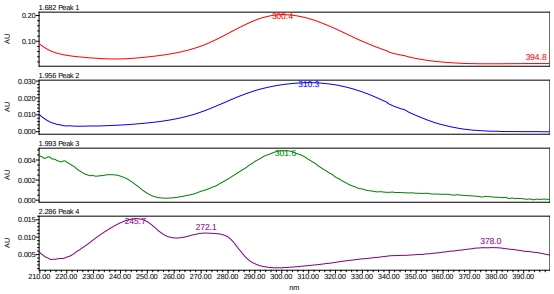

	Retention Time	Area	% Area	Height
1	1.682	60457	66.12	19206
2	1.956	2285	2.50	4020
3	1.993	376	0.41	586
4	2.287	28321	30.97	5705

TropB only

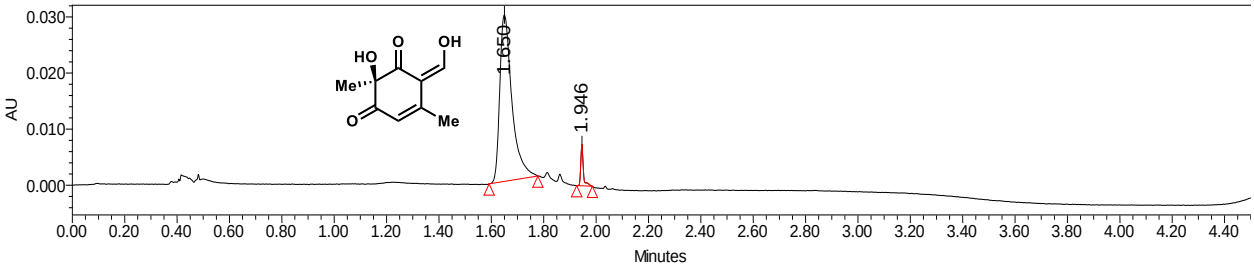

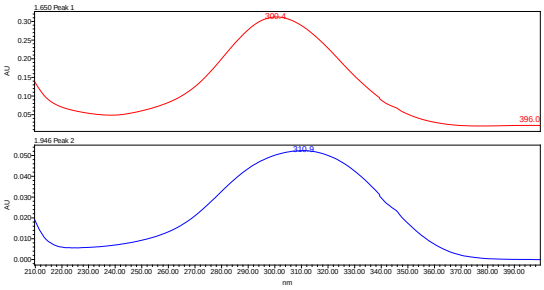

	Retention Time	Area	% Area	Height
1	1.650	96047	95.01	29701
2	1.946	5046	4.99	7337

Supplementary Figure S14. Reaction of TropC F213Y with TropB-generated dienone **10**. PDA traces of enzymatic reaction analyzed at 360 nm.

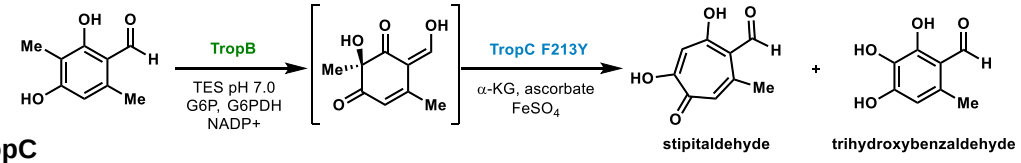

With TropC

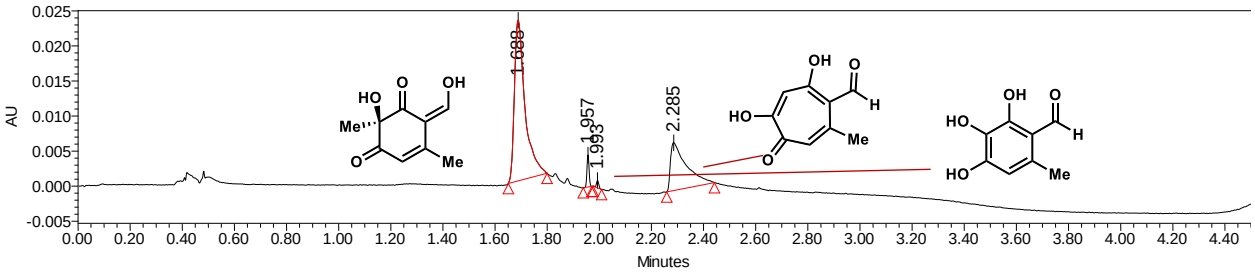

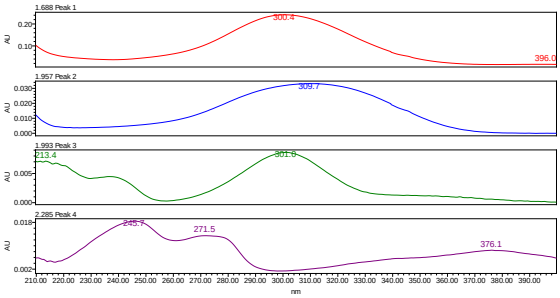

	Retention Time	Area	% Area	Height
1	1.688	64855	66.86	22883
2	1.957	2595	2.67	4564
3	1.993	646	0.67	1063
4	2.285	28901	29.80	6834

TropB only

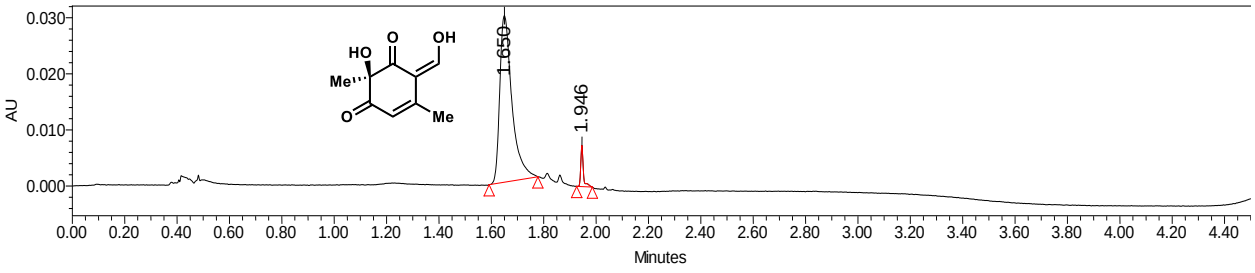

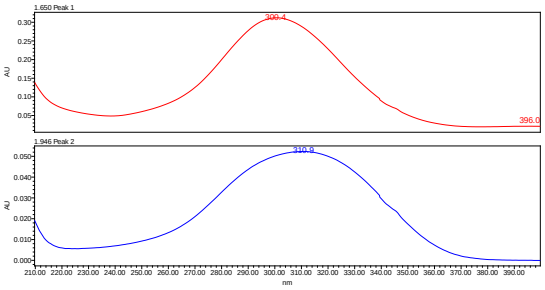

	Retention Time	Area	% Area	Height
1	1.650	96047	95.01	29701
2	1.946	5046	4.99	7337

Supplementary Figure S15. Reaction of TropC F283A with TropB-generated dienone **10**. PDA traces of enzymatic reaction analyzed at 360 nm.

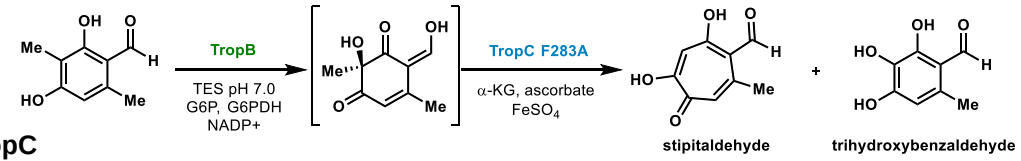

With TropC

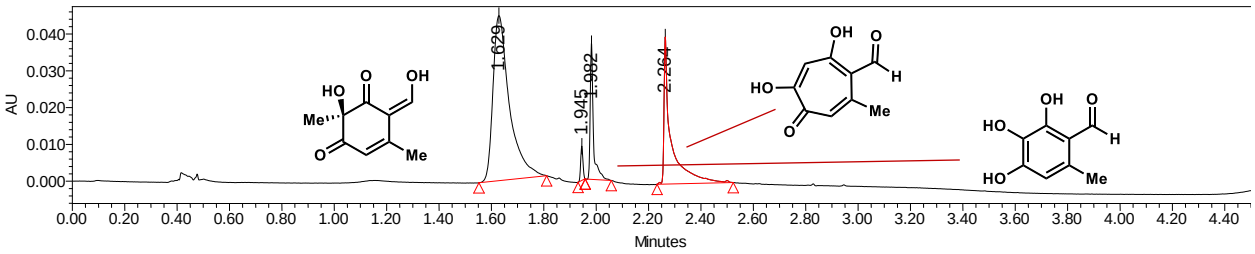

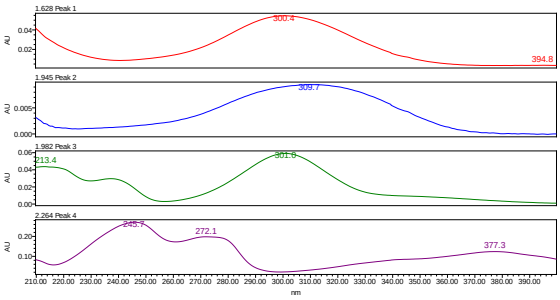

	Retention Time	Area	% Area	Height
1	1.629	195814	63.48	44839
2	1.945	5569	1.81	9326
3	1.982	31658	10.26	37019
4	2.264	75432	24.45	40034

TropB only

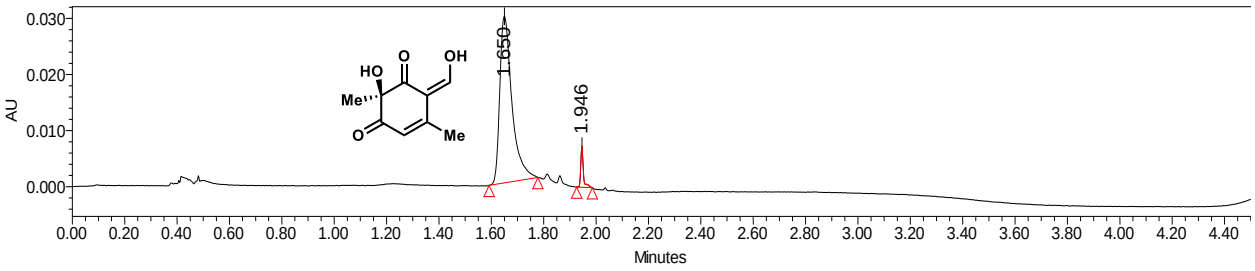

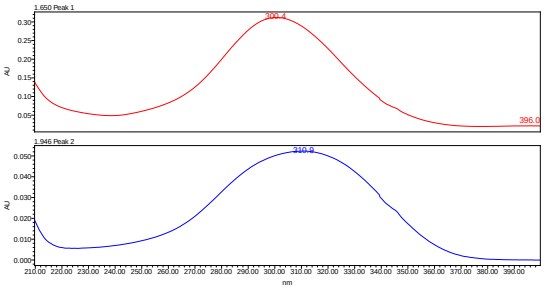

	Retention Time	Area	% Area	Height
1	1.650	96047	95.01	29701
2	1.946	5046	4.99	7337

Supplementary Figure S16. Reaction of TropC F283Y with TropB-generated dienone **10**. PDA traces of enzymatic reaction analyzed at 360 nm.

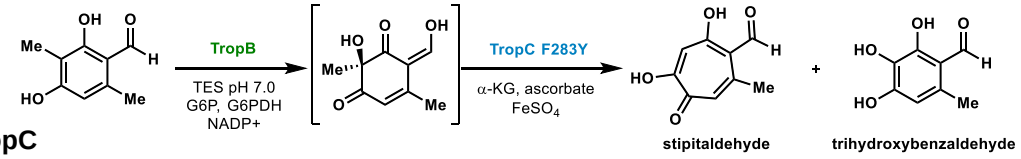

With TropC

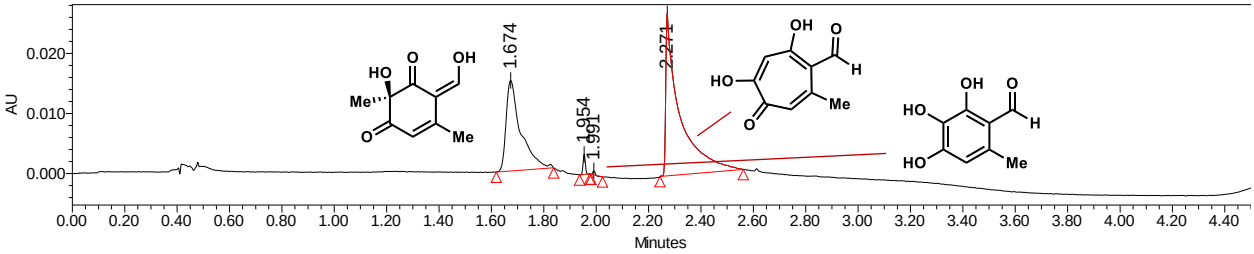

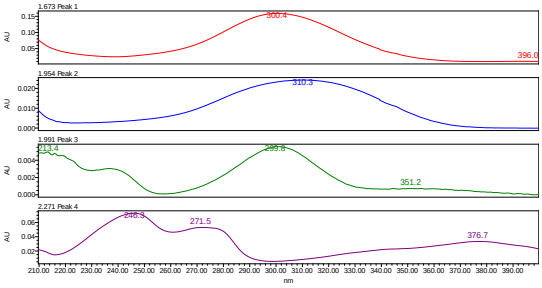

	Retention Time	Area	% Area	Height
1	1.674	58765	36.59	15106
2	1.954	1990	1.24	3339
3	1.991	463	0.29	700
4	2.271	99381	61.88	27052

TropB only

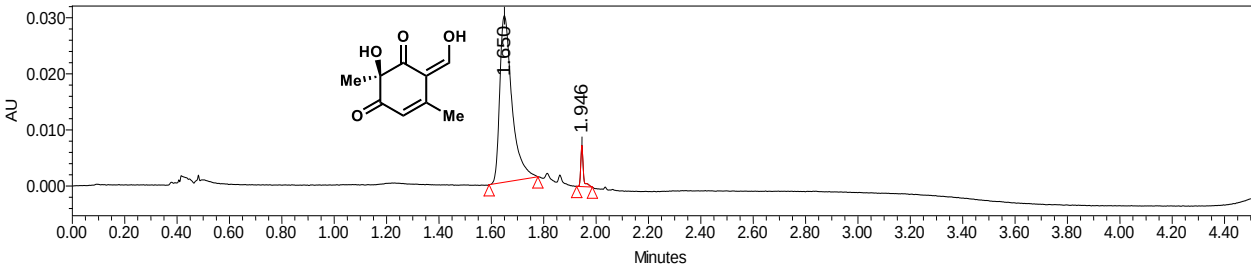

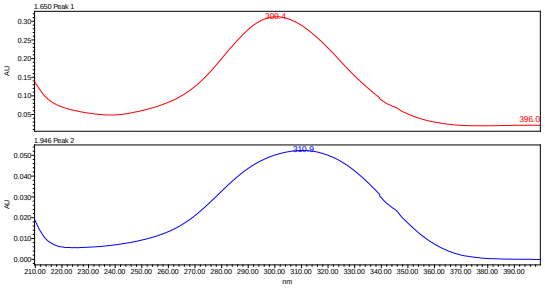

	Retention Time	Area	% Area	Height
1	1.650	96047	95.01	29701
2	1.946	5046	4.99	7337

Supplementary Figure S17. Reaction of TropC F86A with TropB-generated dienone **10**. PDA traces of enzymatic reaction analyzed at 360 nm.

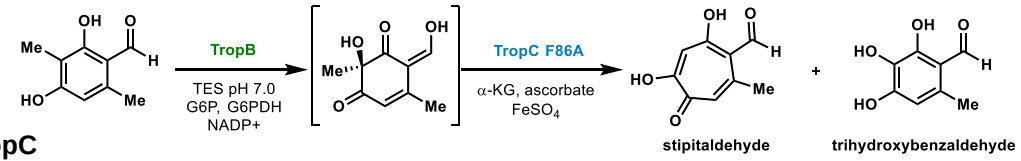

With TropC

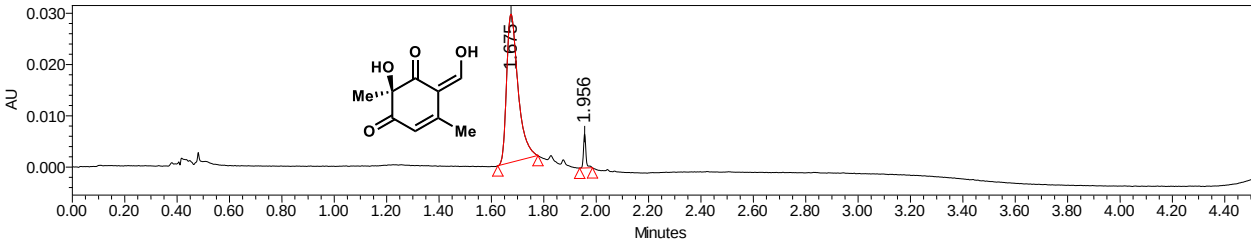

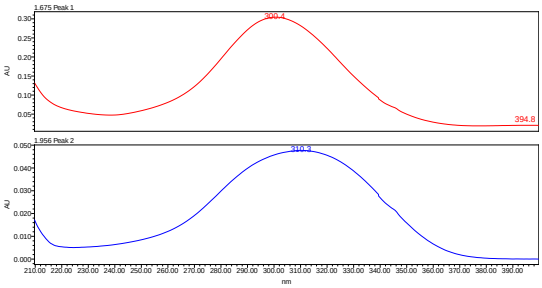

	Retention Time	Area	% Area	Height
1	1.675	87718	95.29	28900
2	1.956	4337	4.71	6627

TropB only

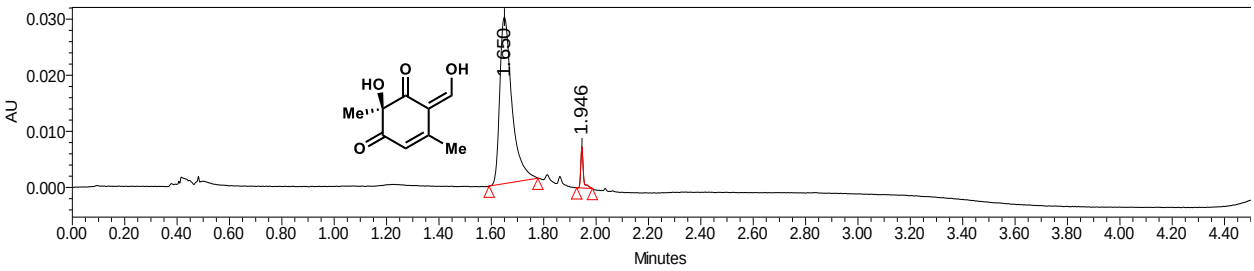

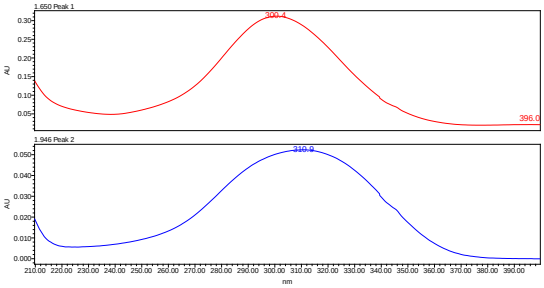

	Retention Time	Area	% Area	Height
1	1.650	96047	95.01	29701
2	1.946	5046	4.99	7337

Supplementary Figure S18. Reaction of TropC F86Y with TropB-generated dienone **10**. PDA traces of enzymatic reaction analyzed at 360 nm.

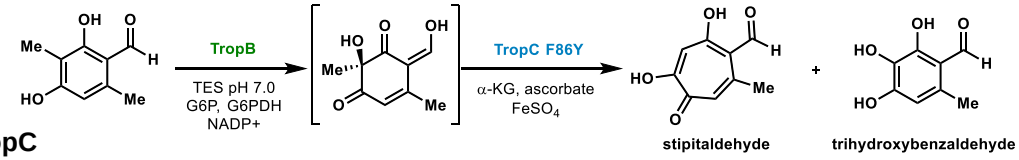

With TropC

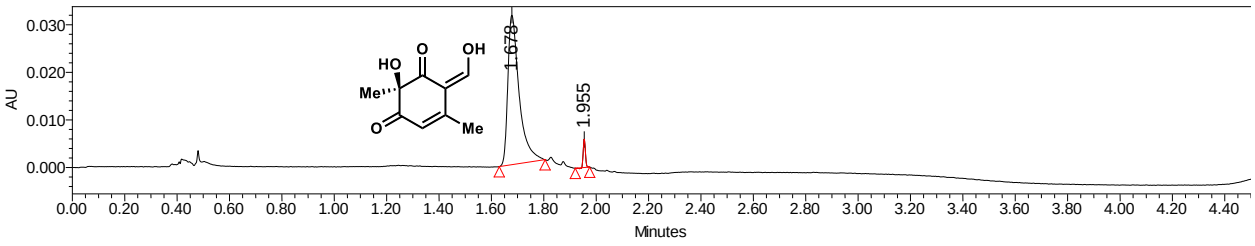

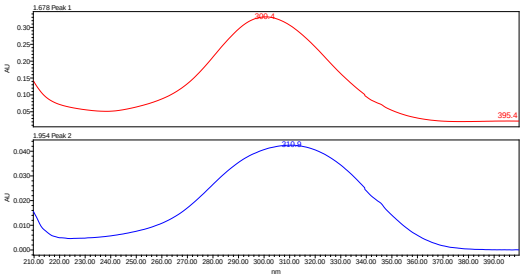

	Retention Time	Area	% Area	Height
1	1.678	94345	96.33	31408
2	1.955	3599	3.67	5966

TropB only

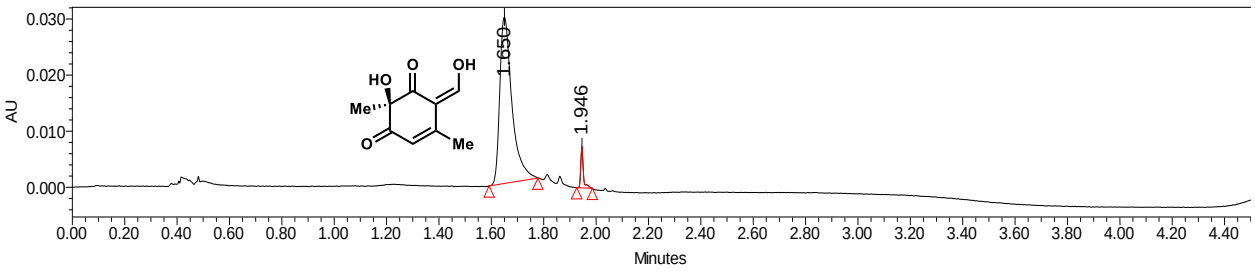

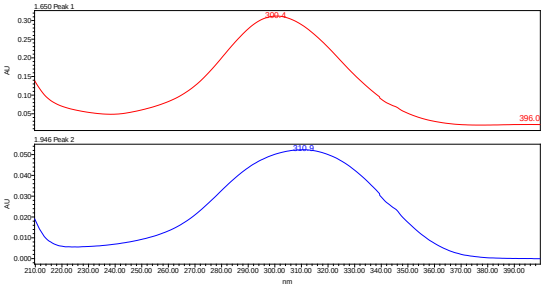

	Retention Time	Area	% Area	Height
1	1.650	96047	95.01	29701
2	1.946	5046	4.99	7337

Supplementary Figure S19. Reaction of TropC S217A with TropB-generated dienone **10**. PDA traces of enzymatic reaction analyzed at 360 nm.

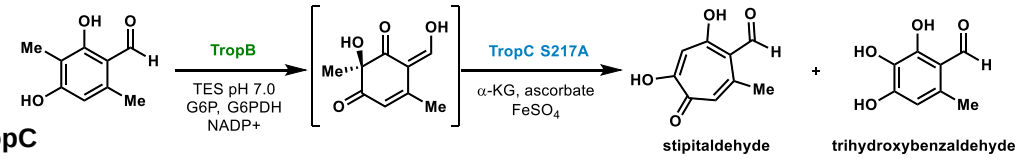

With TropC

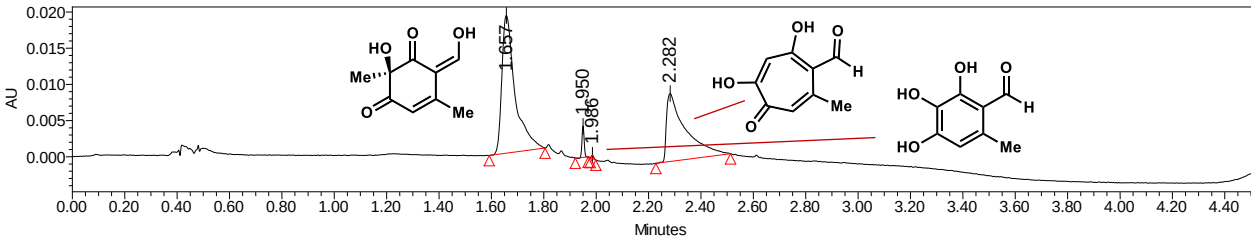

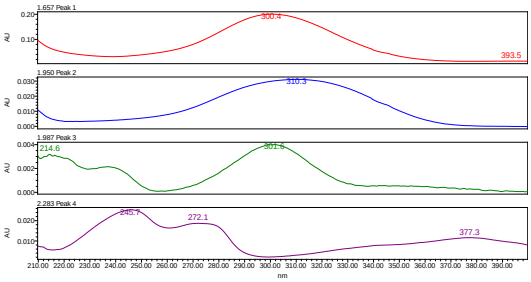

	Retention Time	Area	% Area	Height
1	1.657	67041	57.09	19048
2	1.950	2538	2.16	4320
3	1.986	270	0.23	477
4	2.282	47580	40.52	9389

TropB only

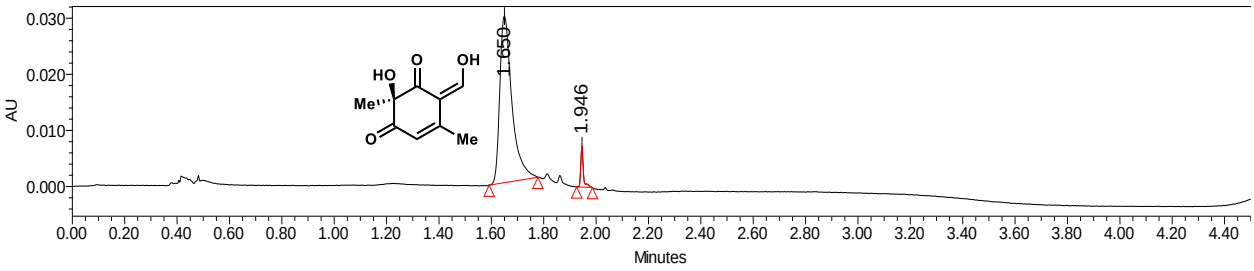

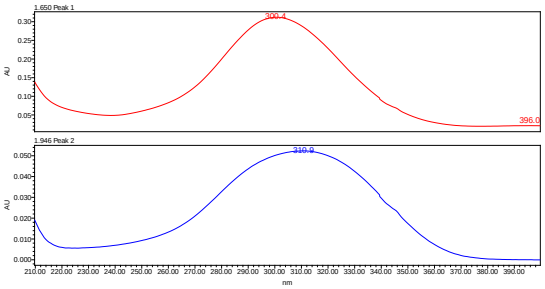

	Retention Time	Area	% Area	Height
1	1.650	96047	95.01	29701
2	1.946	5046	4.99	7337

Supplementary Figure S20. Reaction of TropC S217T with TropB-generated dienone **10**. PDA traces of enzymatic reaction analyzed at 360 nm.

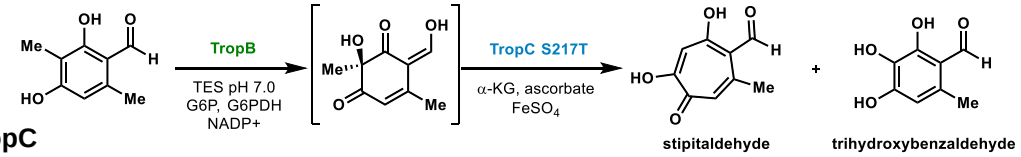

With TropC

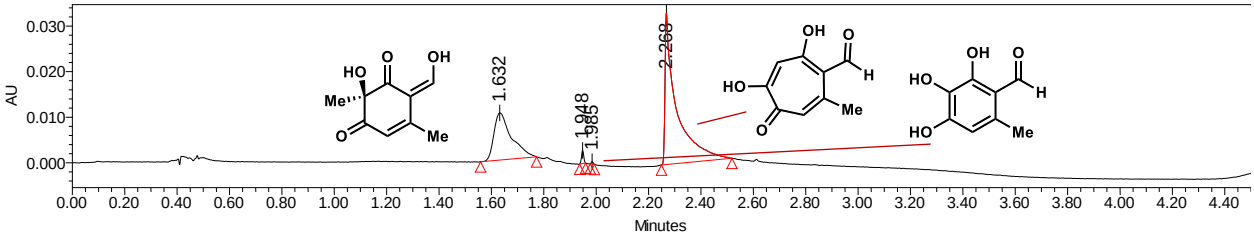

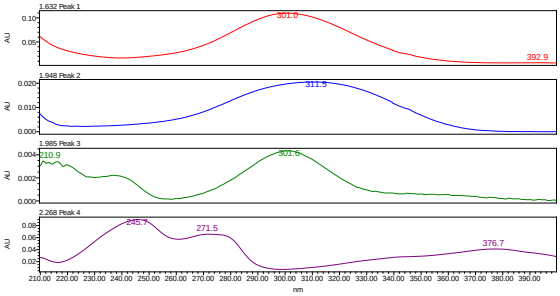

	Retention Time	Area	% Area	Height
1	1.632	47777	31.65	10364
2	1.948	1693	1.12	2886
3	1.985	268	0.18	546
4	2.268	101199	67.05	33239

TropB only

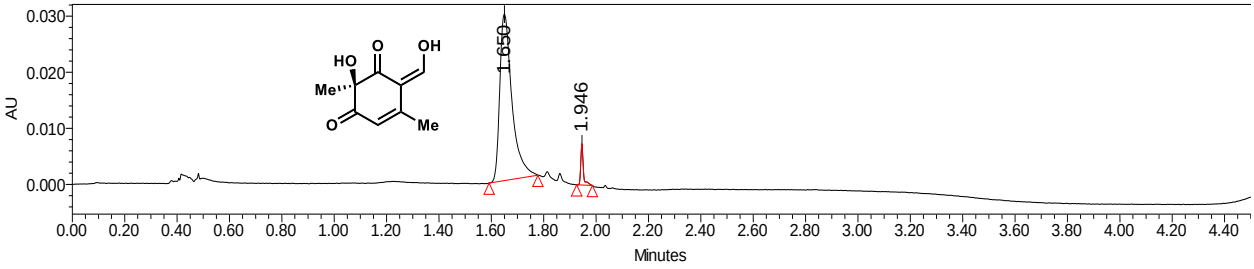

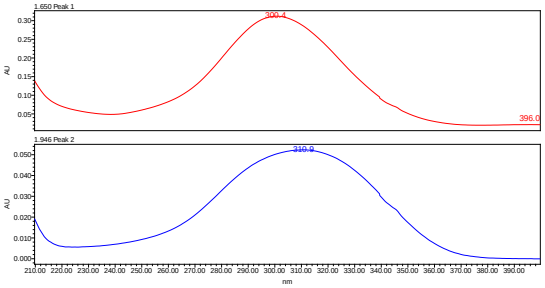

	Retention Time	Area	% Area	Height
1	1.650	96047	95.01	29701
2	1.946	5046	4.99	7337

Supplementary Figure S21. Reaction of TropC C108A with TropB-generated dienone **10**. PDA traces of enzymatic reaction analyzed at 360 nm.

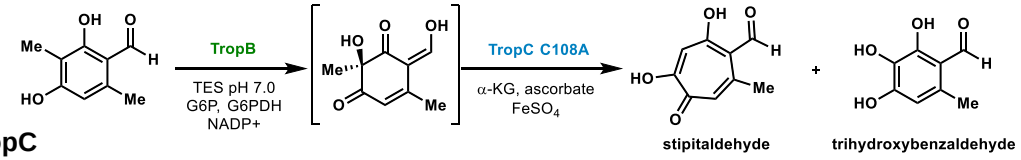

With TropC

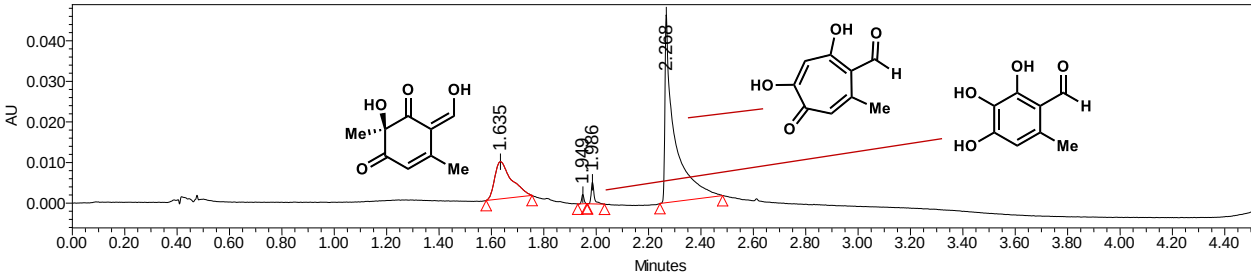

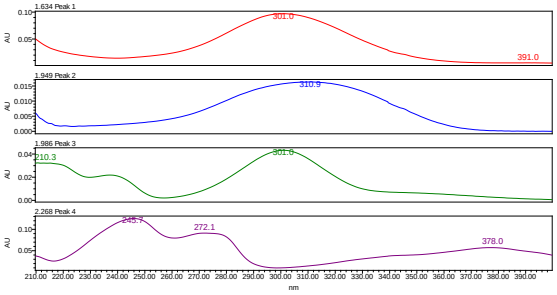

	Retention Time	Area	% Area	Height
1	1.635	40674	24.93	9174
2	1.949	1422	0.87	2302
3	1.986	4246	2.60	5332
4	2.268	116799	71.59	46252

TropB only

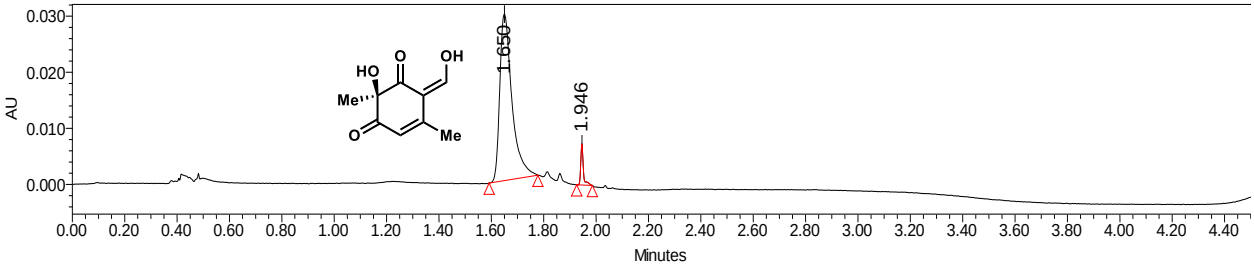

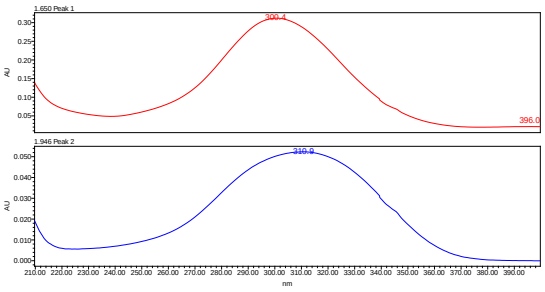

	Retention Time	Area	% Area	Height
1	1.650	96047	95.01	29701
2	1.946	5046	4.99	7337

Supplementary Figure S22. Reaction of TropC Q95A with TropB-generated dienone **10**. PDA traces of enzymatic reaction analyzed at 360 nm.

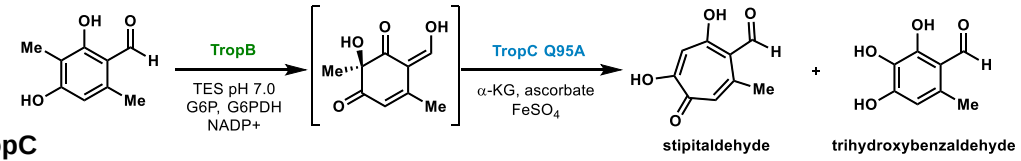

With TropC

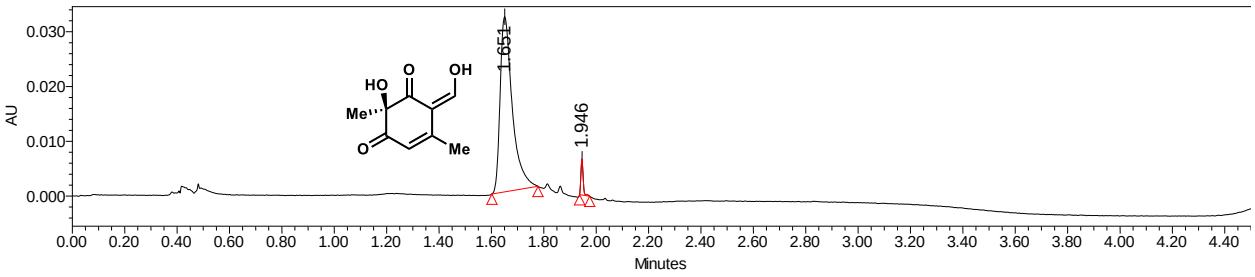

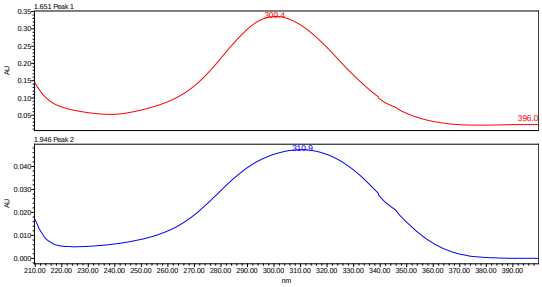

	Retention Time	Area	% Area	Height
1	1.651	103456	96.37	31979
2	1.946	3896	3.63	6593

TropB only

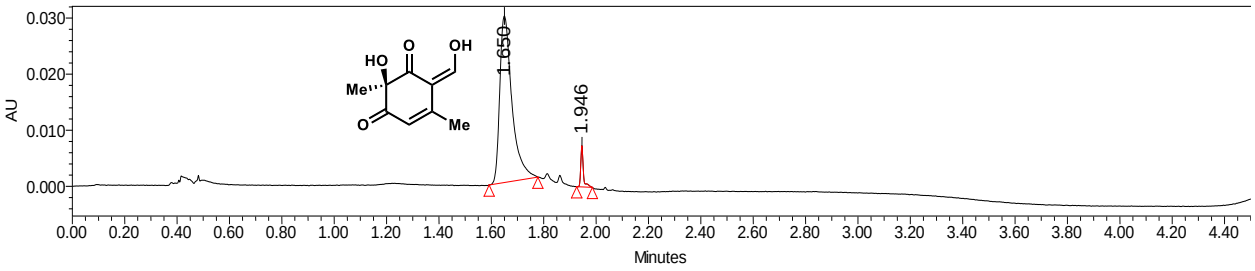

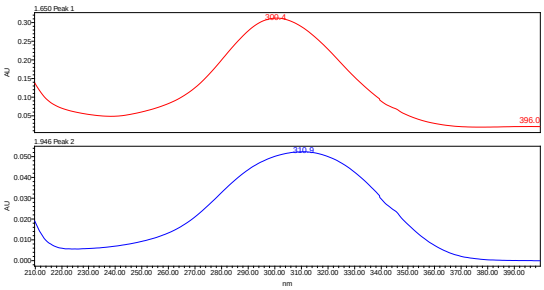

	Retention Time	Area	% Area	Height
1	1.650	96047	95.01	29701
2	1.946	5046	4.99	7337

Supplementary Figure S23. Reaction of TropC R278A with TropB-generated dienone **10**. PDA traces of enzymatic reaction analyzed at 360 nm.

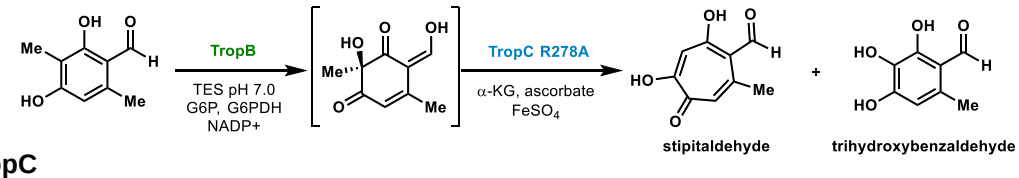

With TropC

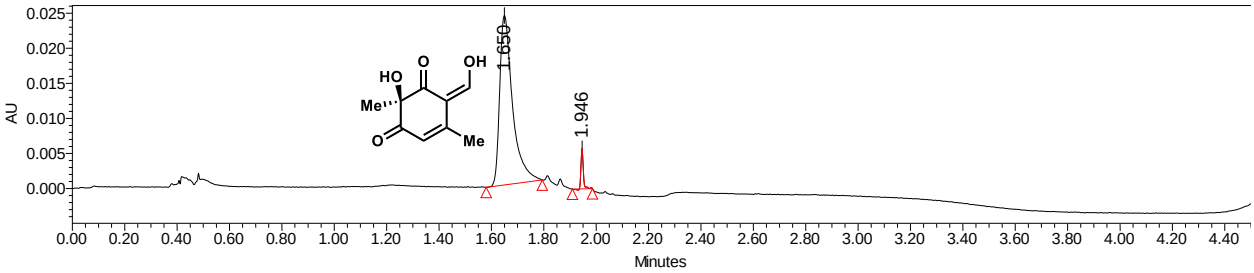

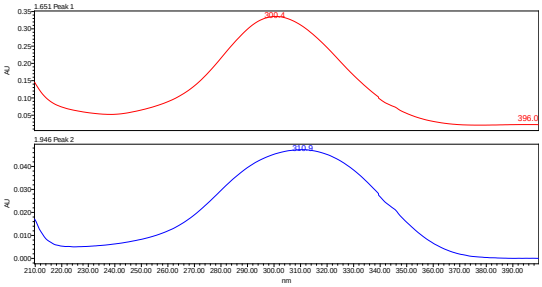

	Retention Time	Area	% Area	Height
1	1.650	82678	95.66	24152
2	1.946	3749	4.34	5727

TropB only

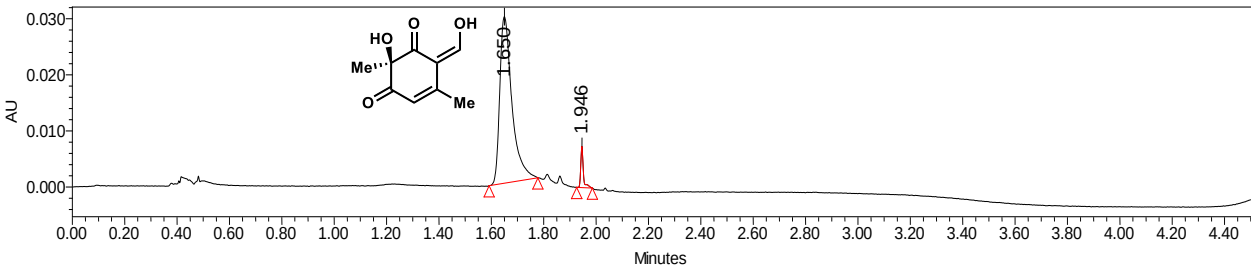

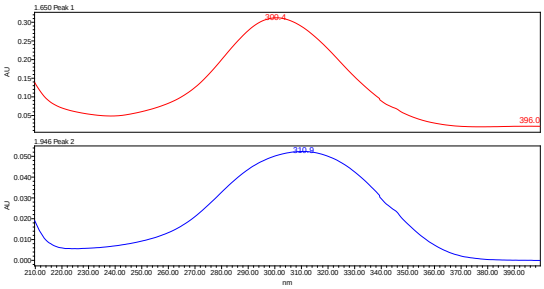

	Retention Time	Area	% Area	Height
1	1.650	96047	95.01	29701
2	1.946	5046	4.99	7337

Supplementary Figure S24. Reaction of TropC R278K with TropB-generated dienone **10**. PDA traces of enzymatic reaction analyzed at 360 nm.

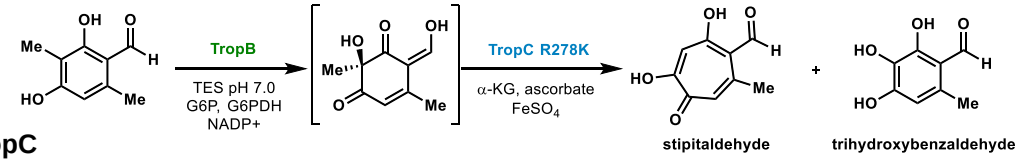

With TropC

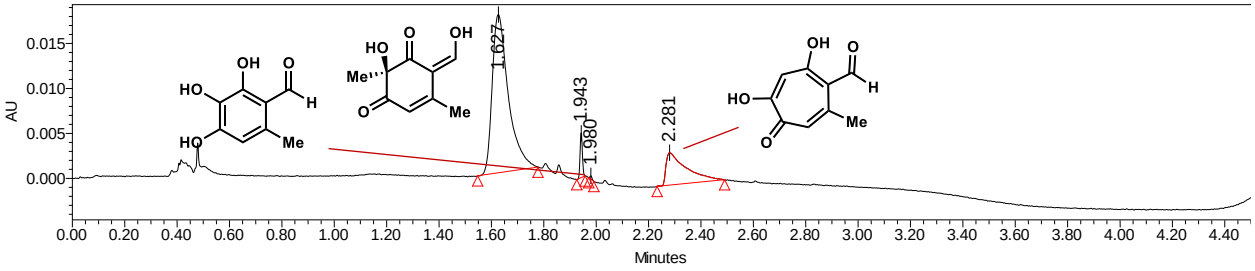

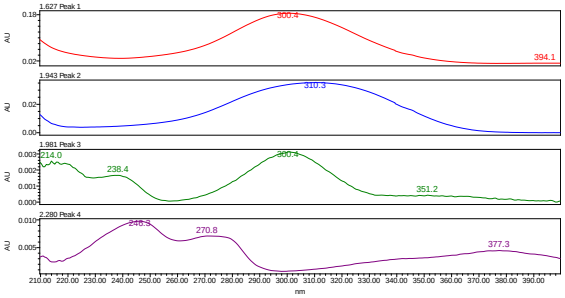

	Retention Time	Area	% Area	Height
1	1.627	75546	76.95	17601
2	1.943	3035	3.09	4982
3	1.980	207	0.21	372
4	2.281	19389	19.75	3622

TropB only

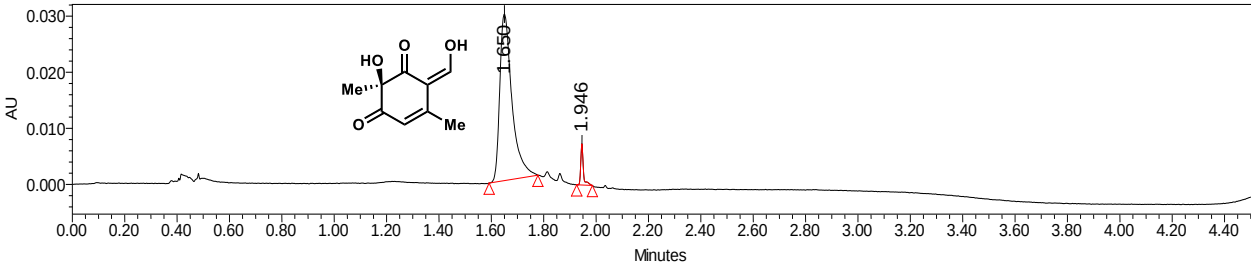

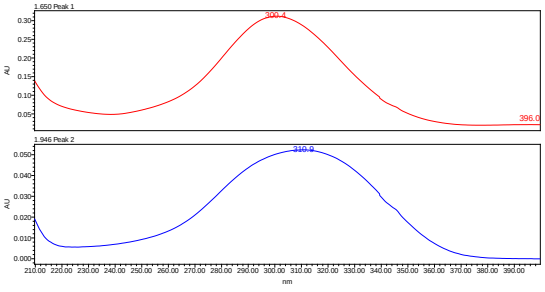

	Retention Time	Area	% Area	Height
1	1.650	96047	95.01	29701
2	1.946	5046	4.99	7337

Supplementary Figure S25. Reaction of wild-type TropC with dienone **10**. PDA traces of enzymatic reaction analyzed at 300 nm.

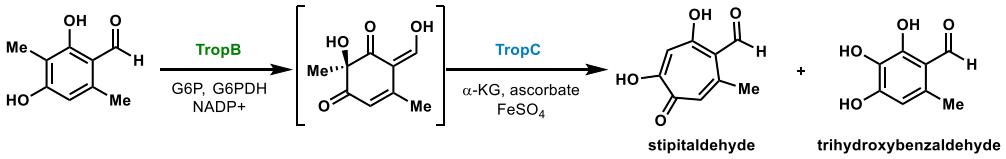

With TropC

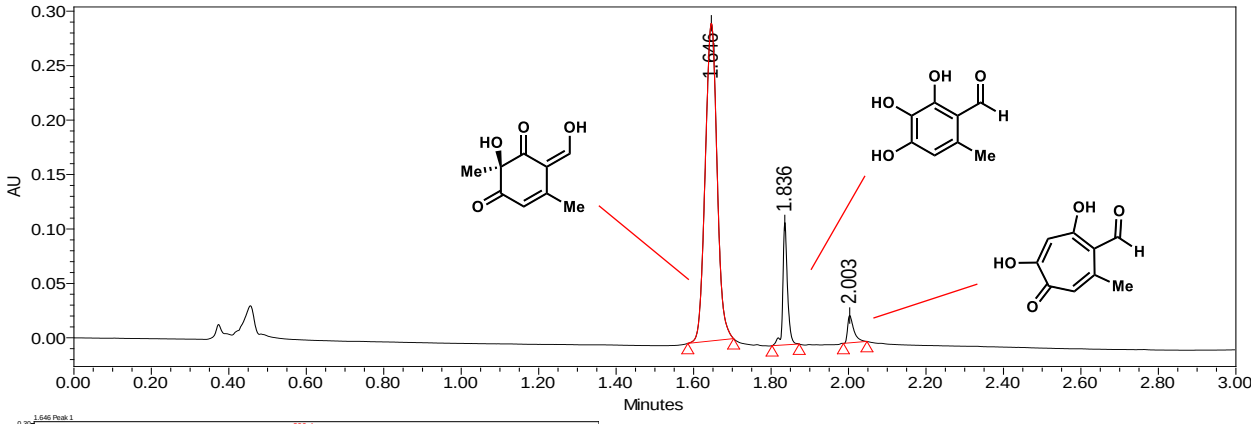

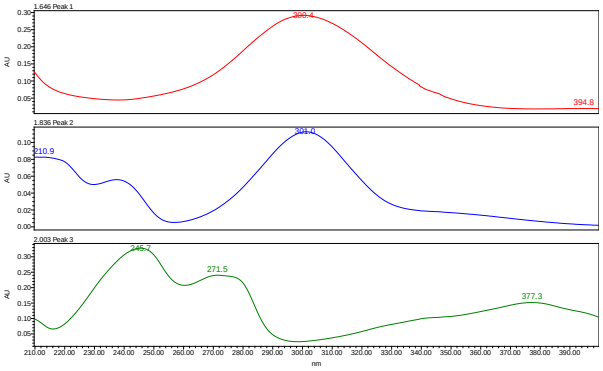

	Retention Time	Area	% Area	Height
1	1.646	620887	83.70	291746
2	1.836	93090	12.55	112386
3	2.003	27801	3.75	25219

Supplementary Figure S26. Reaction of wild-type CitB with substrate **9**. PDA traces of enzymatic reaction analyzed at 300 nm.

With CitB

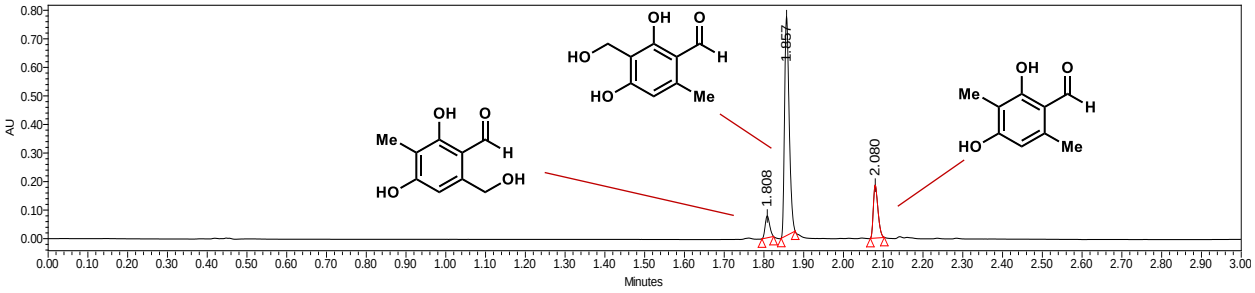

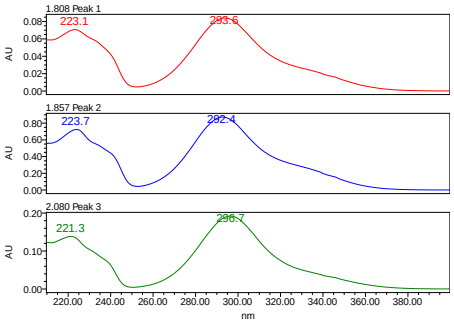

	Retention Time	Area	% Area	Height
1	1.808	60277	7.28	76765
2	1.857	617301	74.60	767275
3	2.080	149848	18.11	185817

No enzyme control

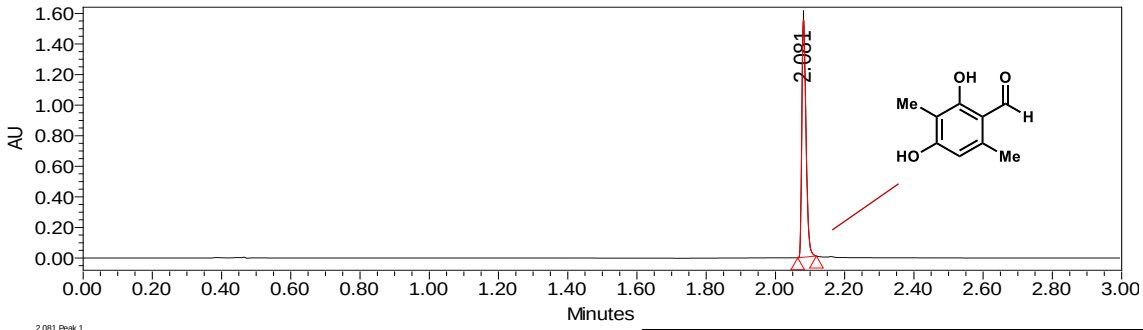

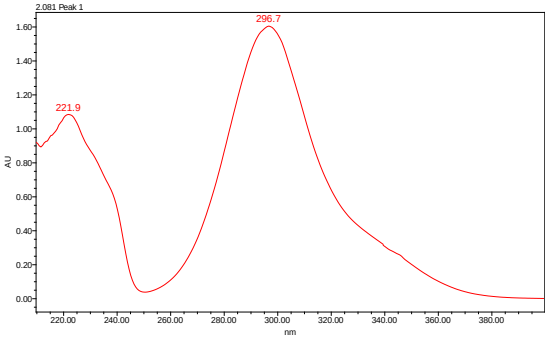

	Retention Time	Area	% Area	Height
1	2.081	1311812	100.00	1557555

Supplementary Figure S27. Reaction of TropB with benzylic alcohol **25**. PDA traces of enzymatic reaction analyzed at 300 nm.

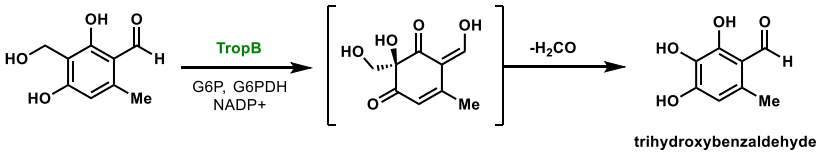

With TropB

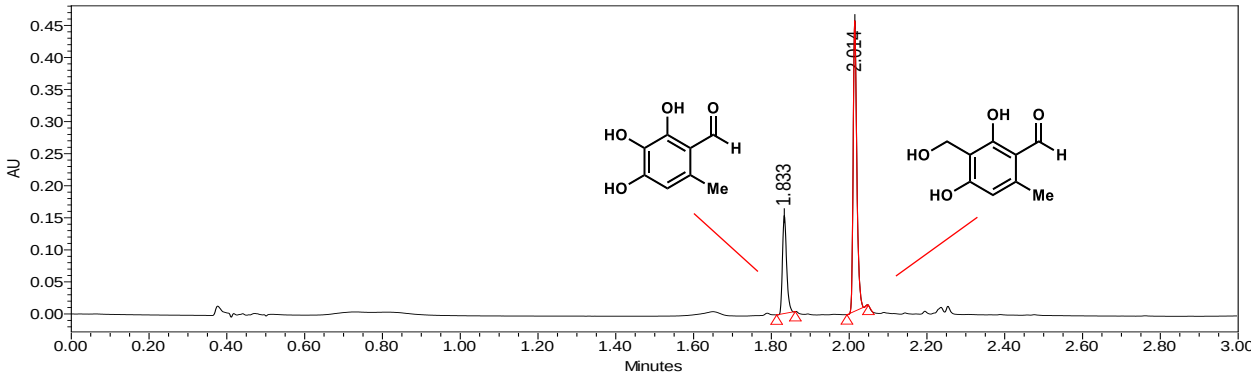

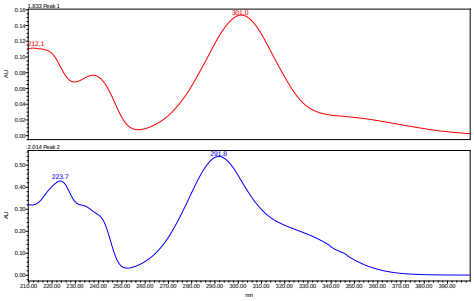

	Retention Time	Area	% Area	Height
1	1.833	112936	27.55	152592
2	2.014	296957	72.45	453413

Trihydroxybenzaldehyde (18) product standard

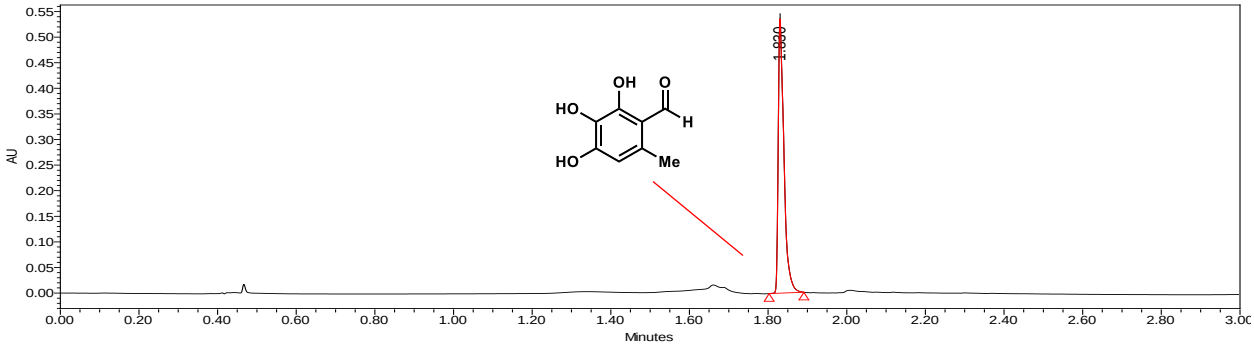

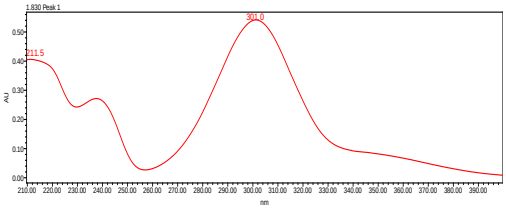

	Retention Time	Area	% Area	Height
1	1.830	538937	100.00	537068

Supplementary Figure S28. Reaction of TropB and TropC with benzylic alcohol **25**. PDA traces of enzymatic reaction analyzed at 300 nm.

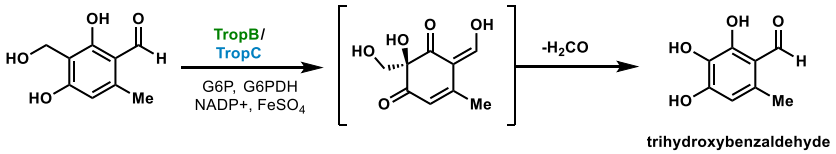

With TropB and TropC

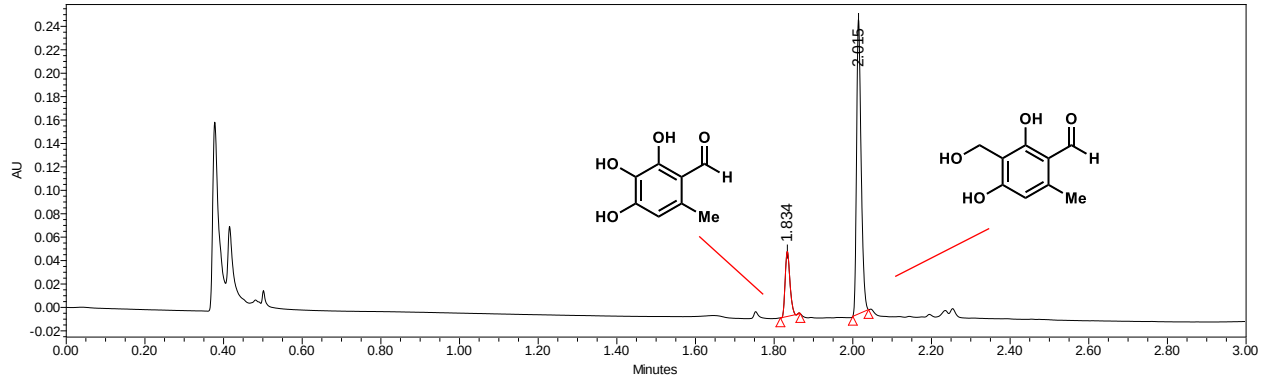

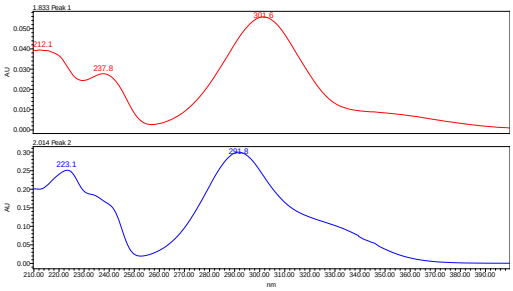

	Retention Time	Area	% Area	Height
1	1.834	47107	18.87	55552
2	2.015	202502	81.13	251750

Trihydroxybenzaldehyde (18) product standard

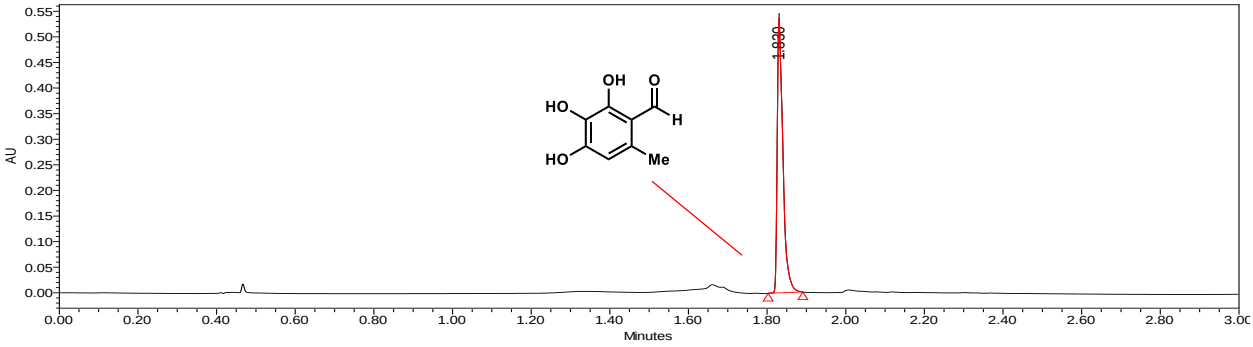

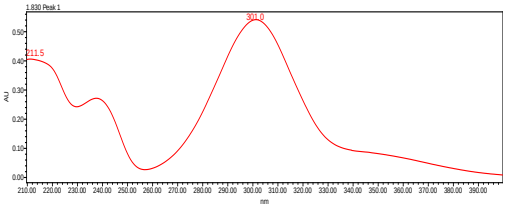

	Retention Time	Area	% Area	Height
1	1.830	538937	100.00	537068

Supplementary Figure S29. Previously reported rearomatization reactivity of *ortho*-dearomatized phenols.[4]

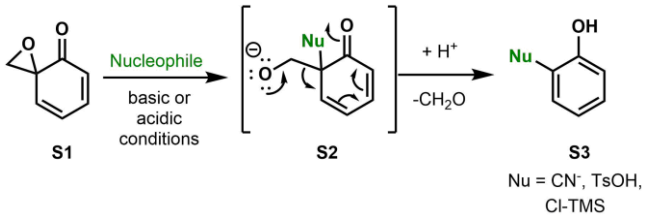

Part VII. NMR spectra of isolated products

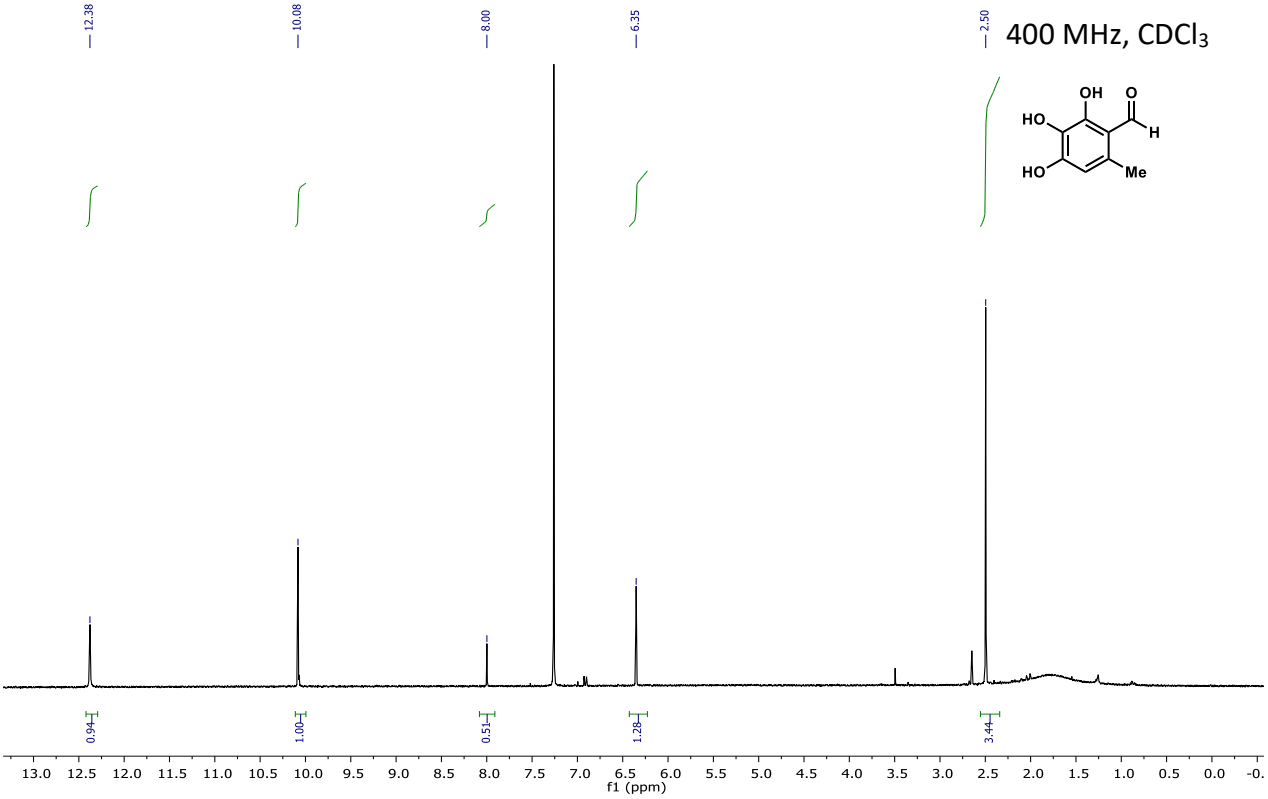

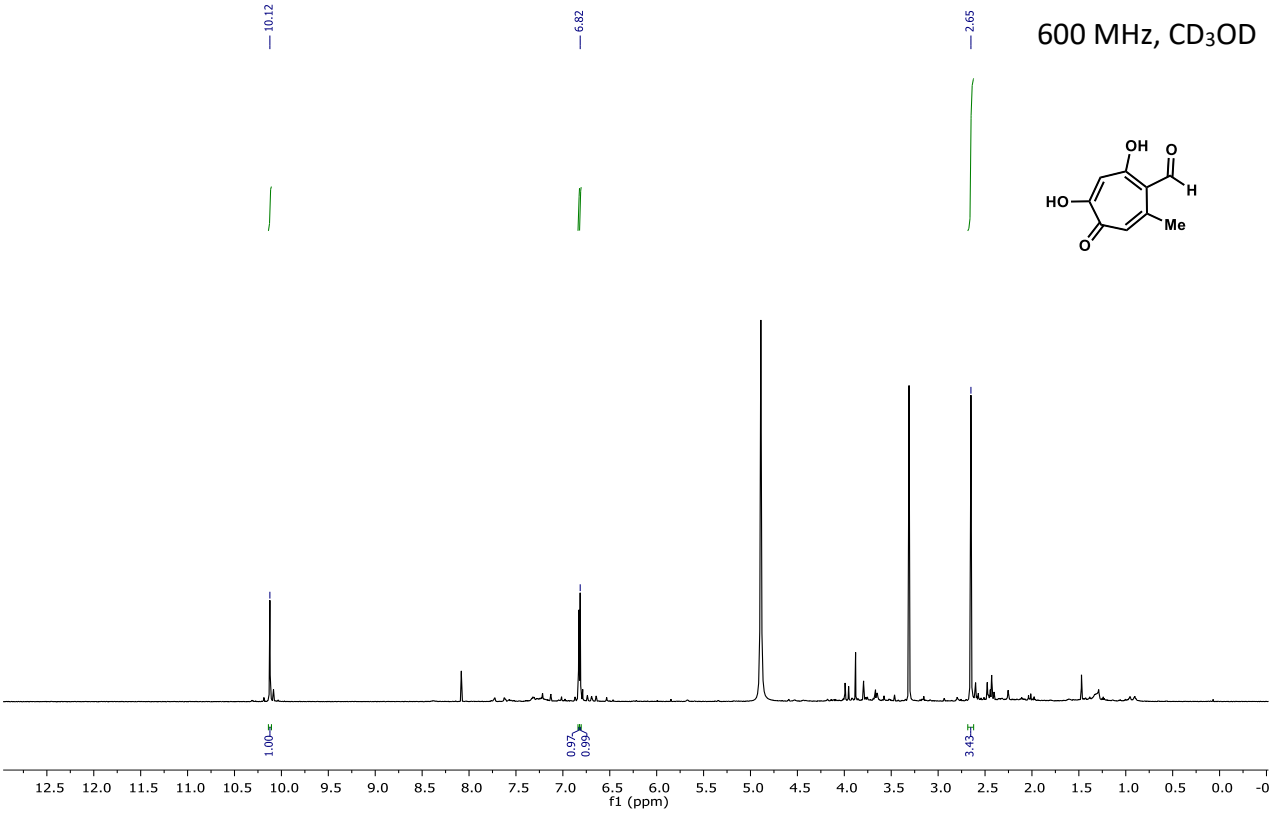
600 MHz, CD3OD
10.12
6.82
2.65
OH
O
H
HO
Me
O
1.00
0.97
0.99
3.43
f1 (ppm)

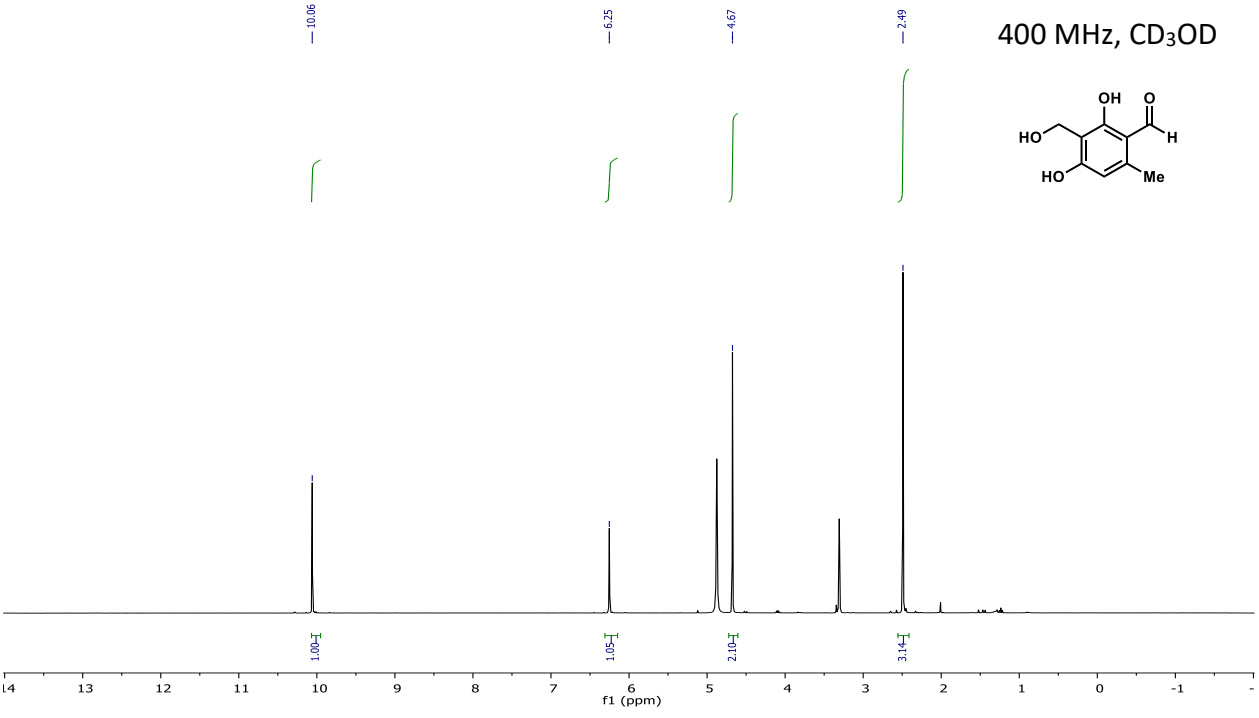
400 MHz, CD3OD
10.06
6.25
4.67
2.49
OH
O
H
HO
HO
Me
1.00
1.05
2.10
3.14
f1 (ppm)

Part VIII. X-ray crystallography

General considerations: Our initial structure prediction analysis of TropC using the JPRED server suggested that the N-terminal region could be disordered, leading to potential challenges in crystal generation. In an effort to develop a TropC variant amenable to crystallization, we generated a construct containing a 7-residue N-terminal truncation (TropC-7N).[5] TropC-7N was purified to homogeneity and the N-terminal 6x His tag was removed by incubation with TEV protease (see Section II for details).

Crystallization: Crystals of TropC were grown using the sitting drop vapor diffusion method. Crystallization of the purified TropC was initially performed with commercially available screens from Rigaku and Molecular Dimension at 20°C and 4° C. Each drop consisted 1:2 mixture of protein solution (10-12 mg/ml in 50 mM Tris-HCl pH 7.4, 0.2 M NaCl and 1 mM TCEP) with reservoir solution. TropC crystals were observed after two weeks at 4˚C. TropC was crystallized in the condition of 0.2 M Magnesium Acetate, 20% PEG 8000, 0.01 M Yttrium (III) Chloride hexahydrate. Crystals were transferred to a cryo-protectant solution containing the corresponding conditions described above and 20% (v/v) glycerol before harvesting. The crystals were harvested and flash-frozen in liquid nitrogen prior to data collection.

Data collection and processing: Diffraction data were collected on LS-CAT 21-ID-D beamline at Advanced Photon Source (APS), Argonne National Laboratory using Eiger-9M detector. Data collection and processing statistics are summarized in Supplementary Table S2.

Structure solution and refinement: The structure of TropC was determined by molecular replacement method with MOLREP3 [6] in CCP4 suite, using the structure of T7H *Neurospora crassa* as a search model[7]. Model was built manually using the program Coot[8] and structure refinement was performed using refmac5[9-10] in CCP4 suite.[11] The structure was validated using MolProbity.[12] Open source program, PyMOL, was used for molecular visualization and generating figures.[13]

Supplementary Table S2: Data collection and refinement parameters.

	TropC
Data collection	
Beamline	APS, LSCAT 21-IDD
Wavelength (Å)	1.0332
Temperature (K)	100
Resolution (Å)	48.07-2.7 (2.873-2.7)
Space group	$P3_121$
Cell dimensions (Å)	a = 111.0, b = 111.0, c = 89.9
Cell dimensions (°)	α = β = 90, γ = 120
Observed reflections	100802 (13636)
Unique reflections	17040 (2288)
R_{merge} (%)	0.070 (1.073)
R_{pim} (%)	0.034 (0.721)
<I/σ>	14.4 (1.7)
CC(1/2)	0.999 (0.766)
Multiplicity	5.9 (6.0)
Completeness (%)	95.4 (71.7)
Overall *B* (Å^2) (Wilson plot)	64.9
Refinement	
Resolution range	48.07-2.7
Number of reflections (work/test set)	17015 (796)
R_{work}/R_{free} (%)	21.3/25.0
No. of non-H atoms	
Protein	2319
Water	5
Ligand	1
B-factors (Å^2)	
Protein	72.83
Water	69.4
Ligand	93.8
Rmsd deviations	
Bond lengths (Å)	0.005
Bond angles (°)	0.890
Ramachandran plot	
Favored/allowed/outliers	96.2/3.8/0
MolProbity Score	1.9 (99th percentile)

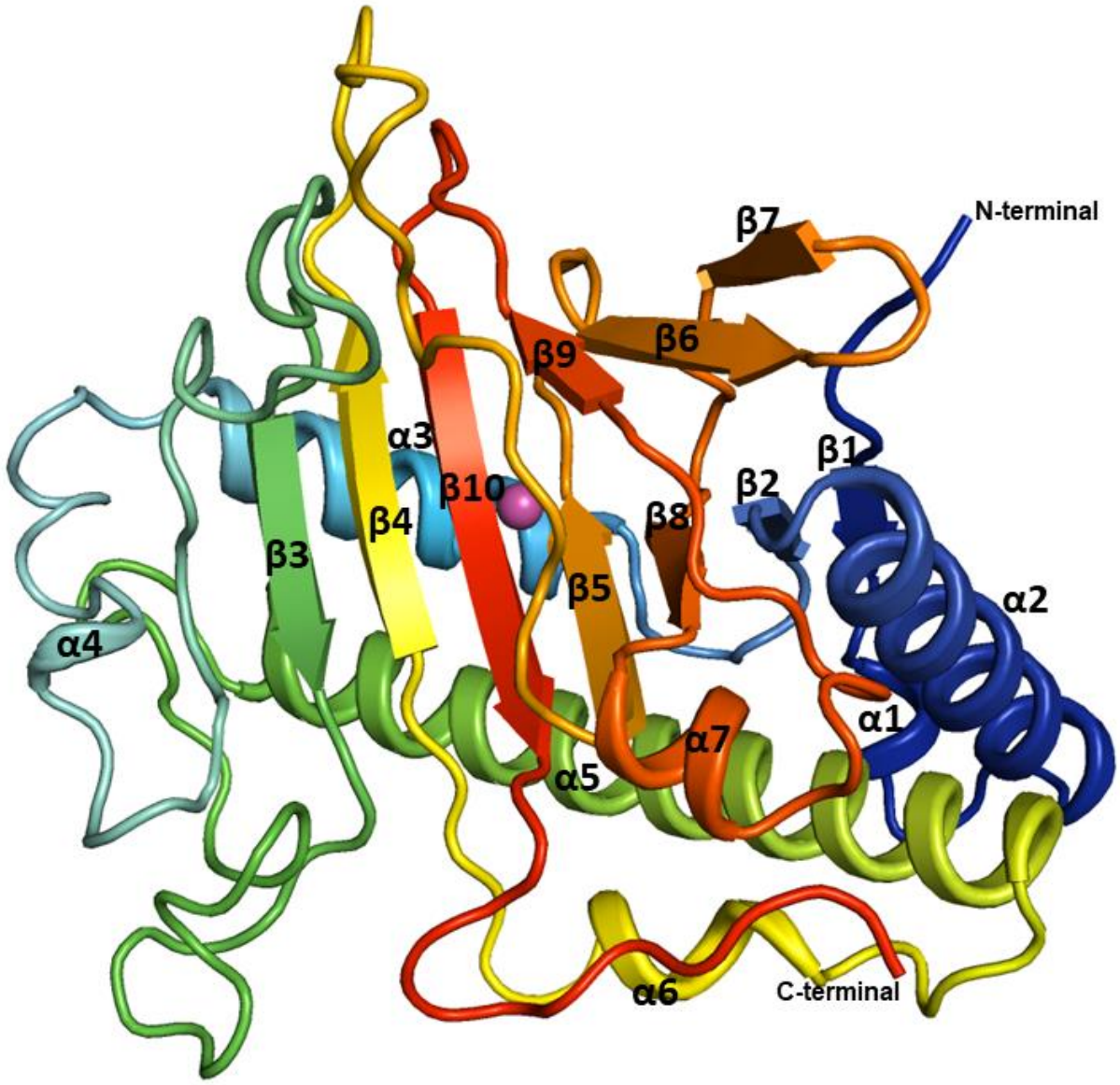

Supplementary Figure S29: Structure of TropC of *T. stipitatus*. Overall structure of TropC (PDB ID: 6XJJ) shown in ribbon representation colored in spectrum, which starts with blue (N-terminal) to red (C-terminal). Jelly-roll (or DSBH) motif at the center of the protein, which comprised of major (β1-5, β8 and β10) and minor (β6, β7 and β9) β-sheets. Fe(III) shown in purple sphere, located at the center of major and minor β-sheet, and in close proximity to β10. Helices (α1-7) are wrapped around the β-sheet. The enzymatic metal binding site is located in similar position as *Pal*PNS (6JYV) and T7H (5C3Q), which is positioned toward the C-terminal end of protein and in close proximity to β10.

Supplementary Table S3: Top 30 structures similar to TropC from protein data bank (PDB) listed by DALI server[14]. Structure are ranked based on the Z-score value.

# No	Chain	Z-score	rmsd	%id	
1	6jyv-A	32.2	2.1	32	PROBABLE IRON/ASCORBATE OXIDOREDUCTASE;
2	5c3q-A	31.8	2.1	29	THYMINE DIOXYGENASE;
3	3oox-A	29.9	2.3	26	PUTATIVE 2OG-FE(II) OXYGENASE FAMILY PROTEIN;
4	1gp6-A	29.5	2.2	25	LEUCOANTHOCYANIDIN DIOXYGENASE;
5	5v2z-A	29.2	2.1	22	2-OXOGLUTARATE-DEPENDENT ETHYLENE/SUCCINATE-FORMI
6	5o7y-A	28.9	2.2	27	THEBAINE 6-O-DEMETHYLASE;
7	2vau-A	28.8	2.3	22	ISOPENICILLIN N SYNTHETASE;
8	4xae-A	27.9	2.4	31	FERULOYL COA ORTHO-HYDROXYLASE 1;
9	6tto-A	27.4	2.1	24	HYOSCYAMINE 6 BETA-HYDROXYLASE;
10	3on7-B	24.8	2.4	24	OXIDOREDUCTASE, IRON/ASCORBATE FAMILY;
11	5tcv-A	24.5	2.3	25	1-AMINOCYCLOPROPANE-1-CARBOXYLATE OXIDASE 1;
12	1unb-A	23.3	2.6	20	DEACETOXYCEPHALOSPORIN C SYNTHETASE;
13	5udb-8	19.8	2.4	13	DNA REPLICATION LICENSING FACTOR MCM2;
14	6n1f-D	14.4	3.2	11	OXIDOREDUCTASE, 2OG-FE(II) OXYGENASE FAMILY;
15	4kbz-A	13.3	3.6	16	EGL NINE HOMOLOG 1;
16	4iw3-A	13.2	2.9	16	PUTATIVE UNCHARACTERIZED PROTEIN;
17	5zm3-B	12.8	3.1	13	DIOXYGENASE ANDA;
18	4nhy-A	12.7	3.0	13	2-OXOGLUTARATE AND IRON-DEPENDENT OXYGENASE DOMAI
19	6ec3-C	12.4	3.2	11	METHYLTRANSFERASE DOMAIN-CONTAINING PROTEIN;
20	6iuq-B	12.4	3.1	15	PROLYL 4-HYDROXYLASE;
21	4xbz-C	12.3	2.8	12	EVDO1;
22	6nie-A	12.3	3.3	8	BESD, LYSINE HALOGENASE;
23	5erl-D	12.1	3.1	7	SNON,SNON;
24	5v1b-A	12.1	3.6	12	EGL NINE HOMOLOG 2;
25	4nao-A	12.1	3.7	13	PUTATIVE OXYGENASE;
26	3kt4-A	12.0	3.3	7	PKHD-TYPE HYDROXYLASE TPA1;
27	5nci-B	12.0	3.0	11	LEUCINE HYDROXYLASE;
28	4ie6-A	12.0	3.6	10	ALPHA-KETOGLUTARATE-DEPENDENT DIOXYGENASE FTO;
29	5ybm-A	11.9	3.4	11	PRHA;
30	5epa-A	11.9	3.5	9	SNOK;

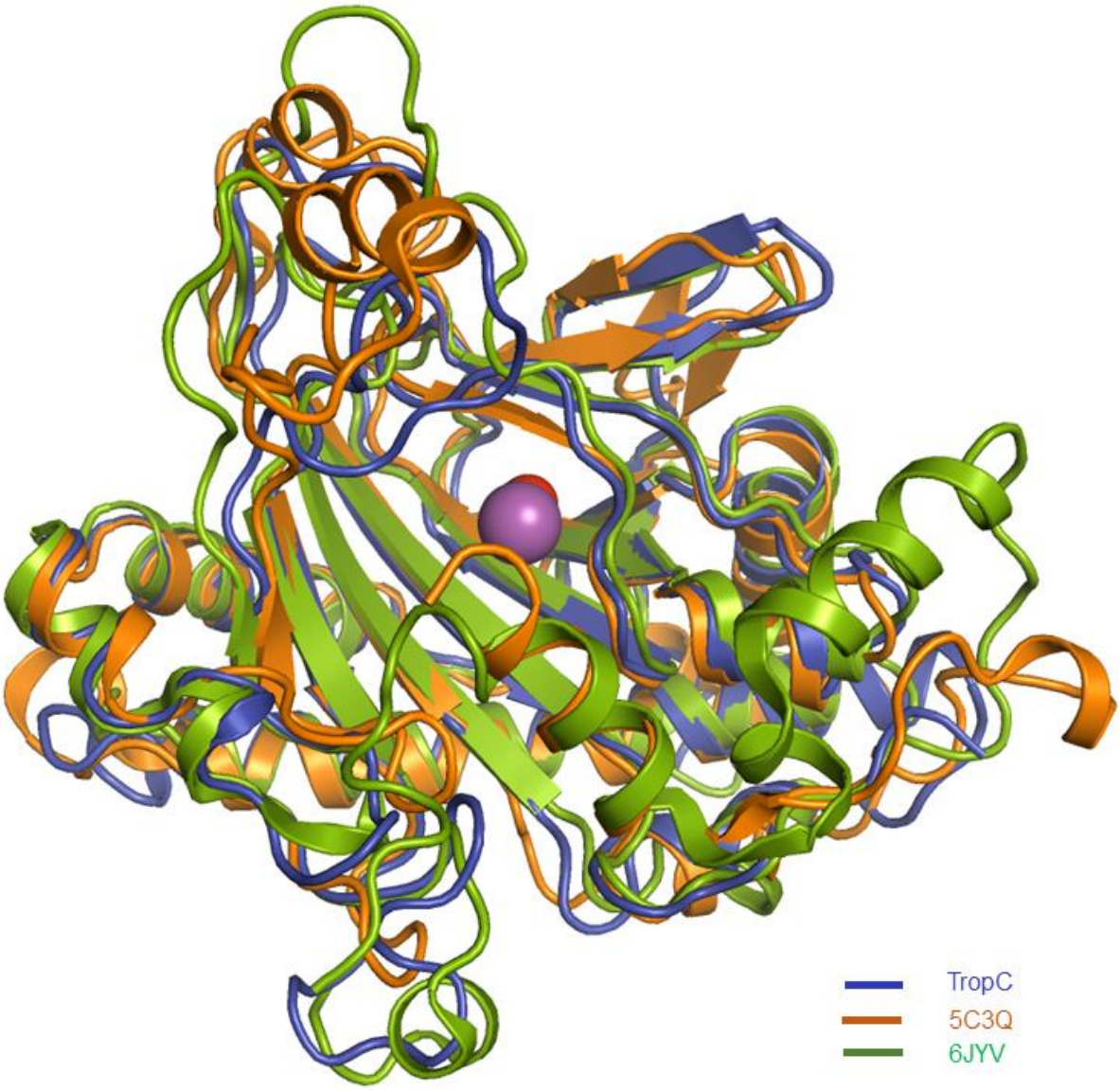

Supplementary Figure S30. Superimposition of TropC (PDB ID: 6XJJ) with isopenicillin N synthase from *Pseudomonas aeruginosa* PAO1 (*Pa*IPNS, PDB ID: 6JYV) and thymine-7-hydroxylase (T7H) of *Neurospora crassa* (PDB ID: 5C3Q).

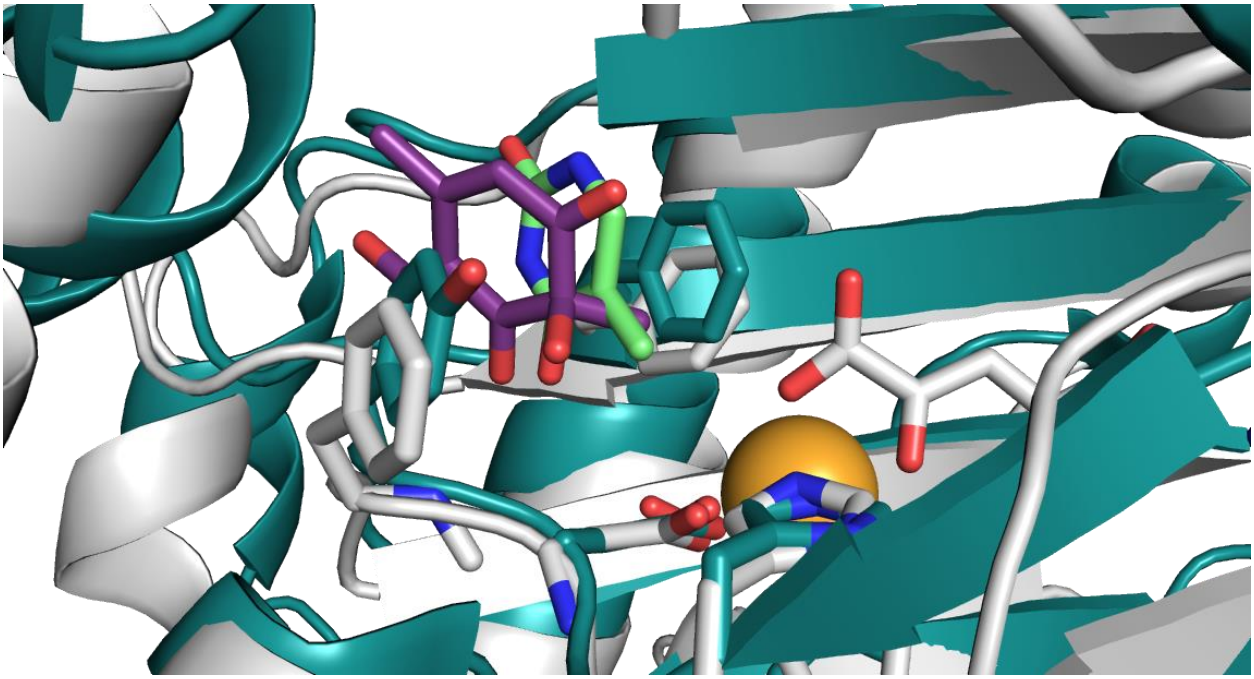

Supplementary Figure S31. Superimposition of TropC thymine-7-hydroxylase (T7H) of *Neurospora crassa* (PDB ID: 5C3Q). Close-up image of active site. TropC is pictured in grey with native substrate **10** in purple. T7H is pictured in teal with thymine shown in green.

Part VIV. Quantum mechanical (QM) analysis of TropC-catalyzed reactions

General Computational Details: All geometries and frequency computations were obtained using the unrestricted B3LYP density functional[15-16] and 6-311++G** basis set.[17-18] Reaction pathways were calculated using the single-ended growing string method.[19] Initial alignment of substrate and iron model was obtained using ZStruct.[20-22] All ground state geometries were confirmed to have no imaginary frequencies, and transition states were confirmed to have one imaginary frequency. Solvent corrections were performed using the SMD implicit solvent model (water)[23-25] and the cc-pVTZ basis set.[26-31] Reported energies are Gibbs free energies in solvent with gas-phase entropy and enthalpy corrections (at 298.15 K). Most simulations were performed using the Q-Chem 5.0 package,[32] except for the solvent computations, which were performed using ORCA 4.0.[33] A small non-heme iron model (Supplementary Figure S32) was used mimic the active site of TropC. Methylimidazoles represent histidine side chains, acetates represent aspartate side chains and succinate, respectively. A hydroxyl group was placed in a productive orientation for catalysis, and as a mimic of the Fe(III)-OH group after initial H-atom abstraction.

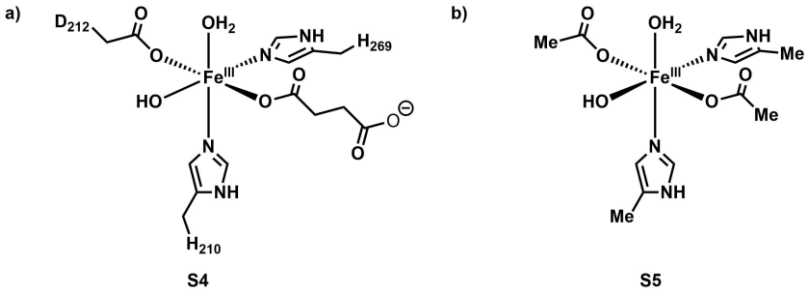

Supplementary Figure S32. Active-site model before (a) and after (b) truncation of His210, Asp212, His269 and succinate.

Part X. XYZ Coordinates for QM calculations

Integers preceding the coordinates represent the charge and multiplicity of the model, respectively.

Compound **14**

-1 2

C	-1.36405068	-1.04444925	0.16913242
C	-1.45915056	0.31190738	-0.26869486
C	-0.28554711	0.95947356	-0.85288205
C	1.09466613	0.30994795	-0.49075439
C	1.01915666	-1.23660759	-0.40613088
C	-0.19132751	-1.78476718	0.09622804
O	-0.30044119	1.98364475	-1.52269526
C	-2.66921645	1.09132468	-0.24942917
O	-3.78685400	0.76992397	0.17727125
O	2.09452996	0.67636495	-1.41848883
C	1.41357514	0.83748332	0.87600449
O	2.02539566	-1.87024130	-0.75775811
C	-2.59608233	-1.75803877	0.67311221
H	0.85725578	0.50641152	1.74369756
H	2.04446893	1.71572266	0.93543639
H	-2.52506060	2.10689144	-0.66221531
H	-3.39790032	-1.73035359	-0.06811200

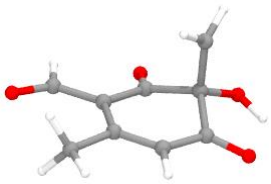

14

H	-3.00415839	-1.25585346	1.55358611
H	-2.36068665	-2.79609046	0.92170180
H	2.61511614	-0.14068631	-1.51516834
H	-0.20483860	-2.84690128	0.31666894

Compound **16**

-1 2

C	-1.32321465	-1.03988654	0.21419164
C	-1.39007402	0.32425418	-0.17447546
C	-0.18009975	1.04298777	-0.60439486
C	1.26948593	0.17963835	-0.46201451
C	1.05672415	-1.31453846	-0.41919394
C	-0.16039692	-1.80299589	0.12094035
O	-0.14164956	2.08361048	-1.28715414
C	-2.60283559	1.09865564	-0.21585736
O	-3.75096181	0.74966098	0.09616481
O	2.27250203	0.55020730	-1.33546093
C	1.07409494	0.99782463	0.70972805
O	1.97743103	-2.01000848	-0.90395541
C	-2.57108589	-1.75422595	0.68295646
H	0.65745715	0.57791273	1.61415998
H	1.55603390	1.96477056	0.73476049
H	-2.43421348	2.13590494	-0.56102868
H	-3.34757052	-1.73755859	-0.08530076
H	-3.01348004	-1.25411600	1.54812585
H	-2.33859154	-2.79054105	0.94265854
H	2.58639562	-0.30700825	-1.68045282
H	-0.21119599	-2.87162435	0.30082671

16

Compound **19**

-1 2

C	-2.51544722	-1.71261253	0.73291417
C	-1.31723648	-0.93897085	0.20358618
C	-0.19146631	-1.71504774	-0.01064276
C	1.09187639	-1.37259732	-0.56825818
O	1.86803001	-2.22061600	-1.11646024
C	1.59730649	-0.03726647	-0.45888863
C	0.96967314	1.05507017	0.30802773
C	-0.43814432	1.43606988	-0.21626141
O	-0.56398938	2.58604909	-0.65545511
C	-1.51185653	0.46793074	-0.08365824
C	-2.82907289	1.04187117	-0.26258200
O	-3.93577462	0.48863803	-0.22679102
O	2.80062695	0.16222538	-1.02297890
H	0.86430425	0.74632632	1.35888882
H	1.58410863	1.95342826	0.25823812
H	-2.78638526	2.12780156	-0.45781491
H	-3.30001380	-1.79170083	-0.02155678
H	-2.97696943	-1.19782104	1.57964654
H	-2.20810635	-2.71304784	1.04700828
H	3.00127970	-0.73918939	-1.38088968
H	-0.29581195	-2.78232256	0.16380103

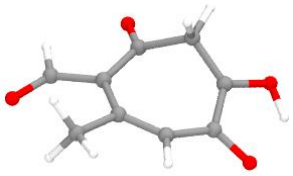

19

Compound **20**

-1 1

C	-2.21373926	-1.72739805	0.83750339
C	-1.22169769	-0.69199008	0.32730357
C	0.09972721	-1.12083985	0.39560405
C	1.32780725	-0.56850947	-0.10206171
O	2.40551081	-1.17106760	-0.06260436
C	1.33538123	0.86758082	-0.64930370
O	2.01827171	1.19075901	-1.59684813
C	0.46764691	1.83574440	0.11149114
C	-1.01396650	1.77850110	-0.33269154
O	-1.48195146	2.83216749	-0.77381117
C	-1.77185872	0.54880576	-0.15689623
C	-3.17865129	0.68808963	-0.49225195
O	-4.06912070	-0.16814836	-0.47660367
H	0.51511053	1.59164814	1.17939501
H	0.80738191	2.85482845	-0.06459116
H	-3.43231565	1.71294587	-0.81091656
H	-2.96065266	-1.27759343	1.49402980
H	-1.68738022	-2.52110903	1.37150574
H	-2.77855585	-2.16339358	0.01093572
H	0.25961745	-2.10733123	0.82185875

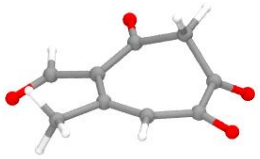

20

Compound **13**

-1 1

C	-1.29438791	-1.03884351	0.19797988
C	-1.45664211	0.30204921	-0.24074957
C	-0.28614153	1.11253935	-0.54693263
C	1.12812135	0.52401174	-0.27055120
C	1.16750040	-0.95953795	0.14290246
C	-0.04552971	-1.62914569	0.38223867
O	-0.33134983	2.26635259	-0.97033814
C	-2.74007501	0.94336319	-0.42549600
O	-3.86374138	0.46624630	-0.23605586
C	1.69247770	1.36284179	0.91047298
O	3.00885254	0.98292189	1.31003137
O	1.89184003	0.72827388	-1.45239656
O	2.30165941	-1.49085238	0.29768675
C	-2.50146428	-1.89908807	0.48386328
O	4.68512743	-0.43512533	-0.80821939
H	1.00220068	1.29934316	1.76333682
H	1.73893020	2.39772717	0.56975567
H	-2.64888075	1.98784727	-0.77129720
H	-3.13791803	-1.43995314	1.24338391
H	-2.19082307	-2.89303871	0.81419119
H	-3.13510154	-1.99021423	-0.40153735
H	2.77711864	0.35508475	-1.32492888
H	3.00227839	0.01382494	1.37952026
H	0.02123743	-2.66303475	0.70398755

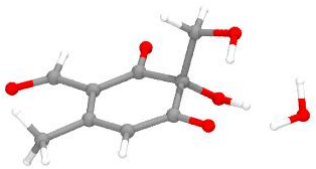

13

H	3.99032565	-1.03282560	-0.47279428
H	4.63979630	0.30785011	-0.19237772

Compound **21**

-1 1

C	1.66584328	1.14862049	0.72194060
C	1.30004206	0.14491849	-0.23662013
O	1.91202776	0.02791017	-1.39888957
C	1.06282759	-1.20094689	0.48678287
O	2.08057320	-1.74624542	0.96672238
C	-0.24340562	-1.73919809	0.60470045
C	-1.40296429	-1.05636302	0.28978850
C	-2.70139489	-1.78923268	0.53789581
C	-1.44637497	0.27329527	-0.24429853
C	-2.67461685	0.97038542	-0.57672242
O	-3.83632692	0.58286374	-0.42797168
C	-0.25281583	1.02406318	-0.54527983
O	-0.15790683	2.07435613	-1.13734568
O	3.53385955	0.53363876	1.34904372
O	4.29287218	0.85926760	-1.21462365
H	1.23776767	1.11346010	1.71723486
H	2.00458213	2.11284433	0.36258720
H	-2.49386048	1.97564377	-0.99804195
H	-3.33236126	-1.24856279	1.24668862
H	-2.50131297	-2.79311490	0.91897574
H	-3.29167932	-1.85644797	-0.37816810
H	3.31535772	0.55625621	-1.39838709
H	3.24256284	-0.41126905	1.30428002
H	-0.31373666	-2.73089249	1.04052893
H	4.84302630	0.19105141	-1.63226123
H	4.00578860	0.67669524	0.48571617

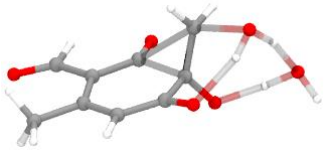

21

Compound **22**

-1 1

C	-2.25401026	-1.75617440	0.76590681
C	-1.25372999	-0.70106981	0.32139887
C	0.07508605	-1.14386310	0.40799575
C	1.31639352	-0.60605482	-0.01985828
O	2.37512390	-1.27049518	-0.00694604
C	1.42542246	0.85503036	-0.47758075
O	2.29103006	1.20339461	-1.25394801
C	0.45891698	1.82017907	0.15002069
C	-0.97693855	1.72907084	-0.41104900
O	-1.39320889	2.72609722	-0.99955866
C	-1.77906944	0.53762810	-0.15282249
C	-3.19794603	0.73707673	-0.42589698
O	-4.12109347	-0.07354403	-0.33774280
O	4.86330784	-0.51778568	-1.05924377
O	4.91999847	-1.37214971	1.73885531
H	0.41619932	1.60820485	1.22522267
H	0.80375699	2.83749599	-0.02474090
H	-3.42095547	1.76749496	-0.74948867

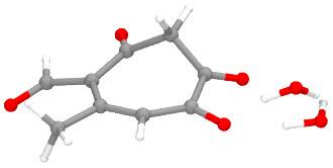

22

H	-3.00532217	-1.33874610	1.43741236
H	-1.73823427	-2.58255824	1.25743182
H	-2.81469026	-2.14238546	-0.08845610
H	4.73744343	0.37266880	-1.40237037
H	3.99137031	-1.55121921	1.54049150
H	0.20102893	-2.15734910	0.77681724
H	3.94644159	-0.78425808	-0.83687898
H	5.23217196	-1.00761762	0.89490779

Compound **11**

0 1

C	-0.85439202	1.68563917	-0.36326391
C	-1.71234651	0.57156895	-0.12297394
C	1.48873710	0.78367638	-0.12003378
C	1.27938417	-0.65675756	0.20366492
C	-0.01113898	-1.26007927	0.32683275
C	-1.29011572	-0.77202637	0.19606475
C	0.56378187	1.75399660	-0.35401837
C	-3.14061480	0.83110182	-0.21475631
C	-2.37273202	-1.81997771	0.42451121
O	2.77708068	1.09680858	-0.17161068
O	2.32762589	-1.30416952	0.36305958
O	-1.38797411	2.86594568	-0.64431437
O	-3.65784830	1.92692051	-0.47532417
H	-3.03803062	-1.54766948	1.24823117
H	-1.91997812	-2.77835817	0.67123625
H	-2.99143547	-1.96737555	-0.46514929
H	0.95137246	2.74303070	-0.57229337
H	3.23891283	0.24595211	0.02701084
H	-3.81593197	-0.01150886	-0.03992552
H	0.08284370	-2.31234044	0.57117286
H	-2.39177514	2.76887516	-0.64196393

11

Compound **13**

-1 1

C	1.32100899	0.26418288	-0.37478702
C	1.27503132	-1.26558389	-0.26315958
C	0.03045125	-1.79757631	0.20637017
C	-1.14395862	-1.07343043	0.23351158
C	-1.23059529	0.28569895	-0.23399977
C	-0.03861443	0.90398429	-0.74002563
O	2.27669274	-1.95204738	-0.49773944
C	-2.38789320	-1.77718379	0.71705182
C	-2.44957813	1.05112473	-0.32237119
O	-3.58777062	0.72138462	0.02760597
O	0.03089452	1.94226218	-1.42068726
O	2.28173262	0.70199434	-1.32857826
C	1.69489141	0.84953305	1.03081984
O	2.85009581	0.29511280	1.62104940
O	4.68862162	-0.48210547	-0.51191699
H	0.87353172	0.68013974	1.73009939
H	1.80551853	1.93268382	0.87518461

13

H	-2.28945230	2.05868538	-0.74970151
H	-2.83054447	-1.24764455	1.56430175
H	-2.15493678	-2.80356802	1.01050947
H	-3.16159704	-1.78226632	-0.05407308
H	1.83497112	1.46301019	-1.74962220
H	3.56130334	0.20120437	0.96102703
H	0.02730673	-2.84789842	0.47672019
H	4.04983114	-1.22147756	-0.51673861
H	4.21408402	0.14600479	-1.07664368

Compound **23**

23

-1 1

C	1.31544095	0.27238757	-0.44239450
C	1.26896676	-1.19486812	-0.25018860
C	0.06980728	-1.78134729	0.14701800
C	-1.13701692	-1.07166703	0.19711175
C	-1.22106789	0.27897950	-0.21184467
C	-0.02489527	0.91324595	-0.73086785
O	2.34144262	-1.92369798	-0.35754406
C	-2.35933824	-1.81544666	0.66973084
C	-2.44120786	1.05937986	-0.23347677
O	-3.56471301	0.70878914	0.13193907
O	0.00047277	1.98172078	-1.36409411
O	2.25802968	0.68468323	-1.41828891
C	1.80144293	0.93920762	1.04519690
O	2.96674894	0.48050515	1.49516454
O	4.42339843	-0.57819943	-0.16190066
H	0.95413742	0.75848951	1.73204013
H	1.79523876	2.00842273	0.74573894
H	-2.28880013	2.08538671	-0.61438480
H	-2.79046559	-1.33459338	1.55137398
H	-2.10918695	-2.85159129	0.90845732
H	-3.14908486	-1.79251208	-0.08474810
H	1.84179221	1.48159255	-1.79497589
H	3.87781263	-0.02528555	0.60470743
H	0.09257052	-2.83097338	0.41542866
H	3.25625638	-1.37169427	-0.37636340
H	4.40504843	0.02718918	-0.91178226

Compound **24**

-1 1

C	1.16226593	-0.04795429	-0.98214112
C	1.18881948	-1.33768179	-0.49907100
C	-0.00017014	-1.88049954	0.04972638
C	-1.16943847	-1.14736563	0.13037308
C	-1.20336571	0.20473908	-0.33737424
C	-0.01271755	0.78131956	-0.91318224
O	2.29130145	-2.14375757	-0.53037436
C	-2.39159886	-1.80329367	0.73165138
C	-2.37263483	1.05537297	-0.28788378
O	-3.49068253	0.78525442	0.16136253
O	0.12393779	1.96809539	-1.37292856
O	2.23187594	0.57561537	-1.59975804
O	4.48499912	-0.31823596	-0.31519501
O	3.01207510	0.80213915	2.05969664
C	1.93463272	1.20509940	1.67293292
H	1.00022317	0.94994854	2.20354846
H	1.83032420	1.86379817	0.79620664
H	-2.18951108	2.05810626	-0.71587995
H	-2.75271039	-1.25666992	1.60645557
H	-2.15818767	-2.83160957	1.02386019
H	-3.22795064	-1.81423397	0.02786833
H	1.81388514	1.45014988	-1.81582363
H	4.31850864	0.02660594	0.57448182
H	0.04264983	-2.89972257	0.41740736
H	3.11111898	-1.61114950	-0.55856107
H	3.89485639	0.21868083	-0.87674231

24

Compound **18**

0 1

C	0.41330517	0.08871090	-0.20328194
C	-0.88184378	-0.28298158	0.24161843
C	1.15856433	-0.76712725	-1.00694048
C	0.62833964	-1.99918700	-1.37605378
C	-0.65056107	-2.38070180	-0.94358524
C	-1.41335529	-1.54630579	-0.14458297
O	2.41159037	-0.44488187	-1.45791220
O	1.34079278	-2.84275506	-2.15762872
O	0.99437284	1.26314146	0.11336597
C	-1.60659284	0.64809196	1.07647815
O	-1.17070395	1.74970047	1.42930754
H	-2.60995103	0.34626573	1.41425796
C	-2.78777252	-2.00001197	0.29432678
H	-3.57178132	-1.31586967	-0.04271847
H	-2.86519466	-2.07884881	1.38271306
H	-3.00598565	-2.98315735	-0.12373088
H	2.64348183	0.43161154	-1.12287824
H	2.19054396	-2.42968112	-2.36537576
H	-1.02444142	-3.34884992	-1.25423749
H	0.35489495	1.76110362	0.68487562

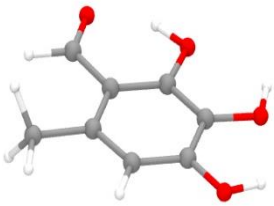

18

[Fe^{III}]

0 4

C	38.23926701	38.29629874	29.53710554
N	37.51798914	36.53354383	31.20562786
H	36.57979369	36.42065883	30.85451949
C	38.47794332	37.40109561	30.70591902
C	38.04802096	35.87599426	32.27156015
H	37.52185157	35.15020117	32.86958055
N	39.28494611	36.26706861	32.47751634
C	39.56590086	37.21519536	31.51655407
H	40.52482129	37.70584044	31.48585394
C	43.17144571	38.99031542	34.13308757
C	42.29929121	37.89270308	34.72239123
O	41.81177984	37.05054528	33.86259073
O	42.10233410	37.85427623	35.94139009
C	42.35063634	31.20755424	31.36745326
N	43.24710579	33.45069629	32.12753254
H	44.18388292	33.32551282	31.77660085
C	42.20717619	32.53510038	32.03066067
C	42.80204263	34.54207495	32.79466044
H	43.39294733	35.41270229	33.02047687
N	41.53826112	34.38048108	33.12648486
C	41.15541594	33.13769466	32.66220200
H	40.15958826	32.76864523	32.83712342
Fe	40.45422521	35.67867455	34.27965033
O	41.76393178	35.02188784	35.96638579
H	41.91088933	35.86532866	36.42605115
H	41.08838887	34.50407100	36.47718862
O	39.64345087	33.64057732	36.74668694
C	38.90092945	33.66328621	35.75878925
O	39.18269509	34.21179155	34.61874976
C	37.53237688	33.00691561	35.82810828
O	39.47350152	36.73538467	35.34864171
H	43.37302269	38.82858090	33.07435629
H	44.10751694	39.04958309	34.69209629
H	42.65822947	39.94753440	34.25938393
H	43.11736403	30.59335687	31.85068902
H	42.61405175	31.30528297	30.30919715
H	41.40657325	30.66468441	31.42637224
H	38.00518255	37.73104235	28.62875809
H	39.13480814	38.88665977	29.33901725
H	37.41555410	38.99416356	29.72014118
H	37.27644531	32.52731764	34.88140651
H	36.78976652	33.78715730	36.02249251
H	37.49881859	32.28424651	36.64273759
H	40.04210171	37.39867676	35.76639073

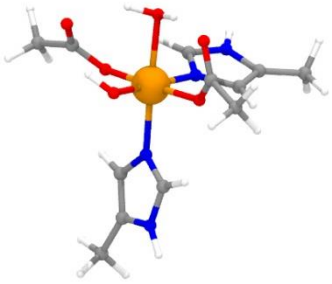

[Fe^{III}]

[Fe^{II}]

0 5

C	38.00896528	38.60216009	29.69941967
N	37.44311767	36.57497726	31.10723864
H	36.54072433	36.39738663	30.69423179
C	38.31091978	37.60279442	30.76403270
C	38.00814300	35.85188438	32.10860738
H	37.55700287	34.99686361	32.58628125
N	39.18365426	36.35258700	32.42217182
C	39.38424709	37.44098206	31.59759418
H	40.28446955	38.02884196	31.67266600
C	43.41914438	38.92014552	34.22782020
C	42.37756387	37.87552887	34.60258657
O	41.92761656	37.12994751	33.67064669
O	42.02355685	37.80990186	35.80655036
C	42.67677952	30.91175014	31.56208238
N	43.31056064	33.34787845	31.84365942
H	44.20186027	33.28922231	31.37617348
C	42.42062681	32.30082291	32.04018472
C	42.78370610	34.46959952	32.39942085
H	43.25848974	35.43774302	32.40695228
N	41.61239275	34.20336176	32.93598990
C	41.37437380	32.86052796	32.72218952
H	40.46981128	32.39741540	33.08122287
Fe	40.42007432	35.63146877	34.03791049
O	41.50236339	35.06648185	35.92094104
H	41.82624773	35.94452257	36.20268891
H	40.74049714	34.84705401	36.49473509
O	38.88011645	34.59535533	36.68499048
C	38.49125303	33.95855439	35.67381698
O	38.91179853	34.15450913	34.48556742
C	37.44625394	32.87164224	35.87981002
O	39.37128366	37.05835820	35.43679881
H	43.66423760	38.88583723	33.16633306
H	44.32129016	38.75931581	34.82349839
H	43.04003076	39.91218399	34.48621897
H	43.58396715	30.48771493	32.00529078
H	42.78229310	30.86608781	30.47287584
H	41.84086406	30.26930209	31.84161017
H	37.88323416	38.13085291	28.71888556
H	38.83105670	39.31483774	29.62206095
H	37.09824332	39.16945284	29.91861256
H	37.13523466	32.42476027	34.93556981
H	36.58154758	33.29282079	36.39810905
H	37.86155953	32.09724618	36.53044688
H	40.14321330	37.52446195	35.81591985
H	39.05735289	36.43225593	36.11794302

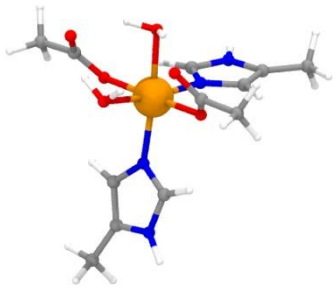

[Fe^{II}]

[Fe^{II}_{W}]

1 5

C	38.29039775	38.83670376	29.75970800
N	37.53658237	36.77152669	31.01303247
H	36.64900671	36.67456191	30.54167423
C	38.47470056	37.76259298	30.77755892
C	37.99765570	35.95779952	31.99438327
H	37.46624044	35.10388307	32.38327543
N	39.18400406	36.36718042	32.40646501
C	39.49047876	37.49087017	31.65574539
H	40.41310258	38.02923278	31.79963147
O	41.85072243	36.97229884	34.00977936
C	43.57033631	31.09423871	32.04199166
N	42.31206030	33.04076490	31.02418044
H	42.52637202	32.81918015	30.06272176
C	42.73306810	32.32422057	32.13438580
C	41.56117085	34.08597233	31.44022500
H	41.10549373	34.80007754	30.77370156
N	41.47280941	34.09040688	32.75946760
C	42.19988722	32.99525887	33.20039016
H	42.27404820	32.76830220	34.25038761
Fe	40.30225156	35.37404145	33.97139581
O	41.34696423	34.47121405	35.85400523
H	42.05698111	34.85023568	36.38219507
H	40.55814752	34.42433131	36.44137962
O	38.78087868	34.65033772	36.67645302
C	38.26068040	34.08817947	35.67774007
O	38.69486787	34.25298052	34.48107801
C	37.08552476	33.16530788	35.88259347
O	39.65143149	36.94327308	35.57106427
H	44.52848132	31.29140487	31.55179241
H	43.06194389	30.30230089	31.48388474
H	43.77916042	30.71432595	33.04216421
H	38.17329681	38.42358495	28.75336053
H	39.16047797	39.49362371	29.75134665
H	37.41096354	39.45129745	29.97460169
H	36.64628194	32.85713869	34.93562238
H	36.33978036	33.65398027	36.51211032
H	37.42898568	32.28031518	36.42529186
H	38.94075657	37.55949548	35.36168237
H	39.27579006	36.28775687	36.20999533
H	42.80309956	36.90259275	33.88383372
H	41.67882363	37.51081912	34.79463246

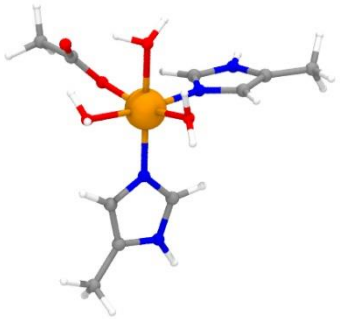

[Fe^{II}_{W}]

Part XI. Molecular dynamics (MD) simulations

Model Construction

To construct the model of TropC, we used the partial crystal structure described in this report and the Modeller software to model the C-terminal region for which no density was observed in X-ray crystallography experiments.[34] To develop a homology model for this region, we submitted the TropC amino acid sequence to the RCSB PDB[35] and JPred4 server for secondary structure prediction. These programs indicated that thebaine 6-O-demthylase crystal structure (PDB ID: 5O7Y, 27% sequence identity, Pymol superalign Cα-RMSD: 4.378) as the closest predicted related structure.[5, 36] Based on the structure prediction results, residues 307-323 of the C-terminal region were modeled as a helix.

To generate an initial substrate-bound structure for MD simulations, further analysis of the RCSB PDB structure revealed that non-heme iron enzyme thymine-7-hydroxylase (T7H) possesses structural similarity to the *apo* crystal structure of TropC (PDB ID: 5C3Q, 28% sequence identity, Pymol superalign Cα-RMSD: 3.139).[37] The deposited crystal structure of T7H was co-crystallized with substrate, nickel, and α-KG. In addition, similarities between the native substrates of TropC and T7H are evident. They are both small, cyclic substrates with a similar substitution pattern of a methyl group ortho to a hydroxyl group. To establish an initial substrate-bound structure for MD simulations, we overlaid the TropC coordinates with the T7H substrate, co-substrate and Fe coordinates. We then computationally replaced thymine with TropC native substrate **10** and converted the nickel atom to an iron atom to prepare our model for MD simulations.

System Preparation

We submitted the TropC model coordinates to the CHARMM-gui for addition of all hydrogen atoms and protons, which were added according to their canonical protonation states.[38] These protonation states were determined based on the use of the Propka-3.1 software.[39-40] The tautomeric forms of histidine were assigned to maximize hydrogen bonds. To obtain an overall electrically-neutral charge model, 47 potassium and 42 chlorine atoms were added. A water box was used with periodic boundary conditions, and the particle mesh Ewald method was used to describe long-range electrostatic effects. Dimensions of the water box were established to fit the largest dimension of the protein plus 10 Å. All water molecules within 2.8 angstroms of heavy atoms were removed. The final model contained 53,819 atoms. Parameters for the substrate were obtained using CGenFF 4.0.[41-42] Parameters for iron were obtained from those described by Pang and coworkers.[43] A restrained active site was used (50 kcal/molÅ^2 force constant), in which the restraints were based off of crystal structure distances. Included in these restraints were a positional restraint on residue Phe213 to more closely resemble that of the complimentary residue in 5C3Q to maintain closure of the active site, and restraints based on H-bonds within the active site. A 5000 step molecular mechanics (MM) minimization was then was performed using the steepest decent algorithm using the CHARMM36 force field.[44]

MD Simulations

Simulations were performed with the OpenMM/CHARMM interface (version c42b1) using periodic boundary conditions, particle mesh Ewald for long range electrostatic interactions, and a Langevin thermostat (friction coefficient = 5).[45] A three-step MD protocol was used to obtain the pose described in the main text, which all used a 2 fs timestep. The first phase slowly heated the model from 10K to 298 K over 500 ps and included the restrained active site as well as harmonic restraints of 10.0 kcal mol/Å^{-2} on all heavy atoms of the solute. The harmonic restraints were then removed, and temperature was kept constant for an additional 500 ps. The MD simulations were performed for 11 ns, with the first ns used for equilibration.

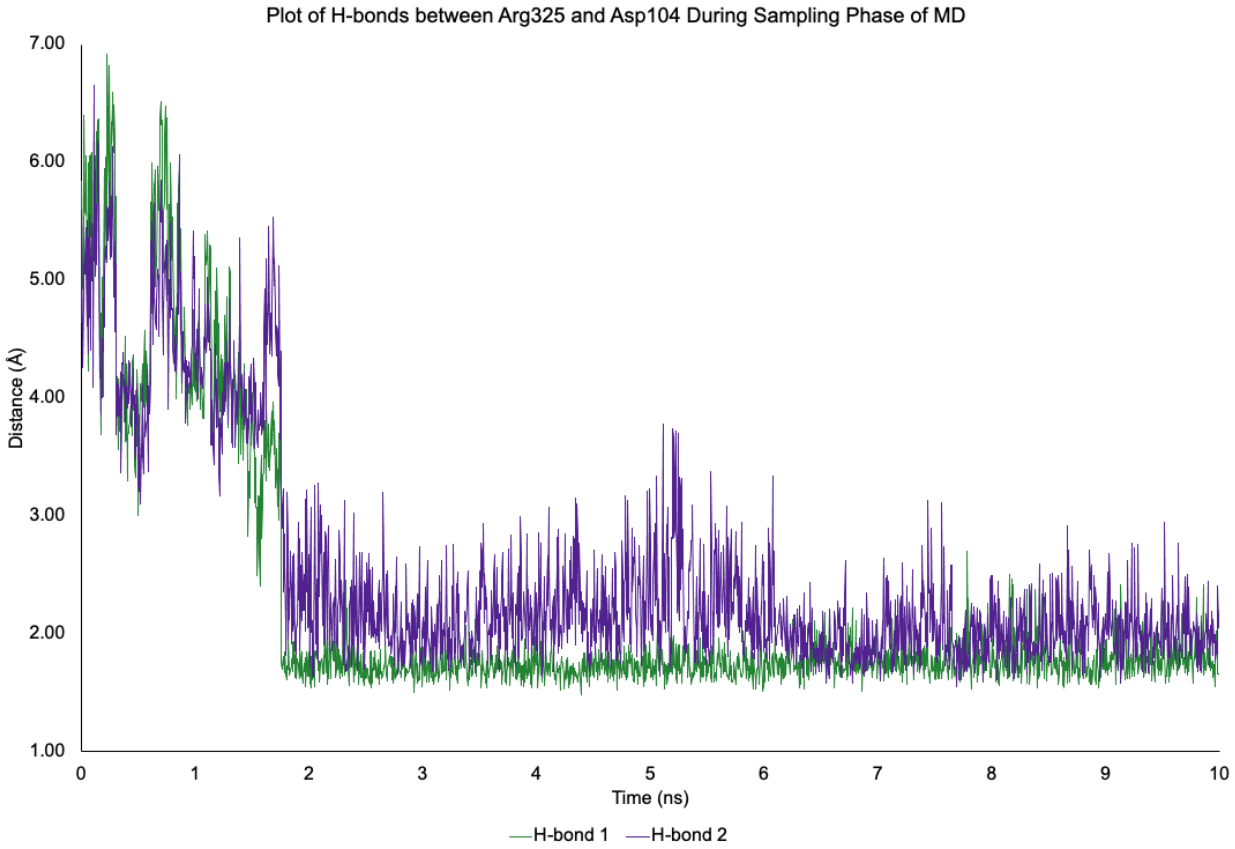

Supplementary Figure S33. Tracking H-bond distance between Arg325 and Asp104 throughout the final 10 ns of sampling (MD). First contact begins, and remains, after ~1.75 ns.

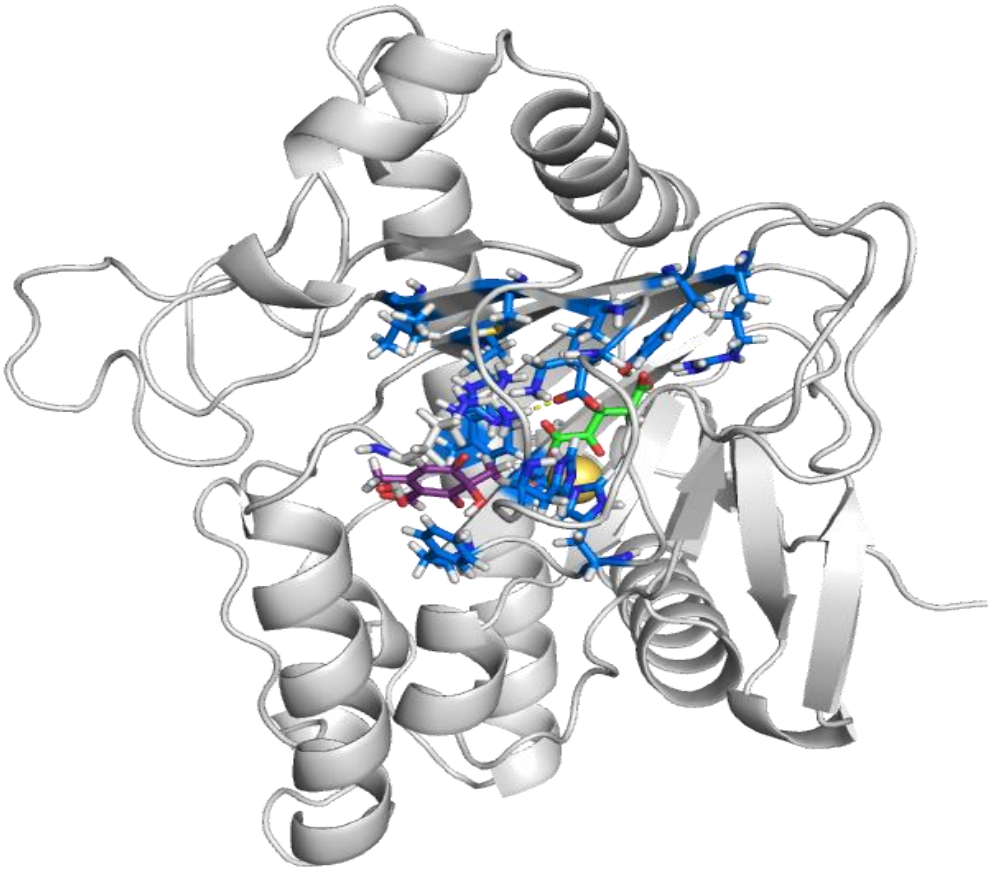

Supplementary Figure S34. Full image of TropC with substrate bound from the final frame of MD simulation. Residues chosen for alanine screening mutagenesis are shown in blue, substrate **10** is shown in purple, cofactor α-ketoglutarate is shown in green and ferrous iron is shown in light brown.

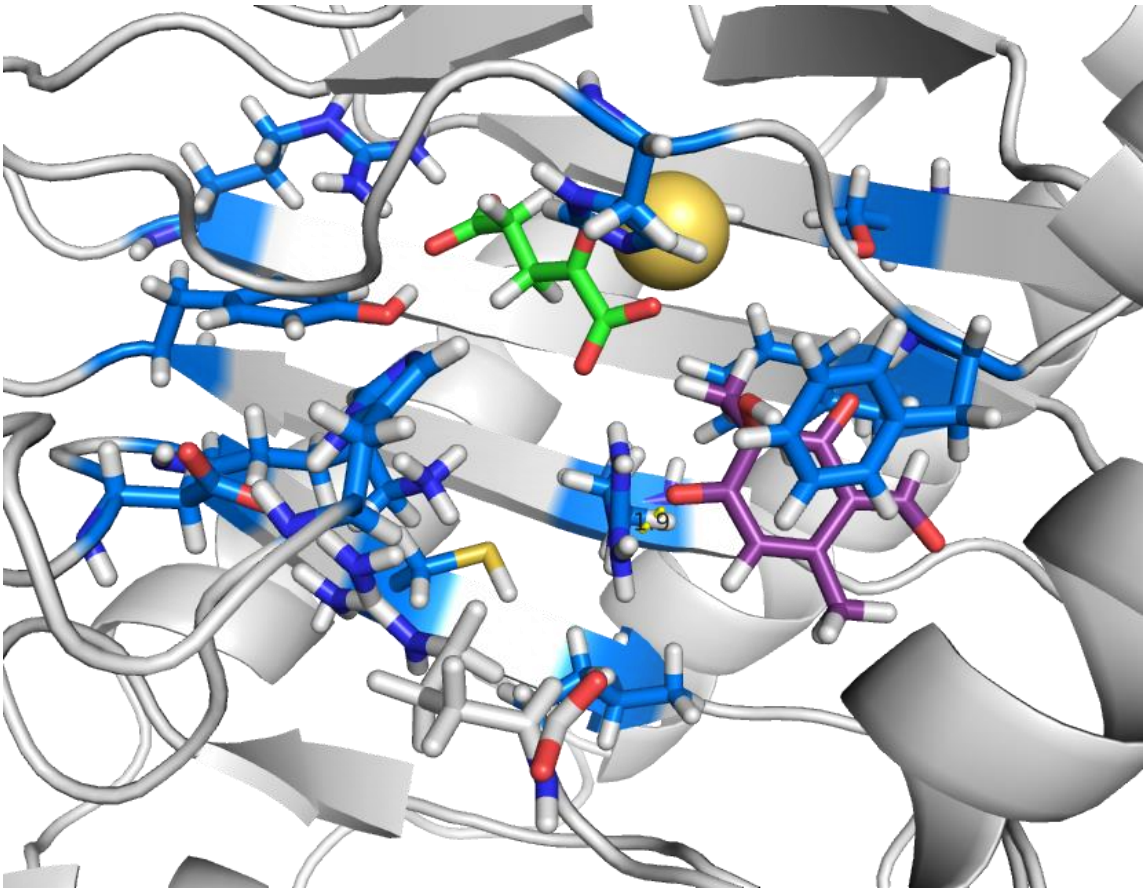

Supplementary Figure S35. Close-up image of TropC active site with substrate bound from the final frame of MD simulation. The hydrogen bonding distance between R186 and substrate **10** is shown. Residues chosen for alanine screening mutagenesis are shown in blue, substrate **10** is shown in purple, cofactor α-ketoglutarate is shown in green and ferrous iron is shown in light brown.

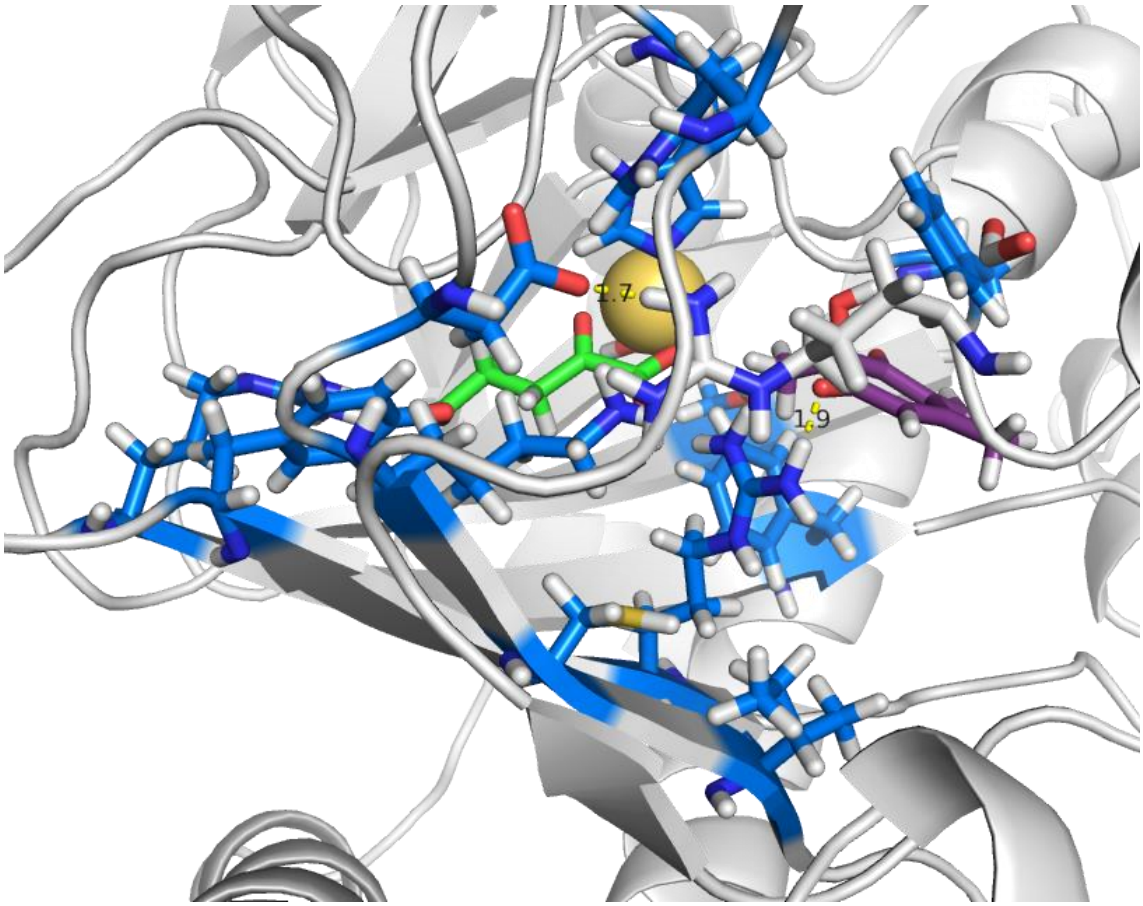

Supplementary Figure S36. Close-up image of TropC active site with substrate bound from the final frame of MD simulation. The hydrogen bonding distance between D100 and R325 is shown. Residues chosen for alanine screening mutagenesis are shown in blue, substrate **10** is shown in purple, cofactor α-ketoglutarate is shown in green and ferrous iron is shown in light brown.

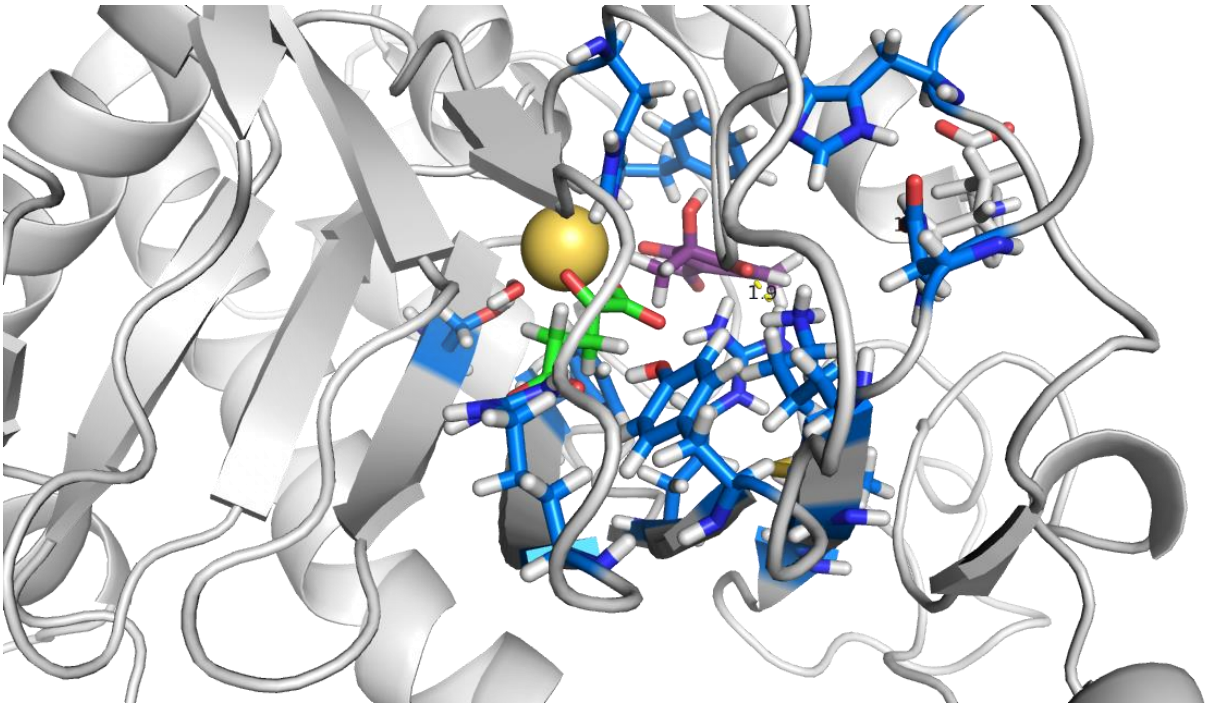

Supplementary Figure S37. Close-up image of TropC active site with substrate bound from the final frame of MD simulation. Residues chosen for alanine screening mutagenesis are shown in blue, substrate **10** is shown in purple, cofactor α-ketoglutarate is shown in green and ferrous iron is shown in light brown.

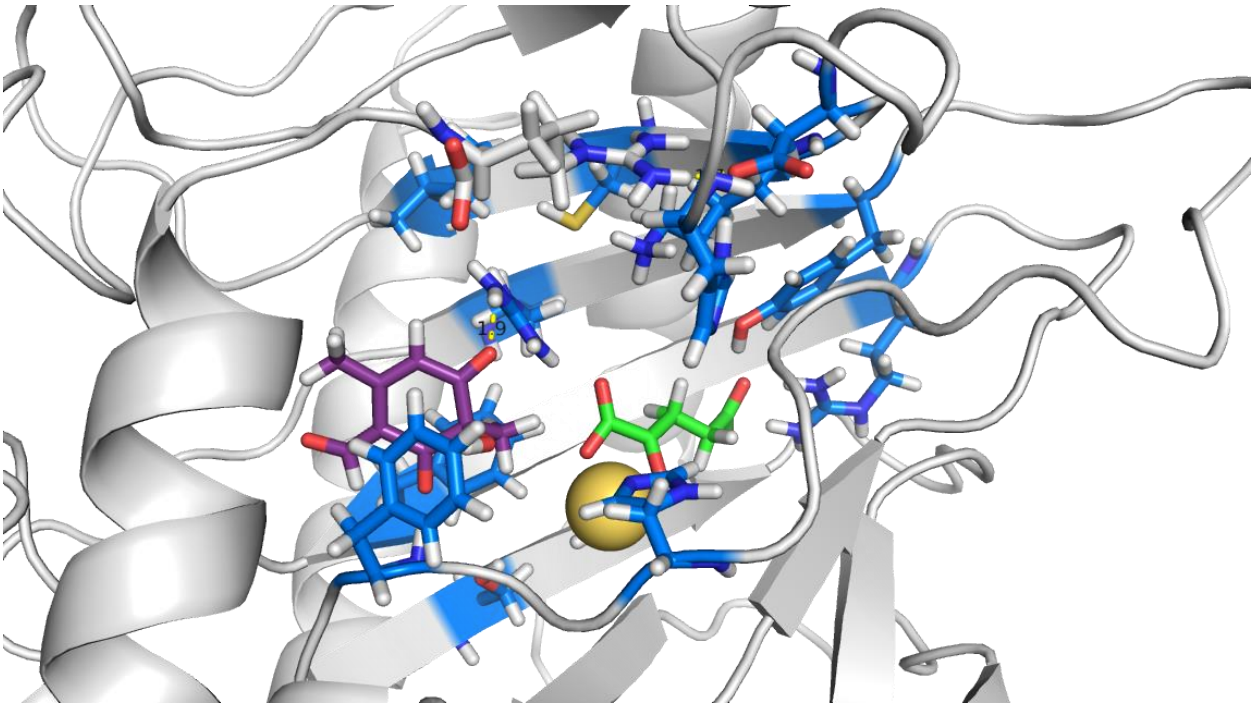

Supplementary Figure S38. Close-up image of TropC active site with substrate bound from the final frame of MD simulation. Residues chosen for alanine screening mutagenesis are shown in blue, substrate **10** is shown in purple, cofactor α-ketoglutarate is shown in green and ferrous iron is shown in light brown.

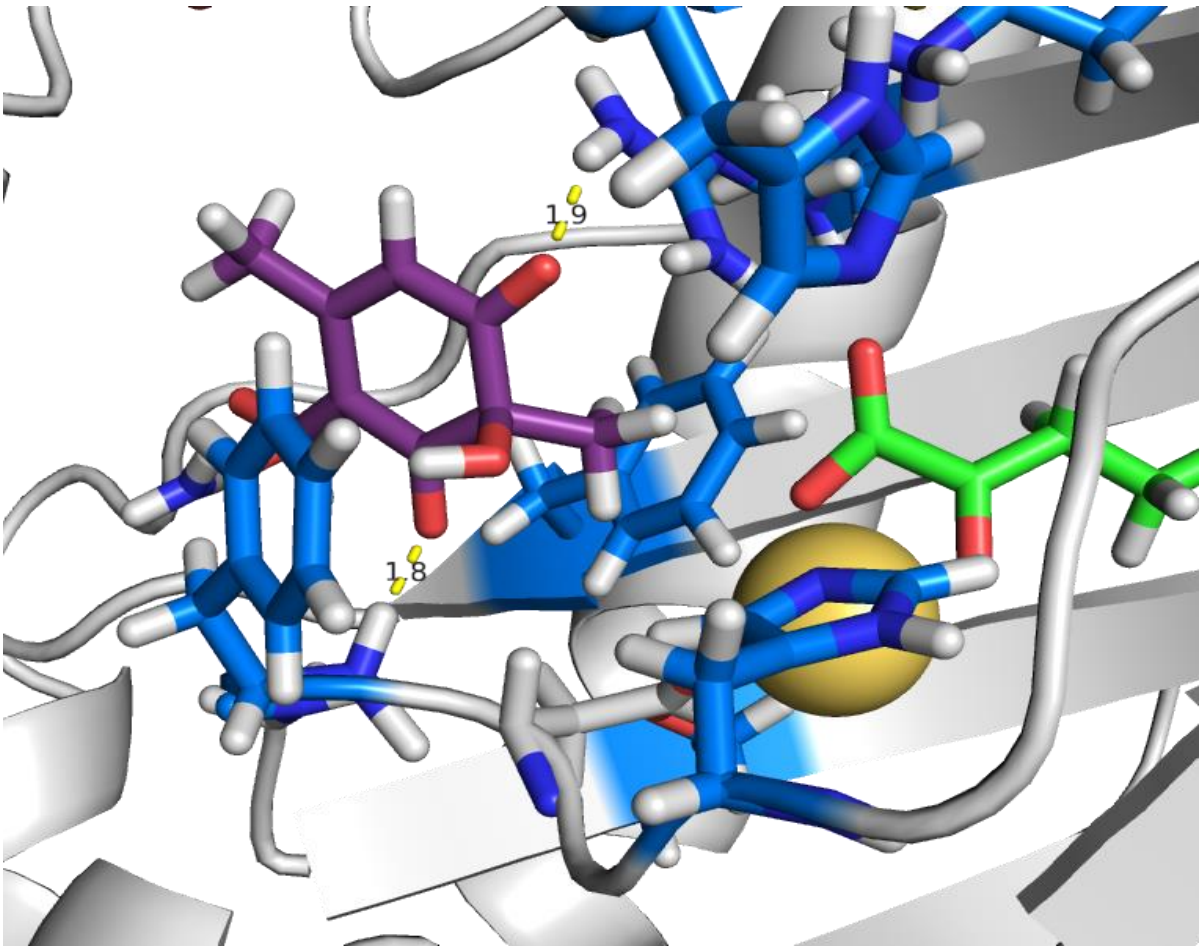

Supplementary Figure S39. Observed 2-point binding between the amide backbone nitrogen of F213, substrate **10** and guanidinium nitrogen of R190 from the final frame of MD simulation. Residues chosen for alanine screening mutagenesis are shown in blue, substrate **10** is shown in purple, cofactor α-ketoglutarate is shown in green and ferrous iron is shown in light brown.

Part XVII. References

1. Baker Dockrey, S. A.; Lukowski, A. L.; Becker, M. R.; Narayan, A. R. H., Biocatalytic site- and enantioselective oxidative dearomatization of phenols. *Nat. Chem.* **2018,** *10* (2), 119-125.
2. Doyon, T. J.; Perkins, J. C.; Baker Dockrey, S. A.; Romero, E. O.; Skinner, K. C.; Zimmerman, P. M.; Narayan, A. R. H., Chemoenzymatic o-Quinone Methide Formation. *J. Am. Chem. Soc.* **2019,** *141* (51), 20269-20277.
3. Davison, J.; al Fahad, A.; Cai, M.; Song, Z.; Yehia, S. Y.; Lazarus, C. M.; Bailey, A. M.; Simpson, T. J.; Cox, R. J., Genetic, molecular, and biochemical basis of fungal tropolone biosynthesis. *Proc. Natl. Acad. Sci. U.S.A.* **2012,** *109* (20), 7642-7647.
4. Cacioli, P.; Reiss, J., Reactions of 1-Oxaspiro[2.5]octa-5,7-dien-4-ones with nucleophiles. *Australian Journal of Chemistry* **1984,** *37* (12), 2525-2535.
5. Drozdetskiy, A.; Cole, C.; Procter, J.; Barton, G. J., JPred4: a protein secondary structure prediction server. *Nucleic Acids Research* **2015,** *43* (W1), W389-W394.
6. Vagin, A.; Teplyakov, A., Molecular replacement with MOLREP. *Acta Crystallogr. D. Biol. Crystallogr.* **2010,** *66* (Pt 1), 22-5.
7. Li, W.; Zhang, T.; Ding, J., Molecular basis for the substrate specificity and catalytic mechanism of thymine-7-hydroxylase in fungi. *Nucl. Acids Res.* **2015,** *43* (20), 10026-38.
8. Emsley, P.; Cowtan, K., Coot: model-building tools for molecular graphics. *Acta Crystallogr. D Biol. Crystallogr.* **2004,** *60* (Pt 12 Pt 1), 2126-32.
9. Murshudov, G. N.; Vagin, A. A.; Dodson, E. J., Refinement of macromolecular structures by the maximum-likelihood method. *Acta Crystallogr. D Biol. Crystallogr.* **1997,** *53* (Pt 3), 240-55.
10. Vagin, A. A.; Steiner, R. A.; Lebedev, A. A.; Potterton, L.; McNicholas, S.; Long, F.; Murshudov, G. N., REFMAC5 dictionary: organization of prior chemical knowledge and guidelines for its use. *Acta Crystallogr. D Biol. Crystallogr.* **2004,** *60* (Pt 12 Pt 1), 2184-95.
11. Winn, M. D.; Ballard, C. C.; Cowtan, K. D.; Dodson, E. J.; Emsley, P.; Evans, P. R.; Keegan, R. M.; Krissinel, E. B.; Leslie, A. G.; McCoy, A.; McNicholas, S. J.; Murshudov, G. N.; Pannu, N. S.; Potterton, E. A.; Powell, H. R.; Read, R. J.; Vagin, A.; Wilson, K. S., Overview of the CCP4 suite and current developments. *Acta Crystallogr. D Biol. Crystallogr.* **2011,** *67* (Pt 4), 235-42.
12. Chen, V. B.; Arendall, W. B., 3rd; Headd, J. J.; Keedy, D. A.; Immormino, R. M.; Kapral, G. J.; Murray, L. W.; Richardson, J. S.; Richardson, D. C., MolProbity: all-atom structure validation for macromolecular crystallography. *Acta Crystallogr. D Biol. Crystallogr.* **2010,** *66* (Pt 1), 12-21.
13. The PyMOL Molecular Graphics System, V., Schrödinger, LLC.
14. Holm, L.; Rosenstrom, P., Dali server: conservation mapping in 3D. *Nucl. Acids Res.* **2010,** *38,* W545-9.
15. Becke, A. D., Density-functional thermochemistry. III. The role of exact exchange. *J. Chem. Phys.* **1993,** *98* (7), 5648-5652.
16. Lee, C.; Yang, W.; Parr, R. G., Development of the Colle-Salvetti correlation-energy formula into a functional of the electron density. *Phys. Rev. B* **1988,** *37* (2), 785-789.
17. Krishnan, R.; Binkley, J. S.; Seeger, R.; Pople, J. A., Self-consistent molecular orbital methods. XX. A basis set for correlated wave functions. *J. Chem. Phys.* **1980,** *72* (1), 650-654.

18. Clark, T.; Chandrasekhar, J.; Spitznagel, G. W.; Schleyer, P. V. R., Efficient diffuse function-augmented basis sets for anion calculations. III. The 3-21+G basis set for first-row elements, Li–F. *J. Comput. Chem.* **1983,** *4* (3), 294-301.
19. Zimmerman, P. M., Single-ended transition state finding with the growing string method. *J. Comput. Chem.* **2015,** *36* (9), 601-611.
20. Zimmerman, P. M., Automated discovery of chemically reasonable elementary reaction steps. *Journal of Computational Chemistry* **2013,** *34* (16), 1385-1392.
21. Zimmerman, P. M., Navigating molecular space for reaction mechanisms: an efficient, automated procedure. *Molecular Simulation* **2015,** *41* (1-3), 43-54.
22. Zimmerman, P., Reliable Transition State Searches Integrated with the Growing String Method. *Journal of Chemical Theory and Computation* **2013,** *9* (7), 3043-3050.
23. Marenich, A. V.; Cramer, C. J.; Truhlar, D. G., Universal Solvation Model Based on Solute Electron Density and on a Continuum Model of the Solvent Defined by the Bulk Dielectric Constant and Atomic Surface Tensions. *J. Phys. Chem. B* **2009,** *113* (18), 6378-6396.
24. Marenich, A. V.; Olson, R. M.; Kelly, C. P.; Cramer, C. J.; Truhlar, D. G., Self-Consistent Reaction Field Model for Aqueous and Nonaqueous Solutions Based on Accurate Polarized Partial Charges. *J. Chemical Theory Comput.* **2007,** *3* (6), 2011-2033.
25. Marenich, A. V.; Cramer, C. J.; Truhlar, D. G., Generalized Born Solvation Model SM12. *J. Chem. Theory Comput.* **2013,** *9* (1), 609-620.
26. Jr., T. H. D., Gaussian basis sets for use in correlated molecular calculations. I. The atoms boron through neon and hydrogen. *J. Chem. Phys.* **1989,** *90* (2), 1007-1023.
27. Wilson, A. K.; Woon, D. E.; Peterson, K. A.; Jr., T. H. D., Gaussian basis sets for use in correlated molecular calculations. IX. The atoms gallium through krypton. *J. Chem. Phys.* **1999,** *110* (16), 7667-7676.
28. Woon, D. E.; Jr., T. H. D., Gaussian basis sets for use in correlated molecular calculations. IV. Calculation of static electrical response properties. *J. Chem. Phys.* **1994,** *100* (4), 2975-2988.
29. Woon, D. E.; Jr., T. H. D., Gaussian basis sets for use in correlated molecular calculations. III. The atoms aluminum through argon. *J. Chem. Phys.* **1993,** *98* (2), 1358-1371.
30. Kendall, R. A.; Jr., T. H. D.; Harrison, R. J., Electron affinities of the first-row atoms revisited. Systematic basis sets and wave functions. *J. Chem. Phys.* **1992,** *96* (9), 6796-6806.
31. Balabanov, N. B.; Peterson, K. A., Systematically convergent basis sets for transition metals. I. All-electron correlation consistent basis sets for the 3d elements Sc–Zn. *J. Chem. Phys.* **2005,** *123* (6), 064107.
32. Neese, F., The ORCA program system. *WIREs Comput. Molec. Sci.* **2012,** *2* (1), 73-78.
33. Shao, Y.; Gan, Z.; Epifanovsky, E.; Gilbert, A. T. B.; Wormit, M.; Kussmann, J.; Lange, A. W.; Behn, A.; Deng, J.; Feng, X.; Ghosh, D.; Goldey, M.; Horn, P. R.; Jacobson, L. D.; Kaliman, I.; Khaliullin, R. Z.; Kuś, T.; Landau, A.; Liu, J.; Proynov, E. I.; Rhee, Y. M.; Richard, R. M.; Rohrdanz, M. A.; Steele, R. P.; Sundstrom, E. J.; Woodcock, H. L.; Zimmerman, P. M.; Zuev, D.; Albrecht, B.; Alguire, E.; Austin, B.; Beran, G. J. O.; Bernard, Y. A.; Berquist, E.; Brandhorst, K.; Bravaya, K. B.; Brown, S. T.; Casanova, D.; Chang, C.-M.; Chen, Y.; Chien, S. H.; Closser, K. D.; Crittenden, D. L.; Diedenhofen, M.; DiStasio, R. A.; Do, H.; Dutoi, A. D.; Edgar, R. G.; Fatehi, S.; Fusti-Molnar, L.; Ghysels, A.; Golubeva-Zadorozhnaya, A.; Gomes,

J.; Hanson-Heine, M. W. D.; Harbach, P. H. P.; Hauser, A. W.; Hohenstein, E. G.; Holden, Z. C.; Jagau, T.-C.; Ji, H.; Kaduk, B.; Khistyaev, K.; Kim, J.; Kim, J.; King, R. A.; Klunzinger, P.; Kosenkov, D.; Kowalczyk, T.; Krauter, C. M.; Lao, K. U.; Laurent, A. D.; Lawler, K. V.; Levchenko, S. V.; Lin, C. Y.; Liu, F.; Livshits, E.; Lochan, R. C.; Luenser, A.; Manohar, P.; Manzer, S. F.; Mao, S.-P.; Mardirossian, N.; Marenich, A. V.; Maurer, S. A.; Mayhall, N. J.; Neuscamman, E.; Oana, C. M.; Olivares-Amaya, R.; O'Neill, D. P.; Parkhill, J. A.; Perrine, T. M.; Peverati, R.; Prociuk, A.; Rehn, D. R.; Rosta, E.; Russ, N. J.; Sharada, S. M.; Sharma, S.; Small, D. W.; Sodt, A.; Stein, T.; Stück, D.; Su, Y.-C.; Thom, A. J. W.; Tsuchimochi, T.; Vanovschi, V.; Vogt, L.; Vydrov, O.; Wang, T.; Watson, M. A.; Wenzel, J.; White, A.; Williams, C. F.; Yang, J.; Yeganeh, S.; Yost, S. R.; You, Z.-Q.; Zhang, I. Y.; Zhang, X.; Zhao, Y.; Brooks, B. R.; Chan, G. K. L.; Chipman, D. M.; Cramer, C. J.; Goddard, W. A.; Gordon, M. S.; Hehre, W. J.; Klamt, A.; Schaefer, H. F.; Schmidt, M. W.; Sherrill, C. D.; Truhlar, D. G.; Warshel, A.; Xu, X.; Aspuru-Guzik, A.; Baer, R.; Bell, A. T.; Besley, N. A.; Chai, J.-D.; Dreuw, A.; Dunietz, B. D.; Furlani, T. R.; Gwaltney, S. R.; Hsu, C.-P.; Jung, Y.; Kong, J.; Lambrecht, D. S.; Liang, W.; Ochsenfeld, C.; Rassolov, V. A.; Slipchenko, L. V.; Subotnik, J. E.; Van Voorhis, T.; Herbert, J. M.; Krylov, A. I.; Gill, P. M. W.; Head-Gordon, M., Advances in molecular quantum chemistry contained in the Q-Chem 4 program package. *Molec. Phys.* **2015,** *113* (2), 184-215.

34. Martí-Renom, M. A.; Stuart, A. C.; Fiser, A.; Sánchez, R.; and, F. M.; Šali, A., Comparative Protein Structure Modeling of Genes and Genomes. *Annu. Rev. Biophys. Biomol. Struct.* **2000,** *29* (1), 291-325.
35. Berman, H. M.; Westbrook, J.; Feng, Z.; Gilliland, G.; Bhat, T. N.; Weissig, H.; Shindyalov, I. N.; Bourne, P. E., The Protein Data Bank. *Nucl. Acids Res.* **2000,** *28* (1), 235-242.
36. Kluza, A.; Niedzialkowska, E.; Kurpiewska, K.; Wojdyla, Z.; Quesne, M.; Kot, E.; Porebski, P. J.; Borowski, T., Crystal structure of thebaine 6-O-demethylase from the morphine biosynthesis pathway. *J. Struct. Biol.* **2018,** *202* (3), 229-235.
37. Li, W.; Zhang, T.; Ding, J., Molecular basis for the substrate specificity and catalytic mechanism of thymine-7-hydroxylase in fungi. *Nucl. Acids Res.* **2015,** *43* (20), 10026-10038.
38. Jo, S.; Kim, T.; Iyer, V. G.; Im, W., CHARMM-GUI: A web-based graphical user interface for CHARMM. *J. Comput. Chem.* **2008,** *29* (11), 1859-1865.
39. Søndergaard, C. R.; Olsson, M. H. M.; Rostkowski, M.; Jensen, J. H., Improved Treatment of Ligands and Coupling Effects in Empirical Calculation and Rationalization of pKa Values. *J. Chem. Theory Comput.* **2011,** *7* (7), 2284-2295.
40. Olsson, M. H. M.; Søndergaard, C. R.; Rostkowski, M.; Jensen, J. H., PROPKA3: Consistent Treatment of Internal and Surface Residues in Empirical pKa Predictions. *J. Chem. Theory Comput.* **2011,** *7* (2), 525-537.
41. Vanommeslaeghe, K.; Hatcher, E.; Acharya, C.; Kundu, S.; Zhong, S.; Shim, J.; Darian, E.; Guvench, O.; Lopes, P.; Vorobyov, I.; Mackerell Jr., A. D., CHARMM general force field: A force field for drug-like molecules compatible with the CHARMM all-atom additive biological force fields. *J. Comput. Chem.* **2010,** *31* (4), 671-690.
42. Yu, W.; He, X.; Vanommeslaeghe, K.; MacKerell Jr., A. D., Extension of the CHARMM general force field to sulfonyl-containing compounds and its utility in biomolecular simulations. *J. Comput. Chem.* **2012,** *33* (31), 2451-2468.

43. Pang, X.; Han, K.; Cui, Q., A simple but effective modeling strategy for structural properties of non-heme Fe(II) sites in proteins: test of force field models and application to proteins in the AlkB family. *Journal of computational chemistry* **2013,** *34* (19), 1620-1635.
44.Huang, J.; MacKerell Jr, A. D., CHARMM36 all-atom additive protein force field: Validation based on comparison to NMR data. *J. Comput. Chem.* **2013,** *34* (25), 2135-2145.
45. Eastman, P.; Swails, J.; Chodera, J. D.; McGibbon, R. T.; Zhao, Y.; Beauchamp, K. A.; Wang, L.-P.; Simmonett, A. C.; Harrigan, M. P.; Stern, C. D.; Wiewiora, R. P.; Brooks, B. R.; Pande, V. S., OpenMM 7: Rapid development of high performance algorithms for molecular dynamics. *PLOS Comput. Biol.* **2017,** *13* (7), e1005659.